PHOSPHORUS IN CAVES: OXYGEN ISOTOPES IN PHOSPHATE AS A NOVEL SPELEOTHEM PALAEOTHERMOMETER

Contemporary study at Poole's Cavern with the British Cave Science Centre

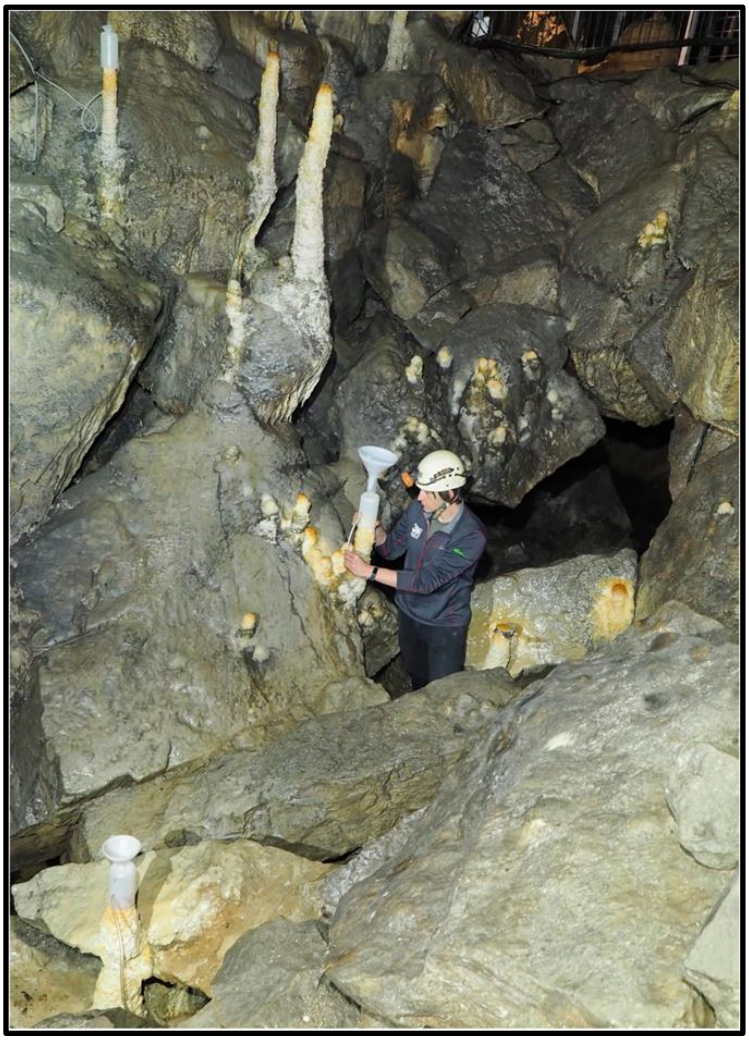

MSc by Research Dissertation by Alistair W. Morgan (Oct. 2021)

Supervisors: Dr. Peter Wynn, Dr. Ben Surridge, Dr. Andrew Smith

Lancaster Environment Centre | Lancaster University

ABSTRACT

ALISTAIR W. MORGAN - PHOSPHORUS IN CAVES: OXYGEN ISOTOPES IN PHOSPHATE AS A NOVEL SPELEOTHEM PALAEOTHERMOMETER (OCTOBER 2021) – MSc BY RESEARCH

Speleothems are key archives for palaeoclimatological study, yet current methods for palaeotemperature records are often affected by processes independent to temperature. Phosphorus is a ubiquitous component of speleothem calcite in caves, yet its efficacy as a palaeothermometer has not yet been fully explored. The fractionation of phosphate-oxygen-isotopes ($\delta^{18}O_{PO4}$) to temperature by pyrophosphatase (PPase) enzymes is frequently mentioned throughout the literature as a chemical thermometer but has yet to be tested in speleothems. This dissertation therefore aimed to evaluate the efficacy of $\delta^{18}O_{PO4}$-thermometry in a contemporary cave monitoring and palaeoclimatic context. This was accomplished through $\delta^{18}O_{PO4}$-temperature-equilibration experiments of drip-waters and speleothem material collected from Poole's Cavern, Buxton. Also tested were two speleothems grown over the last 100-years from Ethiopia and the UK, and two palaeo-$\delta^{18}O_{PO4}$-archives from Australian speleothem YB-F1 (99-37 ka) and the Archean Ocean (3.2-3.5 Ga). Results show that a PPase fractionation equation for Poole's Cavern of $1000Ln \propto (PO_4 - H_2O) = 15.801 \cdot \left(\frac{1000}{T}\right) - 29.106$ (R^2 = 0.69 P <0.01) describes a viable $\delta^{18}O_{PO4}$-temperature relationship between 7 and 30 °C. This has a similar overall trend to current literature (-0.2‰/°C) but is demonstrates a positive shift compared to previously determined relationships due to the hyperalkaline pH of Poole's Cavern drip-waters. $\delta^{18}O_{PO4}$ of calcite material shows mixed results, partly due to acid hydrolysis during late sample prep, but can be mitigated stoichiometrically in the future. Nonetheless, natural $\delta^{18}O_{PO4}$ in Poole's cavern waters translated into in-situ calcite with minimal (±1‰) fractionation, and $\delta^{18}O_{PO4}$-thermometry correctly predicted temperatures for Rukiesa Cave, Ethiopia. Moreover, $\delta^{18}O_{PO4}$ data from YB-F1 shows good correlation to expected temperature change 99-37 Ka but with exaggerated temperature readings. In all, this marks a critical 'first-step' in showcasing promise for $\delta^{18}O_{PO4}$-thermometry in speleothem palaeoclimatology.

Word Count of Main Text = 34,988

CONTENTS

FIGURE LIST

TABLE LIST

ACKNOWLEDGEMENTS

It's safe to say this has been an unusual year for science and certainly a risky year for getting back into academia. For myself leaving the animal feed industry in October 2020, the unknown of whether any cave research could be undertaken at all with the Covid-19 pandemic was only matched by the unknown of subject matter at hand.

It is truly a testament to all involved who went the extra mile to get this project off the ground in the face of adversity (and especially writing an almost endless torrent of extra safety forms).

For that I thank you all.

Dr. Peter Wynn; Who might possibly be the 'dream' supervisor that every good student hopes for. The incredible introduction to speleothem science I have received this year is only matched by your hard work, patience, keen eye, and drive for novel research. Thank you.

Dr. Andi Smith; It was through your recommendation that I landed the gig at Lancaster in the first place. Your expertise in phosphate cycling and isotope geochemistry at the NERC Isotope Geosciences Laboratories, and curating the British Cave Science Centre, has been key to keeping this project afloat. Thank you.

I would also like to thank: the **Buxton Civic Association** for continued access to Poole's Cavern despite the coronavirus pandemic. Similar testaments to **John Connaughton** and the team at **White Scar Cavern**. Cave manager **Alan Walker** for his help in accessing, and almost encyclopaedic knowledge on, Poole's Cavern. **Megan Barnett** and **Jianxun Shen** for the use of microbiological data collected in Poole's Cavern linked to this study. **Catherine Wearing** for her excellent support and guidance at **LEC**. **Ben Surridge** for his insight into $\delta^{18}O_{PO4}$ and use of a much-needed peristaltic pump. **Jo White** for her research materials on White Scar and continued curation of the **BCRA**. **Professor John Gunn** for use of some photos while in Poole's Cavern (including the cover photo). And finally, **Dave Hughes** for the almost endless use of his mg scales.

This work was funded through a Lancaster University Research Training and Support Grant (RTSG) to A. Morgan; and a National Environmental Isotope facility award to P. Wynn (2307.0920).

Upon reflection, this project has succeeded in founding a new avenue of investigation in the arsenal of speleothem palaeoclimatologists. Now moving to start a PhD in speleothem palaeoclimate at Universität Basel (Switzerland), I look forward to the developments to come.

DECLARATION

As author, I declare that this dissertation is my own work and has not been submitted in substantially the same form for the award of a higher degree elsewhere.

i. The lab work associated with the microbiological data for Poole's Cavern was undertaken by Megan Barnett (British Geological Survey), Jianxun Shen (University of St. Andrews) and Andi Smith (British Geological Survey) - Results in prep as of September 2021.

ii. The $\delta^{18}O_{PO4}$ data from the Yarrangobilly speleothem was collected under NERC isotope facility grant IP-1603-11115 to Peter Wynn in 2019.

Alistair William McCubbin Morgan
Dated: 25/09/2021

1 - INTRODUCTION

Producing an absolute temperature record beyond the era of instrumentation has relied upon finding an unambiguous linkage between proxy record and environmental temperature. Records have typically relied on isotope, trace element and biomarker signatures contained within archives such as carbonate deposits, fluid inclusions and ice-cores. However, multiple competing environmental influences on each proxy, and processes of kinetic fractionation, have typically confounded the search for a universal palaeothermometer. This is particularly true for speleothem records of environmental change.

Speleothem formations have proven to be an invaluable resource in terrestrial palaeoclimate studies, benefiting from a robust ^{234}U-series dating system producing high-resolution, long, and often continuous records (Fairchild & Baker, 2012). Cave temperature often represents an average of annual air temperature (McDermott et. al., 2004., Fairchild, et. al., 2006), meaning that there is value in constraining a working palaeothermometer to measure terrestrial temperature through time. However, current traditional archives (e.g. calcite $\delta^{18}O$) also suffer from numerous effects that perturb a clear signal (Fairchild et. al., 2006). While alternatives such as clumped isotope measurements (Ghosh et al., 2006., Bajnai, et.al., 2020) and Mg/Ca ratios (Drysdale et. al., 2020) show promise, there is currently few unambiguous palaeothermometers in speleothem archives.

However, it is thought that the fractionation of oxygen isotopes in phosphate ($\delta^{18}O_{PO4}$) found in speleothems could mitigate this problem. Phosphate is regarded as a ubiquitous component of speleothem material (Fairchild & Baker, 2012), yet its palaeo-

environmental significance has not yet been fully explored (e.g. Chang et. al., 2010). $\delta^{18}O_{PO4}$ is significant, as a mechanism exists driven by the enzymatic action of microbes that can fractionate oxygen isotopes to equilibrium with temperature (Chang & Blake, 2015). This has largely been explored through the soil literature as an environmental proxy, and in archaeological investigations of bones and teeth as a palaeothermometer (Longinelli and Nuti, 1973., Shen et. al., 2020). But recent methodological advances (Grant IP-1603-1115) suggest that small volumes of phosphate can be extracted from speleothem material, raising the possibility of reconstructing temperature from well dated speleothem archives.

Therefore, the aim of this research is to:

1. Explore the efficacy of speleothem $\delta^{18}O_{PO4}$-thermometry by producing a contemporary in-cave fractionation equation of $\delta^{18}O_{PO4}$ Vs. temperature (following those already in the literature; Chang & Blake, 2015).

2. To see if this drip-water $\delta^{18}O_{PO4}$ signal transfers into speleothem material without further isotopic fractionation.

3. To test the in-cave equation from this article, against others in the literature, in predicting $\delta^{18}O_{PO4}$ and temperature from speleothems grown in the last 100-years and in two preliminary palaeo-archives.

2 - LITERATURE REVIEW

2.1 PALAEOCLIMATOLOGY AND THE PALAEOTEMPERATURE RECORD

Palaeoclimatology is a vital tool to better our understanding of the current climate system and to predict future climate change (McDermott et.al., 2004., Bradley, et.al., 2008). If characteristics (such as temperature) are understood at a particular location through time, it can help validate and improve the resolution of climate models. (e.g. Vetteoretti & Peltier 2011, and Jones, et.al., 2013). This is important as idiosyncrasies in variables such as ocean currents, air circulation and humidity can have varying consequences globally.

Palaeotemperature is one aspect of palaeoclimatology and will be the primary focus of this dissertation. It is the temperature of a location through geologic time using proxy data as 'thermometers' in the absence of primary data (Hertzberg, et.al., 2017).

It is key that palaeotemperature proxy data must first be 'calibrated' to known environmental parameters. This involves comparing proxy data to modern climatic records, assuming that the relationship between the variables has remained unchanged temporally (Bradley, 2015). However, it is often the case that each proxy 'signal' is influenced by several environmental factors. Non-climatic processes, such as bioturbation, erosion and re-precipitation, can also alter a signal post deposition. This introduces ambiguity, or 'noise', into palaeoclimate signals and can make curating a novel temperature record difficult (McDermott et.al., 2004).

2.1.1 SOURCES OF PALAEOTEMPERATURE RECORDS

Palaeotemperature records can be split between marine and terrestrial archives. Each source, and method of data extraction, comes with its own strengths and caveats. While there are many forms of palaeoclimate records, we will be focusing on the most popular proxies for palaeotemperature. There is a lot of proxy cross over between archives (δ^{18}O can be used somewhat universally for example), but all come with somewhat similar caveats in each case.

2.1.1.1 Marine Archives

Covering >70% of the earth's surface, the oceans are a very important source of palaeotemperature information. 6-11 billion tons of sediment settle on the ocean floors annually, creating a stratified record of environmental data (Bradley, 2015). In historically temperate waters, they are also home to corals which secrete aragonite in bands much like tree-rings (Alpert et. al., 2016). The downside of marine archives is that they are geographically limited and cannot give information on terrestrial or air temperature. Marine archives are also 'tuned' to changes in boundary conditions, such as sea ice extent, which can drastically alter salinity and ocean currents over interglacial timescales. This may perturb a continuous palaeotemperature signal.

2.1.1.1.1 Foraminifera: species assemblage, Mg^{2+}/Ca^{2+}, $\delta^{18}O$ and Δ_{47}

Foraminifera are marine protozoa that are found free-floating near the ocean's surface (planktonic zone) or living on the seafloor (benthic zone), producing a $CaCO_3$ test which accumulates on the seafloor after death. Stratified chronologies can be traced through oceanic drill cores (e.g. the Integrated Ocean Drilling Program (IODP) 2003-2013).

Their strength as palaeo-archives lies in global abundance, primarily in the tropics (Kucera, 2007), and diversity in marine sediment, particularly deep-sea oozes which hold long continuous palaeoclimate records (Pearson, 2012). Planktonic forams are useful as a proxy for sea-surface-temperature (SST) (Marchitto, et.al., 2014). However, as free-floating organisms, a universal caveat is that assemblages represent source, rather than locational, conditions (Hertzberg, 2017). Careful consideration of ocean currents and palaeo-boundary-conditions, such as sea-ice coverage, much be constrained to back-track trajectories and map ocean temperature.

The Mg^{2+}/Ca^{2+} ratios in foraminifera tests can also be used as a temperature proxy. The substitution of Mg^{2+} for Ca^{2+} is endothermic, favouring increased temperature (Hertzberg, 2017). Anand et.al., 2013 used modern foraminifera to constrain a 9-10 % increase in Mg^{2+}/Ca^{2+} per 1°C. However, Mg^{2+}/Ca^{2+} ratios are influenced heavily by salinity and CO_3^{2-} concentration (Bryan and Marchitto, 2008) which can perturb archives. Moreover, foraminifera tend to dwell in the benthic zone for long periods where temperatures are more stable, requiring careful planktonic species selection for palaeotemperature.

SST can also be inferred from the $^{18}O/^{16}O$ ratios of carbonate tests. In modern forams, $\delta^{18}O_{calcite}$ is expressed as $^{18}O/\ ^{16}O$ ratio away from a standard, such as Vienna Pee Dee

Belemnite (VPDB) (Marchitto, et. al., 2014). In general, $\delta^{18}O_{calcite}$ decreases by 0.21–0.23‰ for a 1 °C increase in temperature (Ravelo & Hillaire-Marcel., 2007). However, problems arise in palaeo-records as $\delta^{18}O_{calcite}$ is a dependant factor of temperature and the $\delta^{18}O_{seawater}$ that the foraminifera grew in (Bernard et. al., 2017). $\delta^{18}O_{seawater}$ is itself influenced by salinity, pH and sea ice volume (Hertzberg, 2017). These effects must be constrained to unravel accurate palaeotemperature signals. This, along with diagenetic effects, created problems such as the 'cool tropics paradox' through late Cretaceous and Paleogene archives (D'Hondt & Arthur, 1998) where climate models were being tuned to poorly-presented data (Bernard et.al., 2017).

Multi-proxy studies, such as combining Mg^{2+}/Ca^{2+} and $\delta^{18}O$ from the same test (Schmidt et. al., 2012) or clumping isotopes together (Δ_{47}) (Tripati et. al., 2010), have shown promise in combating ambiguity. The benefit of Δ_{47} is that it removes ambiguous $\delta^{18}O_{seawater}$ signals as a dependant variable for palaeotemperature (Ghosh et al., 2006., Bajnai, et.al., 2020). The downside is that it is a costly laboratory process, often requiring several repetitions to rule out error, and only limited calibration data is available for palaeo studies (Hertzberg, 2017).

2.1.1.1.2 Sediment chemistry: Coccolithophore Alkenone and TEX_{86} biomarkers

Coccolithophores are another form of eukaryotic phytoplankton protected by calcareous plates known as coccoliths. Like foraminifera, they deposit on the seafloor producing a sedimentological record. As phototrophs they reside near the sea surface, making them a useful tool for reconstructing SST (Hertzberg, 2017).

Coccoliths are common in marine sediments, both temporally and spatially, including regions where foraminifera are absent. Biomarkers of coccoliths, such as the alkenone $U^{k'}_{37}$ (Prahl & Wakeham 1987) and TEX_{86} (Schouten et al. 2002) have been used as an alternative SST proxy. These methods benefit by not influenced by changes in ocean salinity or isotropic concentration (Bradley, 2015).

Alkenones are long-chain organic compounds found in the cell membranes of coccolithophores and the $U^{k'}_{37}$ index is based on the proportions of di- and tri-alkenones, which correlate positively with temperature (Hertzberg, et. al., 2017). Based on laboratory experiments that showed a correlation between $U^{k'}_{37}$ and temperature (Prahl & Wakeham., 1987 and Prahl et al., 1988), Conte et al., 2006 developed a core-top SST calibration (Hertzberg, 2017). However, $U^{k'}_{37}$ has an effective temperature limit of 1-28 °C, so does not record regionally warm areas or periods (Herbert, 2014). Moreover, it has since been discovered that alkenone production is seasonally controlled (Chapman et.al., 1996), meaning that SST signals can be biased to the season of maximum production (Bradley, 2015). Again, alkenones are at the mercy of lateral movement in the water column before deposition.

Thaumarchaeota are single-celled microorganisms found in both marine and lacustrine environments and the composition of their lipid membranes is influenced by

temperature. TEX_{86} (TetraEther indeX of 86 carbons) is the number of GDGT cyclopentane rings found within the lipid membrane which increases with temperature (Wuchter, et.al., 2004). Schouten et al., 2002 demonstrated a strongly positive corelation of TEX_{86} to SST in core-top marine sediments, offering its potential as a palaeotemperature proxy. Unlike alkenones, it can reconstruct warmer SSTs between 6-30°C (Hertzberg, 2017) and diagenetic effects seem to be minimal, therefore making them more robust for pre-Quaternary records (e.g. Lawrence et. al., 2020). However, Hertzberg et al. 2016 noted a bias in TEX_{86} to subsurface temperatures rather than SST. Unlike planktonic coccolithophores, thaumarchaeota live throughout the water column which may explain this benthic signal (Schouten et al. 2002). Lawrence et. al., (2020) now suggests a correction for this, showing good correlation between $U^{k'}_{37}$ and TEX_{86} 5-6 Ma, but may only be successful regionally.

2.1.1.1.3 Coral (Sclerochronology): Sr^{2+}/Ca^{2+} ratios

Corals typically grow in warm oceans, making them viable archives for tropical palaeotemperature reconstructions but provide no information on cooler marine regions or at higher latitudes. Corals secrete aragonite as annual bands, producing a potentially high-resolution record much like tree rings. The substitution of Sr^{2+} to Ca^{2+} is exothermic, and is inversely correlated to temperature (McCulloch, et. al., 1994).

This correlation has been shown to provide reliable palaeotemperature reconstructions, such as Gagan et. al., (1998) which showed that temperatures on the Great Barrier Reef, Australia were 1.2 °C higher in the mid-Holocene. However, coral Sr/Ca is also heavily influenced by vital effects such as pH and light source, leading to bias and varying sensitivity to temperature even in the same reef (Alpert, et. al., 2016). Some advances have been made in countering these effects by combining Sr/Ca to U/Ca ratios (DeCarlo et. al., 2016).

More recently, Stylasterid corals have been offered as a new palaeotemperature archive, using $\delta^{18}O$ and $\delta^{13}C$, due to calcification occurring close to equilibrium compared with other deep-sea corals (Samperiz, et. al., 2020).

2.1.1.2 Terrestrial Archives

If the effects on each proxy can be constrained, terrestrial archives provide information on surface air temperature. As of date, very few palaeoclimate archives, outside of the polar regions, transcend continuously through multiple glacial-interglacial cycles (Drysdale et.al., 2020), hence the need to pursue this as an avenue of research. As speleothems are the focus of this dissertation, they will be discussed in their own section.

2.1.1.2.1 Tree Rings (Dendroclimatology)

Tree rings contain the most comprehensive record of palaeotemperature for the last 1-2 ka, with each ring marking a clear annual increment of growth (George & Esper 2019), benefiting from high-resolution and robust radiocarbon chronology (Hernández, et.al., 2020).

Tree rings are wider in the most favourable conditions for that species, however this has had limited success as a proxy for exact temperatures (George & Esper 2019). Maximum Wood Density (MXD) is a robust proxy for summer temperature (Kaczka, et.al., 2018) and shows a good correlation to other records (Esper & Cook, 2002). This has culminated in databases such as N-TREND (Northern Hemisphere Tree-Ring Network Development), which collates dendrochronologies to improve reconstructions (Wilson, et.al., 2016). $\delta^{18}O$ stable isotope chronology has also been implemented, Lavergne et al. 2016, for example, used $\delta^{18}O$ in tree-ring cellulose to reveal data on climate variability in northern Patagonia.

However, tree rings only 'record' data over the summer months, giving a proxy for favourable growth conditions rather than an annual average. Tree growth is also influenced by climatic effects, including precipitation, sunlight, and soil nutrients, as well as non-climate factors including disease and pest outbreaks (Hernández, et.al., 2020). It therefore becomes difficult to constrain a temperature record without proper tuning or comparison to other records.

More recently $\delta^{13}C$ ratios in fossil wood have been used as an approximation for air temperature (Pienkowski et. al., 2020). This offers a promising record from non-marine

archives, however, is still constrained by the multitude of effects that can control isotopic fractionation.

2.1.1.2.2 Ice Core records: δ^{18}O, δD, δ^{15}N and δ^{40}Ar

Glacial Ice serves as a valuable palaeoclimate archive due to the variety of data that can be taken from both the water and trapped air pockets, offering continuous records for up to the last 800,000 years (Bradley, 2015). This includes direct measurements of CO_2, CH_4, dust and proxies of temperature. Primary archives include Antarctica, Greenland, and high-altitude mountain regions in both hemispheres.

There is a strong spatial correlation between mean annual temperatures and the isotopic ratio of δ^{18}O and ^{2}H (δD) within ice core records (Dansgaard, et. al., 1993). Isotopic fractionation occurs because heavier isotopes have a lower vapour pressure than $^{1}H_2{}^{16}O$; the most common isotopologue in water. As such, more energy is required to readily evaporate ^{18}O and ^{2}H. Conversely, ^{18}O and ^{2}H precipitate more readily as they condense first. As meteorological processes transfer water onto the glacier, this isotopic fractionation from source and journey is translated into the ice, with the temperature difference between the evaporative source and the final region of deposition being the primary control (Masson-Delmotte et. al., 2006).

However, there are several other effects that can influence isotopic fractionation that are often not in equilibrium (Darling et. al., 2006). Like other isotopic proxies, it is important that these effects are constrained to identify a palaeotemperature signal, usually through modelling. The isotopic concentration of the water source is dictated by surface conditions, which can vairy spatially and temporally. This includes SST, wind speed and humidity (Hertzberg, 2017). Rough seas, for example, can enrich δ^{18}O with

no change in temperature. Rayleigh distillation fractionates the air mass en-route as it moves poleward, shedding heavier isotopes as they move over distance to the final precipitation area. Latitude, altitude, wind trajectory and the distance from the water source are therefore primary controllers on this. For example, altitude adiabatic cooling accounts for a 11‰ reduction in $\delta^{18}O$ of Andes glaciers (Grootes et. al., 1989) and interior Antarctic ice has some of the lowest $\delta^{18}O$ due to its distance from the oceans (Bradley, 2015). At low latitudes, $\delta^{18}O$ is largely controlled by precipitation amount rather than temperature (Schmidt et. al., 2007). Moreover, fluctuations in circulation currents, such as the Gulf Stream, can have a significant effect on $\delta^{18}O$ and ^{2}H concentrations.

In the absence of primary data, one solution to this problem is to apply the proxy data to general circulation models. Here, boundary conditions are defined mathematically, and the effect of these changing conditions can be subtracted chronologically from the isotopic dataset. This ideally leaves only the desired palaeotemperature signal. Using this method, most reconstructions during the LGM agree that mean annual temperature was 7-8 °C below current (Bradley, 2015). Problems arise, especially in older interpretations, when assumptions are made on effects such as precipitation source, seasonality, and cloud trajectory (Kapsher et. al., 1995). Another issue is that the firn-ice transition depth is different in each hemisphere (77 m in Greenland, 95 m in Antarctica) and between each glacier, meaning that the 'lock in' time for stable isotopes and gases, which can migrate through the firn stratigraphy, can vary and bias interpretation (Landais et. al., 2020). This makes it difficult to cross-correlate signals and can miss out subtle leads and lags in the climate system.

As with foraminifera, clumped isotope methods such as 'deuterium excess' (d = δD – 8(δ^{18}O) helps to solve some ambiguity by correcting for variation in evaporative conditions (Cuffey & Vimeux, 2001). However extreme changes in boundary conditions, such as clouds becoming super saturated when very cold, can alter the relationship of deuterium excess to temperature (Bradley, 2015).

Another major caveat of ice cores is that it can be difficult to date and correlate the chronology between separate sites. Often event horizons, such as a volcanic fallout and 'isotopic events', are used in the absence of direct radiometric dating. There is good continuity for this over the last 60,000 yrs (Rasmussen et. al., 2006), but beyond becomes vague. Over time, metamorphism can alter boundaries, creating age reversal in extreme cases. Moreover, as glaciers are always in motion downslope, the effective altitude and location of the core has changed over time (Dansgaard & Johnsen, 1969). Careful consideration needs to be made when taking core samples because of this. All these effects will detrimentally influence palaeotemperature records.

2.2 SPELEOTHEM RECORDS

A cave is defined as a ''cavity large enough for humans to enter'' (Hill & Forti, 1997). This can range from a single chamber to, as surveyed to date, a staggering 668 km of passage (Mammoth Cave, USA). Many caves are home to geological formations known as speleothems: secondary precipitates that can form both in the abandoned passages of the vadose zone and subaqueously.

Speleothems can be made from any mineralogy but are often composed of calcite, or aragonite in high-Mg areas (McDermott, 2004). They precipitate in response to the chemistry of the water moving into the karst system and the microclimate within the cave itself (Fairchild et. al., 2006). Water entering the cave is a result of interactions in the epikarst and soil system, the surface landscape, local weather and therefore the global climate. It can therefore be argued that the chemistry of speleothems is a distilled representation of the environment at that time. This includes, if appropriately interpreted, analogues for palaeotemperature.

As calcite precipitates, signatures of these numerous environmental factors get 'locked in' (Gascoyne et.al., 1992). Thus, speleothems have the potential to be multi-proxy archives. The presence of calcite itself, as water must be free flowing to facilitate precipitate, is an indicator of non-glacial or non-arid conditions (Gascoyne, 1992). Rainfall and humidity, linked to climate, affect calcite growth directly (Baker et.al., 1998). Importantly, cave ambient temperature and the temperature of the drip water source also control geochemical characteristics of the calcite such as $\delta^{18}O$, Mg and SO_4 ratios. Cave air temperature is relatively stable throughout the year, and often represents the mean annual air temperature outside the cave (McDermott et. al., 2004.,

Fairchild, et. al., 2006). This is important as, if a palaeotemperature signal can be constrained near to or at the time of calcite precipitation, this could provide a very stable record for annual temperature locally.

Speleothems have become attractive to palaeoclimatologists for several reasons. Firstly, continued episodes of speleothem growth can occur for long periods, often $10^4 – 10^6$ years (McDermott et. al., 2004). Moreover, once the hydrological source has ceased, the cave environment can protect speleothems from erosion for potentially millions of years. This puts them chronologically far beyond the realm of other terrestrial archives. Secondly, speleothems are independent of 'orbitally tuned' marine and ice-core records, and therefore have the potential to transcend glacial-interglacial cycles uninterrupted over the last 1 ka to 1 Ma, through which the more traditional proxy records are either destroyed, altered, or do not record continuously (McDermott et.al., 2004). Moreover, speleothems are widespread geographically, not just limited to the poles or high-altitude regions like ice cores. Thirdly, speleothems benefit from robust U-series dating methods, allowing leads and lags in the climate system to be assessed with precision (Fairchild & Baker, 2012). This is significant as there is continued need for well-dated and constrained palaeoclimate data to test and validate general circulation models (GCMs) (McDermott, 2004). Speleothems therefore complement existing records, such as ice cores, which rely upon GCMs heavily for interpretation (e.g. Svensson, et. al., 2008., Cheng et. al., 2016).

However, as with the other archives previously discussed, due to the complex factors that influence speleothem formation and chemistry the challenge is deriving unambiguous environmental signals.

2.2.1 SPELEOTHEM FORMATION

2.2.1.1 Calcite precipitation: a typical cave system of drip-water pH 7-8

As water percolates through soil and the epikarst, the partial pressure of CO_2 increases, sometimes achieving up to 100,000 ppm in soil (McDermott, 2004). This is due to plant root respiration and the decay of organic matter in the soil (Scholz & Hoffmann, 2008). CO_2 becomes concentrated in small pore spaces of the soil matrix, resulting in the production of carbonic acid (equation i). This weak acid dissociates into protons and bicarbonate ions (equation ii), which dominate between pH 7 and 10. Important when considering Poole's Cavern, under high pH bicarbonate further disassociates into carbonate, leading to carbonate oversaturation (equation iii) (Fairchild & Baker, 2012):

(i) $\mathrm{H_2O + CO_{2(aq)} \leftrightarrow H_2CO_3}$

(ii) $\mathrm{H_2CO_3 \leftrightarrow HCO_3^- + H^+}$

(iii) $\mathrm{HCO_3^- + H^+ \leftrightarrow CO_3^{2-} + 2H^+}$

Water below pH 7, enriched in weak carbonic acid (equation i), dissolves the limestone carbonate bedrock (equation iv) (Fairchild & Baker, 2012):

(iv) $\mathrm{CaCO_3 + 2H^+ \leftrightarrow Ca^{2+} + 2HCO_3^-}$

Bicarbonate is now held in solution at equilibrium, dependant on the temperature, pH and pCO_2 concentration of the surrounding environment (McDermott, 2004). If CO_2 held in solution can degas, calcite precipitation dominates (equation v):

(v) $\mathrm{Ca^{2+} + 2HCO_3^- \leftrightarrow CaCO_3 + H_2O + CO_2}$

The slow microbial oxidisation of organic particles in karst aquifers is now thought to be a major CO_2 reservoir, increasing pCO_2 further (Baldini et. al., 2018). However, as bicarbonate rich pore-water enters a void, such as a cave passage, the partial pressure of pCO_2 in the surrounding environment becomes lower than it was in the soil and epikarst. This allows CO_2 to degas from the drip water, leading to oversaturation and calcite precipitation (McDermott et. al., 2004). The pCO_2 in caves is often higher than atmospheric pCO_2, but sufficiently lower than soil and enough to facilitate this. This process is summarised Figure 2.1:

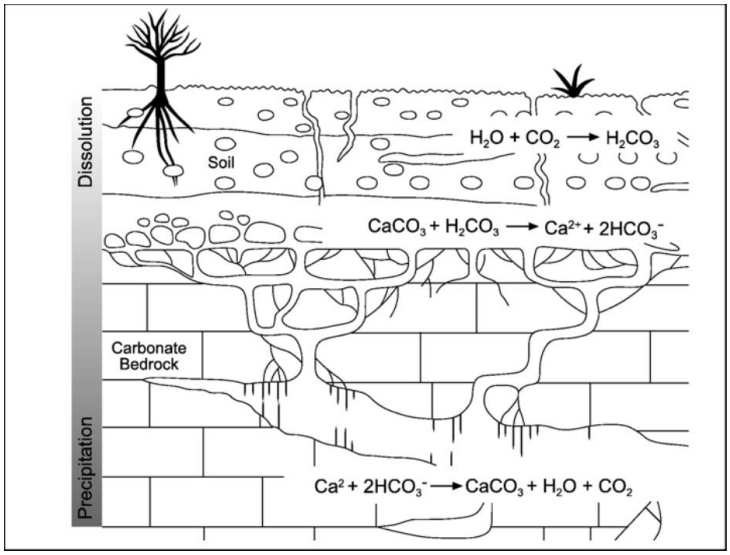

Figure 2.1: Dissolution and precipitative regimes of a typical cave system (Fairchild, et. al., 2006).

In winter, cold dense fresh air tends to move into caves lowering pCO_2 further and increasing calcite production. The growth rate of typical speleothems is therefore seasonal, being greater in winter, if the supply of water continues. Conversely, the opposite is true in summer where air moving out of the cave draws CO_2 from the epikarst, slowing calcite precipitation (Fairchild & Baker, 2012). Over time, precipitated calcite can build layer-by-layer to form speleothems.

2.2.1.2 Calcite Precipitation in hyperalkaline waters: e.g. Poole's Cavern, UK

The precipitation of calcite in hyperalkaline conditions (pH >10), such as those in Poole's Cavern, presents a significant variation on the chemistry previously discussed. Here the relationship with pCO_2 reverses. In areas of old lime kilns, lime waste (CaO) in the soils above the cave reacts with percolating rainwater to produce calcium hydroxide (equation vi). This further disassociates to calcium and hydroxide ions (equation vi):

(vi) $$H_2O + CaO \leftrightarrow Ca(OH)_2 \leftrightarrow Ca^{2+} + 2OH^-$$

The abundance of hydroxide ions greatly increases pH, leading to hyperalkaline waters between pH 9-13 (Hartland et. al., 2010). Above pH 10.3, hydroxylation of CO_2 to produce bicarbonate becomes the dominant reaction (Clark et. al., 1992) (equation vii) further dissociating to carbonate (equation vii) and rapidly precipitating calcite (equation viii):

(vii) $$OH^- + CO_2 \leftrightarrow HCO_3^- \leftrightarrow CO_3^{2-} + H^+$$

(viii) $$CO_3^{2-} + Ca^{2+} \leftrightarrow CaCO_3$$

This marks an alternative reaction for calcite precipitation, where CO_2 is consumed as a reagent rather than degassed. $CO_{2(aq)}$ is so readily consumed that $CO_{2(g)}$ from the cave environment is also taken into solution (Hartland et. al., 2010). Therefore, the relationship between speleothem formation and pCO_2 in the cave also reverses. Hyperalkaline calcite precipitates more readily in areas of high $CO_{2(g)}$, favouring speleothem growth in summer rather than winter (Newton, et. al., 2015). Newton et. al., 2015, in agreement with Hartland et. al., 2014, suggests that pCO_2 in the cave environment is the primary controller on hyperalkaline calcite formation in Poole's Cavern.

Moreover, under this reaction carbonate becomes the dominant ion rather than the bicarbonate found in most cave drip waters at normal pH (see equation iii from Section 2.2.1.1). In hyperalkaline drip waters, the greater the concentration of carbonate and calcium ions leads to a much greater degree of calcite supersaturation, and therefore rapid calcite precipitation once the water is exposed to $CO_{2(g)}$ (Macleod et. al., 1991). Thus, in Poole's Cavern, hyperalkaline calcite grows 25-30x the normal rate (Newton et. al., 2015) at around 1 cm yr^{-1} (Hartland et. al., 2010).

2.2.2 TYPES OF SPELEOTHEM FORMATIONS

Stalactite's form from cave roofs and, in the case of soda-straws, often have a hollow core with growth precipitating at the tip of the tube. Thin and thick annual bands of soda-straws can highlight seasonal variation in growth (Fairchild et. al., 2001), however they are usually very thin and too fragile for sampling.

Flowstones, that form laterally on cave walls and floors, are used less readily but have provided some palaeoclimate information (e.g. Baker et. al., 1995., Hellstrom, et. al., 1998., Webb et. al., 2014., Hellstrom et. al., 2020). Care must be taken when interpreting a flowstone time series, as micro-terraces can induce 'self-damming' of calcite along its growth plane (Fairchild & Baker, 2012) meaning that the location and direction of growth varies.

Stalagmites grow incrementally on cave floors to a minimum thickness of 3-4 cm (Fairchild & Baker, 2012) with clear precipitation regimes compared to flowstones, building parallel to water source. They typically grow 0.01 – 1 mm/yr depending on cave conditions and ionic concentration of drip water (Baker et. al., 1998), but can grow up to 1 cm/yr in hyperalkaline conditions (Hartland et. al., 2010). They are typically less porous than stalactites, but density can vary depending on precipitation rate, with hyperalkaline drip waters forming rapid but lower density speleothems (Hartland et. al., 2010). Thus, stalagmites are often picked for palaeoclimate analysis, due to the extra volume of material that can be used for measurement and laminations that are clear for interpretation (Fairchild & Baker, 2012).

2.2.3 FLUID INCLUSIONS

Speleothems can contain up to 0.1 wt % of palaeo-water in the form of fluid inclusions, trapped as the calcite precipitates (Dennis et. al., 2001). These form as incomplete coalescence of the crystal lattice leaves thin gaps perpendicular to growth, giving a 'milky-white' appearance (Kendall & Broughton, 1978).

Fluid inclusions are significant in offering primary water chemistry at the time of growth (McDermott, 2004). This has marked a significant advance for $\delta^{18}O_{calcite}$ studies, as deuterium excess can be used to estimate the Local Meteoric Water Line for that period, accounting for variations in $\delta^{18}O_{rainfall}$ directly (McGarry et. al., 2004., van Breukelen, et. al., 2008) and estimate the volume of rainfall itself such as monsoon events (McDermott et al., 2006., Griffiths et. al., 2010) and precipitation source during glacial periods (Mathews et. al., 2000).

2.2.4 PALAEOTEMPERATURE RECORDS FROM CAVES

2.2.4.1 $\delta^{18}O$ of speleothem calcite

Analysing $\delta^{18}O_{calcite}$ is currently the primary method for attempting to reconstruct palaeotemperature in speleothems. When air and water movement within a cave is slow, a thermal equilibrium is maintained between the bedrock temperature and the air within the cave (Bradley, 2015). This often represents mean annual air temperature for the environment above the cave (McDermott et. al., 2004., Fairchild, et. al., 2006). During calcite precipitation, fractionation of oxygen isotopes occurs as a function of cave temperature; roughly -0.24‰ $°C^{-1}$ (O, Neil., 1969). This is because the heavier ^{18}O has a lower vapour pressure than ^{16}O, therefore requiring more energy to degas as CO_2 (Fairchild & Baker, 2012). Thus, in ideal conditions, $\delta^{18}O_{calcite}$ can archive cave palaeotemperatures.

If this was the only effect on $\delta^{18}O_{calcite}$ a clear record of cave palaeotemperature, and therefore the palaeotemperature of the region, could be established. However, as with other $\delta^{18}O$ archives already discussed, cave temperature is one of many effects on $\delta^{18}O$ variation. Moreover, there are numerous sources and sinks of oxygen isotopes throughout the system. The myriad of environmental factors distilled within speleothem growth make it exceedingly difficult to decipher between each factor individually, producing ambiguous palaeotemperature signals (McDermott et.al., 2004).

To describe this problem, Fairchild et. al., (2006) breaks the speleothem hydrological cycle into 'realms' that water travels through towards calcite precipitation (Figure 2.2). Each realm affects the geochemistry of the palaeowater, that is hypothetically translated into precipitated calcite (Gascoyne et.al., 1992).

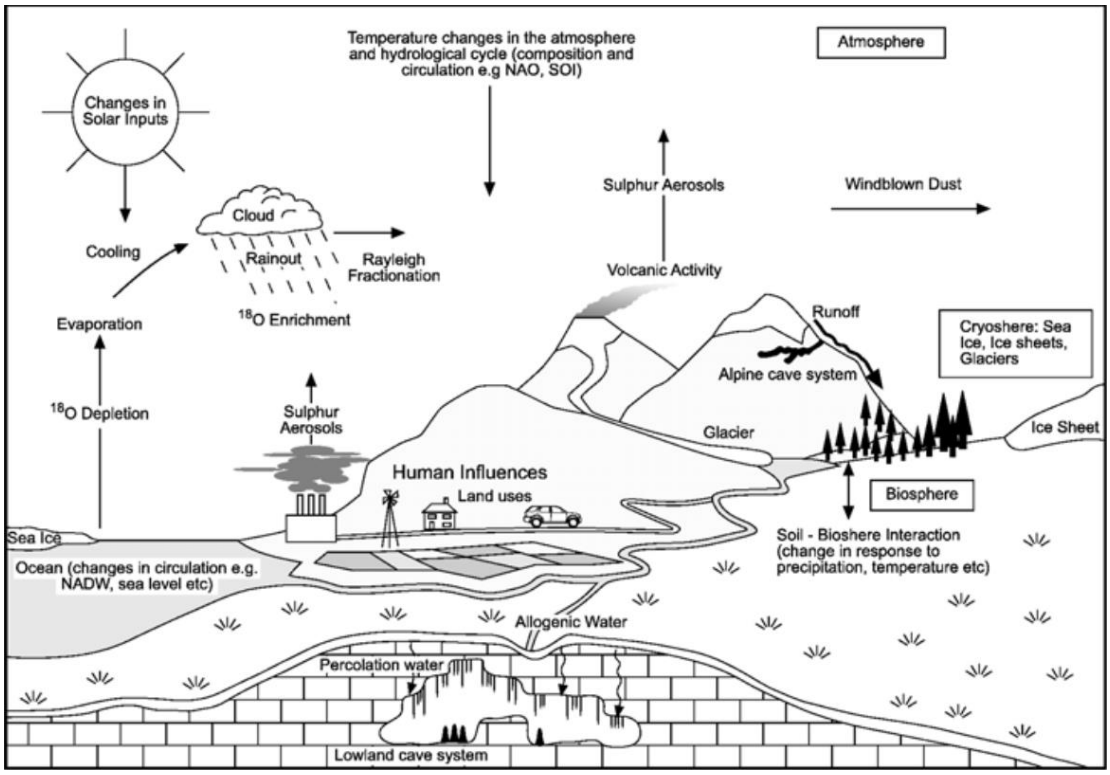

Figure 2.2: A diagram from Fairchild et. al., 2006 depicting the relationship speleothems have to the climate cycle and local environment.

i. Effects from the Atmosphere & the Hydrological Cycle

As with the control on $\delta^{18}O$ in ice-cores and foraminifera, there are several effects independent of temperature that profoundly influence $\delta^{18}O_{rainwater}$ which is translated into $\delta^{18}O_{dripwater}$ and therefore $\delta^{18}O_{calcite}$.

Source Effect: Rainfall source can impart an altered $\delta^{18}O$ ratio into the cave. For example, if precipitation is derived from ^{18}O depleted sources, such as a lake or snow cover, this can bias low $\delta^{18}O_{rainfall}$ values inside the cave (Bradley, 2015). Conversely, during glacial periods, the growth of ^{18}O depleted ice sheets and lowering of sea level leads to a concentration of ^{18}O in the oceans and hence ^{18}O enrichment (McDermott et., al., 2004). This will have a significant impact on interpreting millennial scale records.

While a problem for palaeotemperature, this effect has proven useful in mapping monsoon dynamics through the speleothem record as each monsoon source has its own $\delta^{18}O$ signature (Wolf et. al., 2020). Liu et. al., 2020, for example, builds on $\delta^{18}O$ signatures that identify variation between the Indian and East Asian Monsoons in China to also account glacial-interglacial variability.

Temperature effect: Aside from temperature dependant isotopic fractionation occurring within the cave, $\delta^{18}O$ is also influenced by air temperature above-ground. At lower temperatures ^{18}O less readily evaporates compared to ^{16}O, subsequently leading to lower $\delta^{18}O_{rainfall}$ values.

Continental effect: Rayleigh distillation forces ^{18}O to be preferentially shed with increased distance from the precipitation source, lowering $\delta^{18}O_{rainwater}$ values (Hertzberg, 2017). This is profound if the air mass moves across a large continental region or the direction of precipitation source changes (Bradley, 2015).

Altitude & Topographical Effects: There is an altitude effect where adiabatic cooling and condensation, such as an air mass moving over a mountain range, forces ^{18}O in rainwater to condense more readily leading to preferential loss of ^{18}O and lowering of $\delta^{18}O_{rainwater}$ values (Gat, et. al., 2001). Caves in Alpine regions must be corrected for their altitude as $\delta^{18}O_{calcite}$ values are lower, compared to sea-level, for the same temperature.

Latitude effect: At low latitudes, where mean annual temperatures are >15 °C, $\delta^{18}O$ variation becomes a function of precipitation source rather than temperature (Schmidt et. al., 2007), introducing a regional bias. Oceanic water vapour is more enriched in ^{18}O at lower latitudes due to the higher ambient temperatures facilitating the evaporation

of heavier isotopes. With distance from the low latitude source moving poleward, ^{18}O is shed via Rayleigh distillation (Schmidt et. al., 2007).

Amount Effect: Isotopic ratios can change, up to 10‰, within the same rainfall event (Rozanski, et. al., 1993). Thus, the volume of rainfall itself forces a strong but averaged isotopic signature into the cave.

The Latitude and amount effects, while problematic for palaeotemperature, has yielded positive results in mapping monsoon variability through long periods (Cheng, et. al., 2016., Wolf et. al., 2020). This is fundamental to the discovery of the '8200-year' cold event, marked by a very large decrease in $\delta^{18}O$, signifying a profound change in precipitation source during the Holocene that has been traced through ice-core records (McDermott et. al., 2001., Baldini et. al., 2002 Jaglan et. al., 2020).

ii. Effects from the Soil and upper-epikarst

After deposition above the cave, rainwater incorporates into vegetation, soil system and epikarst. Storage and mixing here can overprint the $\delta^{18}O_{rainfall}$ signal. This can vary significantly depending on the structural geology above the cave.

Before percolating, evaporation from the soil surface leads to a preferential concentration of ^{18}O, increasing $\delta^{18}O$ independent of temperature (Fairchild & Baker, 2012). Moreover, if the conversion of CO_2 to carbonic acid and carbonate within the soil system is slow, kinetic fractionation can occur between different oxygen species (McConnaughey, 1989).

Speleothems are sourced from heterogeneous flow regimes of primary porosity (matrix flow) or secondary porosity (fracture flow), as opposed to a fast-moving tertiary conduit

(Ford & Williams, 2013). An element of secondary porosity, or at least contact with carbonate materials such as limestone, is required for dissolution and calcite formation (Fairchild & Baker, 2012).

Matrix flow, such as through dense soil or porous karst, is slow, introducing long residence times and a lag between precipitation event and the $\delta^{18}O_{rainfall}$ signal reaching the speleothem (Fairchild & Baker, 2012). This disconnects a $\delta^{18}O_{rainfall}$ temperature signal away from $\delta^{18}O_{calcite}$, by months or decades (Baldini, 2002), acting as a 'low-pass filter' on the palaeotemperature record (Bradley, 2015). For a good resolution palaeotemperature signal, the residence time before precipitation calcite should therefore be at least sub-annual.

Fracture flow translates water faster, making the rates of speleothem formation more in-line with precipitation regimes. This influences a rainfall signature on $\delta^{18}O$, with preferential recharge of ^{16}O into drained aquifers, that overwrites $\delta^{18}O_{rainfall}$ temperature signals (Bar-Mathews et. al., 1996).

Variable storage within the karst aquifer leads to mixing of oxygen isotopes because the ratio of fracture to matrix flow alters (2 % is common; Bradley et. al., 2010), or if it is influenced by storage reservoirs. An Overflow storage reservoir, for example, introduce a fossil water source during times of prolonged precipitation, contaminating the $\delta^{18}O_{rainfall}$ signal (Fairchild & Baker, 2012).

The structure of speleothems is a useful indicator to suggest the flow regime into the cave. For example, large numbers of small speleothems are indicative of matrix flow, straight 'candlestick' speleothems suggest consistent drip rate independent of precipitation events (Bradley et. al., 2010) and wide based speleothems suggest a rapid

fracture based hydrological source (Fairchild & Baker, 2012). This interpretation is however not without issues. For example, it is very difficult to differentiate between the wide-based morphology of a speleothem that has formed from fracture flow Vs. intermittent overflow, as both lead to widening of the speleothem base as excess water runs down the sides (Fairchild & Baker, 2012).

It seems the best method to understand and mitigate these effects is to measure $\delta^{18}O_{rainfall}$ at the surface and $\delta^{18}O_{calcite}$ in parallel over extended periods, effectively tracking the impact of variability (e.g. Bar-Mathews et. al., 1996). Karst hydrological models have been introduced to suggest the controls that are likely to explain this variation (e.g. Bradley et. al., 2010).

iii. Effects in the Lower-epikarst and cave

It is noted that calcite precipitation can start occurring en-route through the epikarst, known as Prior Calcite Precipitation (PCP) (Fairchild et. al., 2000) which has connotations for interpreting speleothem oxygen isotopes, depending on the time until final speleothem formation.

iv. Effects during calcite precipitation

The temperature within the cave environment can be translated into the speleothem during calcite precipitation. However, in deriving a palaeotemperature signal, it is important that $\delta^{18}O_{calcite}$ precipitates in isotopic equilibrium with $\delta^{18}O_{dripwater}$. Kinetic fractionation can occur that makes it impossible to trace a $\delta^{18}O_{dripwater}$ backwards and/or introducing noise to a $\delta^{18}O_{calcite}$ temperature signal. For example, precipitation due to evaporation, rather than CO_2 degassing, causes kinetic fractionation along the growth surface that enriches ^{18}O.

In cool temperate regions caves have high humidity levels, meaning that $\delta^{18}O_{calcite}$ is often in equilibrium with $\delta^{18}O_{dripwater}$ (McDermott, et. al., 2004). Thus, evaporation that would increase kinetic isotope fractionation during calcite precipitation is avoided. In these conditions, $\delta^{18}O$ of source water is the biggest factor on $\delta^{18}O_{calcite}$. However, as conditions within the cave might have changed through time. This is a potential source of error especially in arid regions where evaporative processes occur seasonally (McDermott et. al., 2004).

Hendy tests (Hendy, 1971) can be used to evaluate this degree of fractionation by looking at carbon and oxygen isotopes along the growth layer. If dis-equilibrium existed, and kinetic factors were present, the fluctuations of $\delta^{13}C$ and $\delta^{18}O$ would be similar (Bradley, 2015).

However, Dorale & Liu 2009 point out that the test has its limitations. Fractionation can take place at the flanks of a speleothem growth layer while being at equilibrium in the centre, giving mixed results on a drilling regime following the same growth layer. Moreover, the Hendy test makes assumptions that $\delta^{13}C$ is not linked to climate (Hendy, 1971), whereas $\delta^{13}C$ is directly linked to soil CO_2, because of annual bio-productivity (Hellstrom, et. al., 1998 Fairchild et. al., 2006), which has direct links to seasonal rainfall and temperature (Dorale, et. al., 1998). Isotopic coupling can therefore still occur, but not because of kinetic fractionation. To combat this, looking at spatially separated speleothems within the same cave could be useful in ruling out this site-specific fractionation (McDermott et. al., 2004).

As calcite precipitation is seasonally controlled by pCO_2 in the cave atmosphere, this can introduce a seasonal bias to the $\delta^{18}O$ record. Mindful of the ambiguity thus far,

McDermott et. al., 2004 highlighted the significance of systematic monitoring of present-day drip-waters, to better constrain the mechanisms driving δ^{18}O fluctuations between rainfall, drip waters and speleothems. By studying the complex factors controlling δ^{18}O flux, this should renew understanding of current speleothem palaeo-climate records.

v. Post-depositional change

Once the speleothem has been precipitated, and in the absence of major hydrological events that might cause erosion, the preservation of a δ^{18}O signals is very good. However, particular attention should be made in looking for signs of erosion or diagenesis in the speleothem sample as this will affect the coverage and age model.

2.2.4.2 Clumped Isotopes

Like with foraminifera, clumped isotopic studies are useful as an alternative to the ambiguous $\delta^{18}O_{calcite}$ signal, by removing the unknown $\delta^{18}O_{dripwater}$ as a dependant variable (Ghosh et al., 2006., Bajnai, et.al., 2020). The theory of clumped isotopes is that at lower temperature, where there is less energy in a system, heavier isotopes 'clump together' and the variety of isotopes decreases (Peterson, et.al., 2019). At equilibrium, $\delta^{13}C$ and $\delta^{18}O$ reflects the crystallisation temperature of carbonate formation. Thus, no knowledge of the meteoric palaeo-fluid that the speleothem precipitated from is required to correct $\delta^{18}O$ in isolation (Ghosh et al., 2006).

However, this method is still under the mercy of kinetic fractionation that can occur during calcite precipitation: Kluge et. al., 2014, for example, showed temperature variations of 3-18 °C for the formation of cryogenic carbonates, which should form near to, or at, freezing temperatures. Recently however Bajnai, et.al., 2020 suggests that Δ_{48} and Δ_{47} in conjunction can identify some of these kinetic biases. Peterson et. al., 2019 has made some headway in producing a universal temperature calibration in several carbonate studies, that should streamline future work and solve some interlaboratory error.

2.2.4.3 Magnesium

Unlike its success in marine archives such as foraminifera, Mg/Ca partitioning has a limited use as a palaeothermometer in Speleothems. Magnesium's use in caves was first suggested by Roberts et. al., 1998 from a speleothem sample in Uamh an Tartair, Scotland. However, variation in Mg/Ca was too large to be explained by temperature fractionation alone. It was suggested that that varying residence times, inducing varying PCP, might explain this large variation which overwrites any temperature signal (Roberts

et. al., 1998., Hellstrom et. al., 2000., Drysdale et. al., 2020). It has since been noted that other effects such as incongruent calcite dissolution (ICD), where minor ions are released into solution in preference to Ca during calcite dissolution, and dissolution of Mg rich aragonite/dolomite also contribute to Mg/Ca fractionation independent of temperature (Sinclair et. al., 2011). However, Drysdale et. al., 2020 suggested that the Mg concertation in sub-aqueous speleothems, where PCP is reduced, can track regional SST over the last 350 ka, with Mg increasing in warmer climate intervals.

2.2.4.4 Sulphate

Typically sulphate inclusions are associated with volcanic activity (Frisia et. al., 2008), anthropogenic pollution (Wynn et. al., 2010) and wildfires (Nagra et. al., 2016). However, under certain conditions, sulphate concentrations in speleothems have a relationship with annual temperature-controlled calcite precipitation (Wynn et. al., 2014., Wynn et. al., 2018). In winter the cold dense air outside the cave leads to inward ventilation, freshening the cave air and lowering pCO_2, facilitating the precipitation of carbonate. This increases pH which reduces the ratio of sulphate to carbonate in drip waters (Wynn et. al., 2018). This produces a seasonal cyclicity to sulphate concentrations within speleothems that grow within seasonally ventilated caves. The resolution of the speleothems in Obir Cave, Austria is such that annual cyclicity of sulphate can be seen through the 1970s, thus recording a relative signal of temperature (Wynn et. al., 2014). However, to date, this finding has not been constrained to a degree where it can be used as a quantitative palaeothermometer, but more as a proxy of season duration and severity.

2.2.5 SPELEOTHEM DATING

A reliable palaeotemperature record is only as good as its dating method, both for temporal accuracy and to compare to other datasets. It could be argued that the robustness of speleothem dating is the single most important factor for bringing speleothems into the limelight within the field of palaeoclimate (Hoffmann et. al., 2007., Fairchild & Baker 2012). However, it comes with its caveats.

Stalagmite speleothems grow incrementally upwards from the cave floor, with an ascending chronology. Visible laminae form perpendicular to this time series and can be drilled for dating (Figure 2.3). Growth rate is seldom linear, with variation according to climate events and conditions within the cave (Baldini, 2010). Growth hiatuses, marking a temporary pause in growth, are usually identified by dirt horizons and periods of potential desiccation (Figure 2.3). This usually marks a period when the hydrological source to the speleothem has ceased temporarily, such as a local drought or change in drip location (Fairchild et. al., 2006). Moreover, speleothems can break apart and be reincorporated into new growth, muddling a dataset. Therefore, to produce a temporally accurate palaeoclimate data series an age model must first be created.

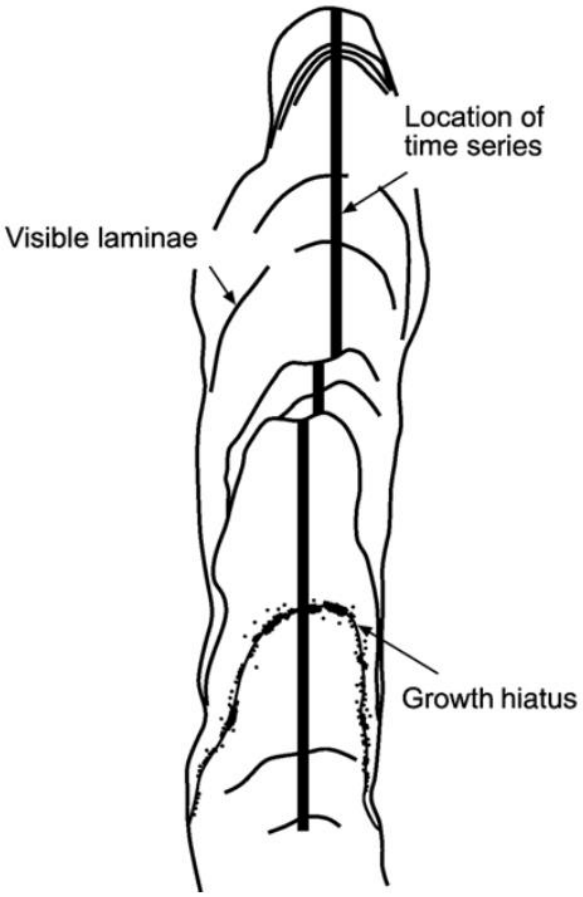

Figure 2.3: A cut and slabbed stalagmite illustrating the relationship of growth features to an ideal time series (Fairchild et. al., 2006).

Somewhat like tree rings, interval dating is particularly useful in showing chronology in caves of rapid and seasonal speleothem growth. Seasonal variation of trace elements, inclusions and fluorescent organic matter produce rhythmic laminae perpendicular to direction of precipitation (e.g. Wynn et. al., 2014). However, while results can be very precise, it is a labour-intensive process to record each lamina quantitatively and a working knowledge of the caves hydrology is required (Fairchild & Baker, 2012). Moreover, irregular precipitation and false banding can introduce bias when trying to construct a linear record on banding alone (e.g. Shen et. al., 2013). Therefore, its real strength lies in complimenting other dating methods.

^{14}C dating was the first method used by researchers to date speleothems (e.g. Geyh, 1970). It however suffers as there are many sources of ^{14}C integrated into the speleothem with varying ages, including the bedrock, overlying soil interactions and cave atmosphere (Fairchild & Baker, 2012). 'Dead Carbon', that has been sitting for long periods, can commonly make up 12-20 % of speleothem calcite (Genty et. al., 2001). However, ^{14}C is particularly useful for modern speleothems post 1960, where a lagged spike in ^{14}C from nuclear testing can be used to date precisely (e.g. Smith, et. al., 2009). Bomb testing with laminae counting can be used to extrapolate an age-depth model further back in time. Hua et. al., 2012, for example, used ^{14}C dating to estimate a chronology for the last 550–750 years as conventional U/Th was too scarce for measurement.

Today, speleothems are primarily dated using U-series ($^{230}Th/^{234}U$). Carbonate rock commonly contains natural uranium minerals, which become coprecipitated as uranyl carbonate as the speleothem forms (Bradley, 2015), effectively locked into a closed system. Normally, speleothems contain no natural ^{230}Th as it is insoluble, getting filtered and absorbed in clay soils or the upper epikarst. The half-life for ^{234}U decay is 245,000 yrs. Thus the decay of ^{234}U to ^{230}Th can give a calendar age in years, up to 640 ka BP (Richards & Dorale, 2003., Cheng et. al., 2016).

Recent improvements in analytical techniques (TIMS, MC-ICP-MS) allow more precise $^{230}Th/^{234}U$-ages to be obtained (Cheng et. al., 2013), now within 1σ of <1 to 0.1% variation (Shen et. al., 2012), from much smaller sample sizes: <100 mg of calcite (Bradley, 2015). As such, speleothems have since been used to correct the timing

discrepancies in ice core records, where $\delta^{18}O$ can be cross-correlated (e.g. Cheng et. al., 2016).

However, the technique still comes with its own set of issues. It is possible that detrital Th can get incorporated into the speleothem, leading to 'age reversals' that can often be difficult to distinguish from natural ^{234}U decay (Fairchild & Baker, 2012). This is particular across growth hiatuses (Figure 2.3) or episodes of sediment wash-in. $^{230}Th/^{232}Th$ ratios less than 300 is suggested to demonstrate a speleothem sample is 'clean from detrital components, requiring low levels of age correction (Hellstrom, 2006), however the flux of $^{230}Th/^{232}Th$ may not be linear through time. U-series dating also assumes decay under a 'closed-system'. Weathering and subsequent calcite re-formation, or aragonite to calcite recrystallization, can allow the sequestration of contemporary radioisotopic material (Richards & Doyle 2003). Moreover, ^{234}U concentrations can simply be too low in the speleothem to date them (as experienced with Hua et. al., 2012).

Given the age of many speleothems, a considerable interest has been put into U-Pb dating beyond 640 ka (Woodhead et. al., 2012). This can theoretically date back millions to billions of years. Again, detrital Pb and U incorporated into the speleothem is the biggest factor in misinterpretation (Porcelli & Swarzenski, 2003).

Since the spatial resolution of dated points on the speleothem is usually lower than that of proxy sampling regime, the age between two adjacent dated points needs to be estimated. This is acquired by calculating a relationship between determined ages along the speleothem growth axis and the distance of a proxy result along the same axis. This relationship is usually referred to as an 'age-depth model' (Scholz et. al., 2012). Several

algorithms have been designed (StalAge, Oxcal) and databases created (SISAL v2) to streamline a consistent process of U-series age modelling, to allow collaborative cross-comparison of data, and to better account for irregularities such as age reversals and hiatus events (Comas-Bru et. al., 2020).

2.2.6 SUMMARY

As discussed, to date there is still not a convincing terrestrial 'palaeothermometer' that can be interpreted without ambiguity. Each proxy is influenced by a myriad of effects independent to temperature. $\delta^{18}O_{calcite}$, for example, is influenced by the $\delta^{18}O$ of the palaeo-fluid from which the carbonate precipitated, itself influenced by changes in atmospheric circulation, storm events and the source of moisture (Spandin et.al., 2015), fractionation away from equilibrium during the precipitation process (Bajnai et. al., 2020), pCO_2 levels and humidity changes in the cave and epikarst (Schwarcz, 1986), temperature inside the cave at the time (McDermott et.al., 2011) and erosional or diagenetic processes (Fairchild et. al., 2006). Similar effects exist for all terrestrial and marine palaeotemperature records.

To combat this, the literature has been moving towards aligning several proxy archives to rule out idiosyncrasies (Dwyer & Chandler, 2008., Zhang et al., 2010., de Boer et al., 2014., Svendsen et al., 2014., Hernández, et.al., 2020) and developing methods such as clumped isotope thermometry (Henkes, et.al., 2018 ., Bajnai, et.al., 2020). However, Blaauw 2010 and Hernandez et.al., 2020 outline the dangers and potential conflicts faced when trying to align different proxy archives due to circular reasoning, calibration not being fully explored to a range of climatic behaviours, and unrecognised chronological uncertainties.

It remains that these factors hamper efforts to develop a coherent picture of site-specific palaeotemperature. As such, a shift in the literature has moved towards more 'attainable' goals of revealing the consequences of major climate events where changes in temperature are significant and can easily be correlated to more established

geological records. This includes glacial-interglacial cycles (Spötl et.al., 2002), D/O events (Spötl & Mangini, 2002), Milankovitch Cycles (Zhao et. al., 2001, Webb et. al., 2014), and mass extinction events (Li et. al., 2020). Spötl et.al., 2002, for example, demonstrated a high $\delta^{18}O$ signal in a cave speleothem from the Austrian Alps that corresponds with the MIS 5e interstadial event highlighted through ice-core records on the Greenland Ice Sheet and Zhao et.al., 2001 tracked the duration of the MIS 5e interstadial based on data from a Tasmanian stalagmite, showing a global relationship driven by the Milankovitch cycle.

Despite this, outside the polar regions only speleothems have the potential to hold a terrestrial proxy record over multiple glacial-interglacial cycles. Moreover, speleothems benefit from long potential chronologies (McDermott et. al., 2004) and robust radioisotope dating methods with precision that outshines current ice-core chronology (Fairchild & Baker, 2012), even being used to correct it (e.g. Cheng et. al., 2016). The stability of cave air temperature, and its relationship to mean external temperature (McDermott et. al., 2004., Fairchild, et. al., 2006), is significant because, if a palaeotemperature signal can be constrained at point of calcite precipitation, this could provide a very stable record for local annual temperature over long periods.

Thus, it remains that there is value in pushing every avenue in assessing potential palaeotemperature proxies within speleothems, either to reinforce other methodologies, such as $\delta^{18}O_{calcite}$, or in the quest for an unambiguous palaeothermometer.

2.3 PHOSPHATE & BIOGEOCHEMISTRY OF THE PHOSPHORUS CYCLE

Phosphorus (P) is naturally found in the environment from the weathering and leaching of P-rich minerals such as apatite. This gets tightly cycled by plants and microbes as well as absorbed into the soil matrix (Fairchild & Baker, 2012). This is because phosphorus is a key component for microorganisms and is essential to life, acting as a limiting nutrient in aquatic and soil environments (Blake et. al., 2005). As such, P is fundamental in making a large proportion of planktonic biomass.

2.3.1 PHOSPHORUS CYCLE

In soils phosphorus is found in many organic (e.g., humic acids) and inorganic forms (e.g., orthophosphate), getting assimilated by these organisms and released back into the soil matter as they decay (George et. al., 2018). Inorganic forms can be more accessible the smaller and less-bonded they are, becoming less accessible if co-precipitated in minerals such as carbonate or metal-rich clays. Both processes are driven by enzyme activity in microbes as they break down the larger organic matter into smaller units including orthophosphate (George et. al., 2018). *Mycorrhiza sp.*, for example, is a symbiotic fungus that aids complex-P breakdown and uptake for plants (Barman et. al., 2016).

Through surface runoff or soil percolation, phosphorus moves through natural waters as dissolved inorganic orthophosphate (P_i), the primary form of P cycled through ecosystems (Nisbeth et. al., 2019), or as P-rich particulates, such as colloids, in inorganic and organic forms (Figure 2.4). In solution, some of this phosphate can flow into karst systems where it can be co-precipitated into speleothem calcite (Fairchild & Baker,

2012). Eventually, the majority of phosphate stores will terminate in ocean biomass and subsequent deposition.

However, if released into the environment in excess, P can induce algal blooms and incidentally facilitate eutrophication and anoxia in lakes, rivers and streams (Schlinder, 1974., Blake et. al., 2005., Lin & Singer, 2006). This is commonly associated with the over-application and poor management of agricultural fertilisers, which can be split into organic (manure) and inorganic (chemical) varieties. Excess P can also leach from septic tanks and wastewater treatment plants (Nisbeth et. al., 2019).

For this reason, the presence of arable land and use of fertilisers has transformed natural P budgets globally (Sharpley & Rekolainen, 1997). Fertilisers are added to boost crop yield as plant growth is typically limited by P in the soil (George et. al., 2018). The study of P is therefore important from the perspective of food security, environmental pollution and drinking water quality (George et. al., 2018., Nisbeth et. al., 2019). As cave systems act as natural ‘sinks’, this is something that could be evaluated through the speleothem archive.

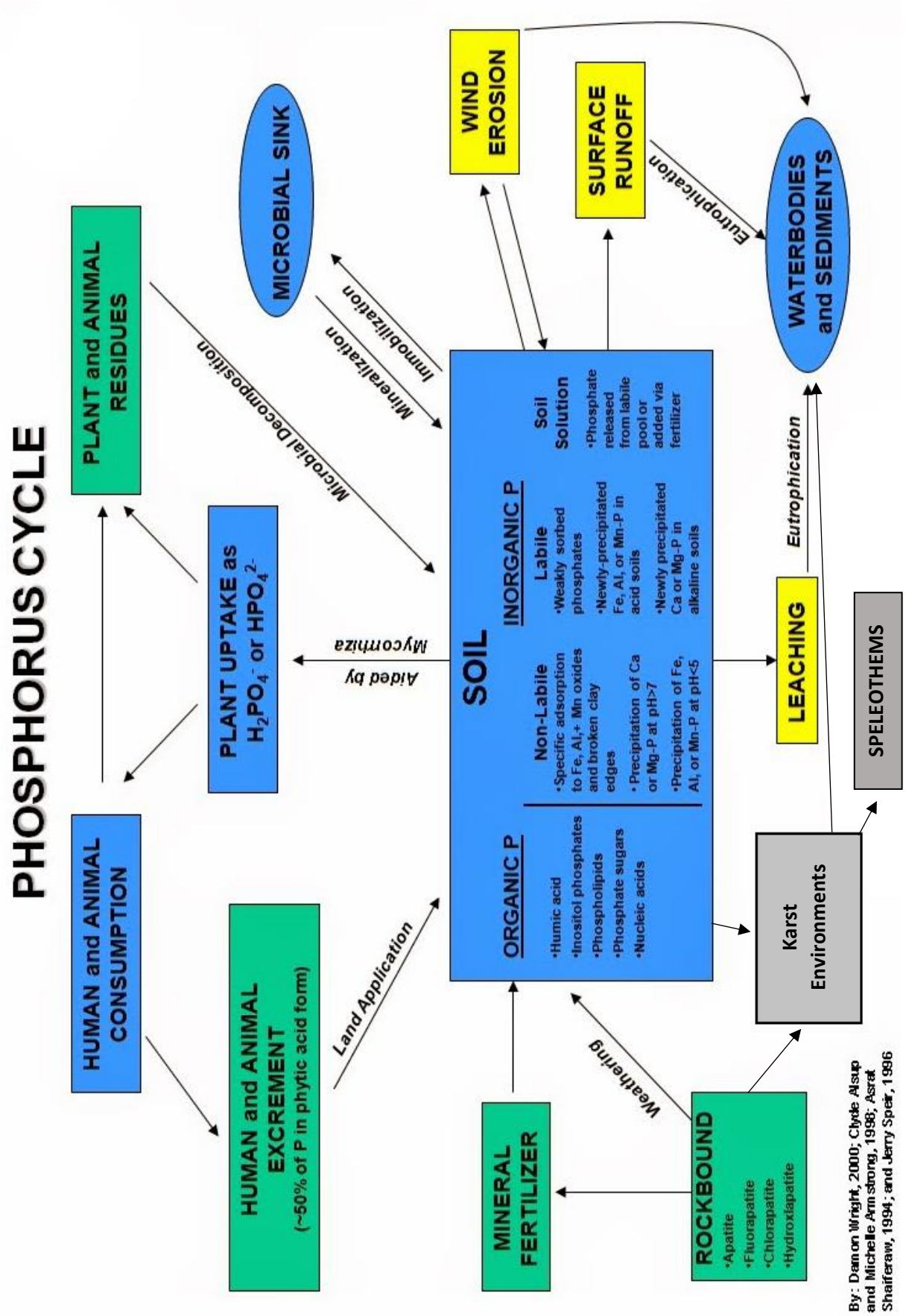

Figure 2.2: Summary of the phosphorus biogeochemical cycle (adapted, Damon Wright, 2000).

2.3.2 SPELEOTHEM PHOSPHORUS CYCLE

Upon percolating into caves, P has been found to incorporate into speleothems both as individual ions co-precipitating in the calcite lattice and as humic P-rich colloidal inclusions (Frisia et. al., 2012), highlighted through organic fluorescing layers at the sub-annual scale (Huang et. al., 2001, Borsato et. al., 2007). $CaHPO_4$ orthophosphate has been shown to compete and inhibit calcite growth, depending on pH, by blocking crystal-growth sites (Lin & Singer, 2006), with 10^{-6} molar concentrations reducing calcite formation by as much as 50 % (Fairchild & Baker, 2012).

Phosphate inclusion in speleothems has historically been viewed as a largely inorganic process, with annual cycles of high-P concentration as an indicator of autumnal flushing events from the surface, to around 80-1700 ppm (Heathwaite, 1997) and 130 ppm (Huang et. al., 2001), following vegetation die-back and increased seasonal rainfall. For example, increased P/Ca ratios in modern speleothems suggests a relationship to increased rainfall and erosion in Western Australia (Trebel et. al., 2003., Lewis et. al., 2011). In the summer, inorganic P is mediated by microbes and held in vegetation which acts as a P-reservoir (Sharpley & Rekolainen, 1997). Frisia et. al., 2012 suggests that P-rich phases seem to co-precipitate with calcite at times of low prior calcite precipitation (PCP), correlated to low CO_2 and high rainfall. Huang et. al., 2001 suggests that the vegetation P-reservoir is opened in autumn/winter as vegetation dies back, aided by freeze-thaw action (Fairchild & Baker et. al., 2001).

However, growing evidence suggests significant microbial mediation of speleothem calcite within the cave itself. For example, stromatolite morphologies, which are a consequence of bacterial action, were found in the Italian Alps (Frisia & Borsato, 2010)

and Spain (Rossi et. al., 2010). This also includes evidence of phosphate inclusion (e.g. Chang et. al., 2010, Frisia et. al., 2012).

Initially, this discovery of biotic phosphate mediation raised scepticism at the efficacy of phosphate as an environmental indicator (e.g. Jones, 2009), as microbes were known to drive non-equilibrium partitioning (Warren et. al., 2001). However, these concerns were notably disregarded in later literature (e.g. Fairchild & Baker, 2012., Frisia et. al., 2012) as phosphate trends show clear seasonal forcing through P/Ca ratios.

2.3.3 ORTHOPHOSPHATE OXYGEN ISOTOPES ($\delta^{18}O_{PO4}$)

The use of trace elements as palaeoclimate and ecosystem process indicators has only gained traction through the past 20-years, partly motivated by the caveats of other methods previously discussed (e.g. Hellstrom & McCulloch 2000., Chang et. al., 2010., Griffiths et. al., 2010). Whilst the biogeochemical cycles of many elements through soil and karst systems have been studied (e.g., carbon, nitrogen, and sulphate), the biochemical cycling of P is less well understood. This is largely because only one stable isotope (^{31}P) exists in nature (Shen, et. al., 2020) and P primarily being in non-specific forms of orthophosphate that are hard to trace to origin (Blake et. al., 2005).

However, P in nature is strongly bound to oxygen which has 2 major stable isotopes (Blake et. al., 1997., McLaughin et. al., 2004). Thus, the stable oxygen isotopes within orthophosphate ($\delta^{18}O_{PO4}$) have been suggested as a biochemical tracer and palaeotemperature indicator. This is because $\delta^{18}O_{PO4}$ seems to be fractionated readily by biotic enzyme processes that map biochemical cycling (Shen et. al., 2020) and transform $\delta^{18}O_{PO4}$ in equilibrium with water temperature (Blake et. al., 2005).

Once oxygen is incorporated into phosphate, it is resistant to inorganic hydrolysis with change in temperature or pH in aquatic ecosystems between 3-37 °C (Chang & Blake, 2015). As such the $\delta^{18}O_{PO4}$ signal is maintained and well preserved (Smith et. al., 2021). This has transformed understanding of phosphate cycling by allowing differentiation between phosphate species (Shen et. al., 2020). For example, it has been used to trace sources and cycling in lakes (Young et. al., 2009) and an estuary affected by fertiliser input (McLaughlin et. al., 2006).

Originally, $\delta^{18}O_{PO4}$ was popular in the archaeological and marine biology fields in using the variation of oxygen species within biogenic appetite to infer environmental conditions for the growth of bone, teeth or shells (Longinelli and Nuti, 1973., Luz et. al., 1985). For example, using $\delta^{18}O_{PO4}$ from the tooth enamel of small rodents to calculate mean palaeotemperatures from the Quaternary (Koch et. al., 1995., Grimes et. al., 2004). $\delta^{18}O_{PO4}$ has also been used to trace phosphate sources and cycling in lakes (Young et. al., 2009), it has more recently been trialled as a DNA 'biothermometer' (Blake et. al., 2016) and is a suggested proxy for Martian microbial activity (Shen et. al., 2020).

However, the isotopic equilibrium of oxygen species between phosphate and source waters by the intracellular enzyme pyrophosphatase (PPase) has recently come into its own significance showing promise as a 'biothermometer'. This has been observed in lab cultures (Blake et. al., 1997, 2005), in seawater (Coleman et. al., 2005), groundwater (Blake et. al., 2001), sedimentary authigenic apatite (Jaisi & Blake, 2010), soils (Tamburini et. al., 2012) and bat guano within cave environments (Chang et. al., 2010).

2.3.4 PHOSPHORUS BIOGEOCHEMISTRY

Assimilated by microbial enzymes, the P-O covalent bond within phosphate is a critical component to ATP energy production: ubiquitous to all cellular life. P also forms the sugar-phosphate backbone of DNA/RNA and the phospholipid-bilayer of cell walls (George et. al., 2018). There is linkage between P and the cycling of carbon, which has a requirement for orthophosphate to function (Maloney, 1992). Nitrogen fixation requires P, with the possibility of N-cycling becoming P-limited (Krom et. al., 2004).

The preferred form of phosphate for cells to metabolise is dissolved inorganic orthophosphate (P_i, PO_4^{3-}) as it is capable of diffusion across cytoplasmic membranes (Liang & Blake, 2006). However, the concentrations of P_i are low in nature (Chang et. al., 2010). For example, Huang et. al., 2001 found 7 and 3 µg/L P in soil and cave waters respectively, suggesting microbiological scavenging of P is taking place from elsewhere (Fairchild & Baker, 2012). As such, microorganisms generate P_i through enzyme degradation of organic-P (P_{org}), naturally abundant in many soil environments, or the dissolution of mineral deposits such as phosphorites and apatite (Chang et. al., 2010).

These enzymes can be broken into extracellular and intracellular forms:

2.3.4.1 EXTRACELLULAR ALKALINE PHOSPHATASE (APASE)

Phosphohydrolases, such as alkaline phosphatase (APase), catalyse the hydrolysis of phosphorester bonds in P_{org}. This takes place outside of the cell or within the periplasmic space outside the cell wall (Blake et. al., 2005). With the addition of water, APase hydrolyses large P_{org} compounds, such as waste sugar-PO_4 and lysed DNA/RNA, into more manageable P_i for consumption within the water column. P_i is then able to enter the cell via diffusion or facilitated transport (Maloney et. al., 1992). However, cells have

varying aptitudes to this function that depends on the species and environment, making it less ubiquitous (Blake et. al., 2005). These enzymes can account for potential negative fractionation of -25‰, (Liang & Blake, 2006., Shen et. al., 2020) but function less profoundly compared to intracellular enzymes (Blake et. al., 2005).

2.3.4.2 INTRACELLULAR ENZYMES

Once inside the cell, P_i is utilised in the aforementioned metabolic processes catalysed by enzymes (Blake et. al., 2005).

Shen et. al., 2020 showed that by looking at the divergence of $\delta^{18}O_{PO4}$ between soil and the igneous bedrock, that enzymes such as DNase (-25‰) RNase (-5‰) and 5'-nucleotidase (-10‰) account for negative isotopic fractionations.

2.3.4.3 Intracellular pyrophosphatase (PPase)

Intracellular pyrophosphatase (PPase) enzymes are ubiquitous to all cellular life, catalysing the hydrolysis of inorganic pyrophosphate (PPi), the product of ATP (adenosine triphosphate) hydrolysis, and water into forms of P_i (Chang & Blake 2015):

$$H_2P_2O_7^{2-} + H_2O_{\text{dripwater}} \xrightarrow{\text{PPase}} 2HPO_4^{2-} + 2H^+$$

The process is rapid and highly exergonic, producing a secondary energy source for cell function after ATP. It is noted that PPase, as a metalloprotease, requires adequate Mg^{2+} concentration for maximal activity (Chang & Blake 2015).

Significantly, enzyme hydrolysis exchanges all four O-atoms from water into phosphate, generating the $\delta^{18}O$ equilibrium observed between P_i in bones, teeth, and shells to the surrounding water (Longinelli and Nuti, 1973., Luz et. al., 1985). Hydrolysis by PPase is a

significant player in this fact and is thought to be a credible 'biothermometer' (Chang & Blake, 2015).

The resulting Pi is then released back into the extracellular environment under two mechanisms (Figure 2.5). Either released as a by-product to maintain non-toxic intracellular P concentrations or following cell lysis/death (Davies et. al., 2014).

The mechanism of these metabolic processes, and isotopic effects, on P_i can be summarised below with a diagram from Davies et. al., 2014.

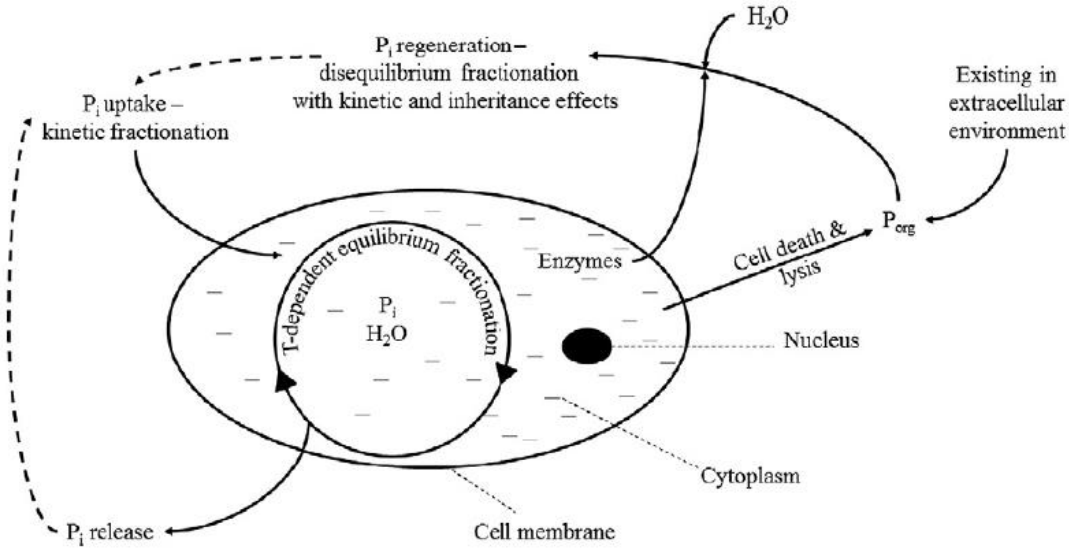

Figure 2.3: Schematic diagram describing the major isotope effects that can occur within the intracellular or extracellular environment due to metabolic processes. P_{org} = organic P compounds; P_i = dissolved inorganic phosphate ion; H_2O = water molecule, T= temperature. (Davies et. al., 2014).

2.3.5 THE PPASE $\delta^{18}O_{PO4}$ 'BIOTHERMOMETER'

The hydrolysis of water by PPase is significant as it forces the fractionation of oxygen species, from the water into stable P_i, as a function of temperature. This effectively translates the $\delta^{18}O$ signature into phosphate: $\delta^{18}O_{PO4}$ (Blake et. al., 1997., Blake et. al., 2005., Chang et. al., 2010., Tamburini et. al., 2012., Davies et. al., 2014).

For apatite, the relationship between $\delta^{18}O_{PO4}$ and temperature has been calculated as follows (Longinelli & Nuti, 1973., McLaughin et. al., 2004) (Equation 2.i):

$$\mathrm{T(°C)} = 111.4 - 4.3(\delta^{18}\mathrm{O_P} - \delta^{18}\mathrm{O_{H2O}}) \quad \text{(2.i)}$$

A refinement of this equation was made by Pucéat et al. (2010) following improvements in P_i purification methods (Davies et. asl., 2014) (Equation 2.ii):

$$\mathrm{T(°C)} = 118.7\ (\pm 4.9) - 4.3(\pm 0.20)(\delta^{18}\mathrm{O_P} - \delta^{18}\mathrm{O_{H2O}}) \quad \text{(2.ii)}$$

Alternatively, if at thermodynamic equilibrium, Chang & Blake 2015 calculated the relationship between $\delta^{18}O_{PO4}$ and temperatures between 3 and 37 °C by PPase as Equation 2.iii (r^2 = 0.99):

$$1000 \ln \alpha_{PO4-H2O)} = 14.43(\mp 0.39)\frac{1000}{\mathrm{T(K)}} - 26.54\ (\mp 1.33) \quad \text{(2.iii)}$$

This equation has been reformulated by Pistocchi et. al., 2017 (2.iv) and subsequently Smith et. al., 2021 (2.v) for different applications:

$$\text{(2.iv)} \quad \delta^{18}\mathrm{O_P} = (\delta^{18}\mathrm{O_{H2O}} + 10^3) \times \mathrm{e}^{\frac{\left[\left(14.43\times\frac{10^3}{\mathrm{T(K)}}\right)-26.54\right]}{10^3}} - 10^3$$

$$\text{(2.v)} \quad \delta^{18}\mathrm{O_P} = -0.18\mathrm{T(°C)} + 26.3 + \delta^{18}\mathrm{O_{H2O}}$$

The equation for Chang & Blake 2015 can be rearranged for temperature (°C) as Equation 2.vi:

$$\mathrm{T(°C)} = \left(\frac{14430}{1000Ln\propto(PO_4-H_2\mathrm{O})+26.54}\right) - 273.15 \quad \text{(2.vi)}$$

Under this mechanism by PPase, any previous $\delta^{18}O_{PO4}$ signal, such as the phosphate source, is effectively overwritten and replaced it with an isotopic signature of temperature (Chang et. al., 2010 Tamburini et. al., 2012). This includes any kinetic fractionation that might have taken place during the initial uptake of Pi into the cell (Davies et. al., 2014). Importantly, excess P_i is exchanged between the intracellular-extracellular environment during cell growth or released following death/lysis (Blake et. al., 2005) releasing it into the water column. The function of PPase imprinting a temperature signal in expelled P_i, through hydrolysis and oxygen isotope exchange, forms the basis of this dissertation.

The rate of PPase hydrolysis is proportional to pH, temperature, the concentration of orthophosphate and the access to Mg^{2+} (Kunitz, 1952). Optimal enzyme function is at 40 °C (Kunitz, 1952) allowing complete equilibration in less than 14 hours (Chang & Blake, 2015), with equilibration taking 3-5 days at 2.5 °C (Chang & Blake, 2015). It is noted that the data of Chang & Blake, 2015 shows signs that equilibrium was not quite reached by the end of the 5-day period at 2.5 °C.

It is likely that any $\delta^{18}O_{PO4}$ temperature fractionation signal is a mixture of intracellular and extracellular enzymes (Blake et. al., 2005) which may be impacted by other external effects. The physical action of bacterial uptake of P by *Escherichia coli*, for example, can fractionate $\delta^{18}O_{PO4}$ by -3‰, showing an uptake preference for the lighter isotopologue through kinetic fractionation (Blake et. al., 2005). However, acting in the case for PPase,

Cohn., 1953 observed that PPase is a highly reversable reaction, meaning that the forward and back reactions are likely to rapidly enforce isotopic equilibrium between P_i and water (Blake et. al., 2005). This is contrast to APase which is strongly unidirectional and likely to suffer from kinetic fractionation away from temperature dependant equilibrium at a slower rate (Blake et. al., 2005). However, the profound action of PPase is likely to overwrite any conflicting fractionation mechanisms or signatures (Davies et. al., 2014), including APase.

In normal soil environments, orthophosphate P has shown to be turned over on timescales from seconds to minutes, oxide-bound P is recycled on weekly to monthly timescales, and Ca-bound P over years to millennia (Helfenstein et al., 2020., Shen et. al., 2020). Therefore, there is a hierarchy of bioavailability of P for PPase in microbes, with Ca-bound P being the least bioavailable (Shen et. al., 2020).

It is noted that if temperature dependant exchange by PPase is taking place, sample storage is important. If the sample is removed from a cave, for example, the PPase enzymes in the water might re-equilibrate with the temperature of the new environment such as a fridge or lab (Blake et. al., 2005). This was a particular problem for Longinelli et. al., 1976 as the collected samples were not originally intended for isotope analysis. Freezing the sample would halt the process but might lyse cells, introducing contamination of unequilibrated $\delta^{18}O_{PO4}$. This is not an issue for digested Total-P analysis but would be for dissolved orthophosphate. The addition of bactericides might introduce a new source of contamination.

2.3.6 SPELEOTHEM $\delta^{18}O_{PO4}$

In cave environments, it is known that P_i can precipitate within calcite that coats speleothems as it forms, therefore preserving a theoretical palaeotemperature record if PPase enzyme function continues. Chang et. al., 2010 found that the $\delta^{18}O_{PO4}$ of hydroxylapatite, a microbially mediated phosphate rich karst mineral from bat guano, was isotopically identical to cave drip water (+14.6 to +15.6‰) and matched the expected $\delta^{18}O_{PO4}$ for mean cave temperature. The previous $\delta^{18}O$ signal of +21.4‰ from the guano was effectively overwritten by a drop of -6‰ (Chang et. al., 2010., Smith et. al., 2021). PPase function in the microbially rich environment was the suspected driver of isotopic equilibrium. It remains to be seen however if this effect can be translated and preserved in speleothem calcite under the P-inclusion mechanisms.

This hypothesis is significant as $\delta^{18}O_{PO4}$ fractionation is taking place in a known location, be it the overlying soil, epikarst or within the cave itself. As $\delta^{18}O$ is being fractionated and 'locked in' at a much later stage, this effectively bypasses the issues associated with conventional $\delta^{18}O_{calcite}$ palaeothermometry, which is at the mercy of numerous environmental effects. P-calcite minerals are very resistant to abiotic breakdown, meaning that any isotopic signature is then long lived (Shen et. al., 2020). Conversely, a lack of PPase activity but presence of P_i in drip water is also informative as this could indicate an efficacy of speleothems to record soil $\delta^{18}O_{PO4}$ temperature fractionation.

At typical cave temperatures, P_i is inert and does not readily exchange oxygen with water without enzymes (Blake et. al., 1997). Therefore, any temperature dependant fractionation between P_i and water is likely to be microbially mediated and gets well preserved.

2.3.7 EXTRACTION METHODS FOR $\delta^{18}O_{PO4}$

Historically, $\delta^{18}O_{PO4}$ was determined through fluorination (Crowson et. al., 1991) or bromination ($BiPO_4$) of the phosphate precipitate (Longinelli & Nuti, 1973). However, both required large samples sizes, significant preparation before isotopic analysis and suffer from hygroscopic contamination (Nisbeth, et. al., 2019). More recently, silver(I) phosphate (Ag_3PO_4) methods (Tamburini et. al., 2010) have been selected due to Ag_3PO_4 being less hygroscopic, more structurally stable, less soluble and yielding more O in a shorter preparation time (Nisbeth et. al., 2019). Moreover, the Ag_3PO_4 precipitation method benefits samples which have low P_i concentrations (Nisbeth et. al., 2019).

A major challenge for this method is removing any oxygen sources other than P_i that might contaminate $\delta^{18}O_{PO4}$ away from isotopic equilibrium with the source water (Tamburini et al., 2010). Dissolved organic matter (DOM) is of particular concern due to its high O content that can persist through all steps to Ag_3PO_4 precipitation (Nisbeth et. al., 2019). Other common oxygen sources include silver nitrate contamination (Pistocchi et. al., 2017). Potential methods to mitigate this include:

i. Adsorption of DOM to a resin such as DAX-8 (Tamburini et. al., 2010).

ii. Repetition of the MagIC step with the intention of further isolation of P_i from a matrix with potential contaminants (Goldhammer et al., 2011).

iii. Acidified pH-specific precipitations of fulvic and/or humic acids (Zohar et. al., 2010).

iv. Sequential precipitation and re-crystallization scheme to efficiently scavenge P_i (Tamburini et al., 2010).

v. A final washing of the Ag_3PO_4 precipitate with hydrogen peroxide to eliminate residual organic matter by oxidation (Tamburini et. al., 2010).

vi. Checking isotope data for peaks in blanks, consistent with contaminants such as silver nitrate.

However, this method suffers from the fact that large volumes of freshwater (1000 L) are often needed to yield enough phosphorus (20 µmol) for enough silver phosphate (300 µg) for isotope analysis (Nisbeth, et. al., 2019). Moreover, resisting the loss of PO_4 through the various filtration steps to remover DOM, cation/anions, and metals, is a technically challenge as these contaminants often far outnumber PO_4 (Liu et. al., 2021).

As such, new methods are continuously being sought after that are more robust, reliable, and efficient. A recent paper has shown some success in using Zr-Oxide gels, a variation on Diffusive Gradients in Thin-films (DGT) (Davidson & Zhang, 1994), to extract phosphate directly from the water column (Liu et. al., 2021). The method known as *In Situ Enrichment, Elution and Purification* (ISEEP) benefits from its simplicity of sampling, high recovery rate of PO_4 (92.8 %), high removal of DOM/cation/anion contaminants (99.7 %) and robust recovery of $\delta^{18}O_{PO4}$ signals comparable to the McLaughlin, 2004 method (Liu et. al., 2021). The gels 'selectively' extract phosphate, precipitating $CePO_4$ and processed to Ag_3PO_4 for isotopic analysis.

However, a caveat here for alkaline waters is that PO_4 absorption by zirconium hydroxide is a reversable reaction. In conditions pH >10 the back-reaction is favoured, eluting PO_4 back into the water column and therefore limiting the extractable fraction (Liu et. al., 2021). For this reason, the method would be unfavourable for the drip waters in Poole's Cavern.

3 – METHODOLOGY

3.1 POOLE'S CAVERN SITE DESCRIPTION

Poole's Cavern, a public show-cave in Buxton (Derbyshire), is a shallow epigenetic cave made of early Carboniferous and Bee Low limestone (Hartland, 2010). It strikes N-S with a total length of 240m (Figure 3.1), with the main passage terminated by a partially cemented boulder choke (Rowberry et. al., 2020., Deakin et. al., 1968).

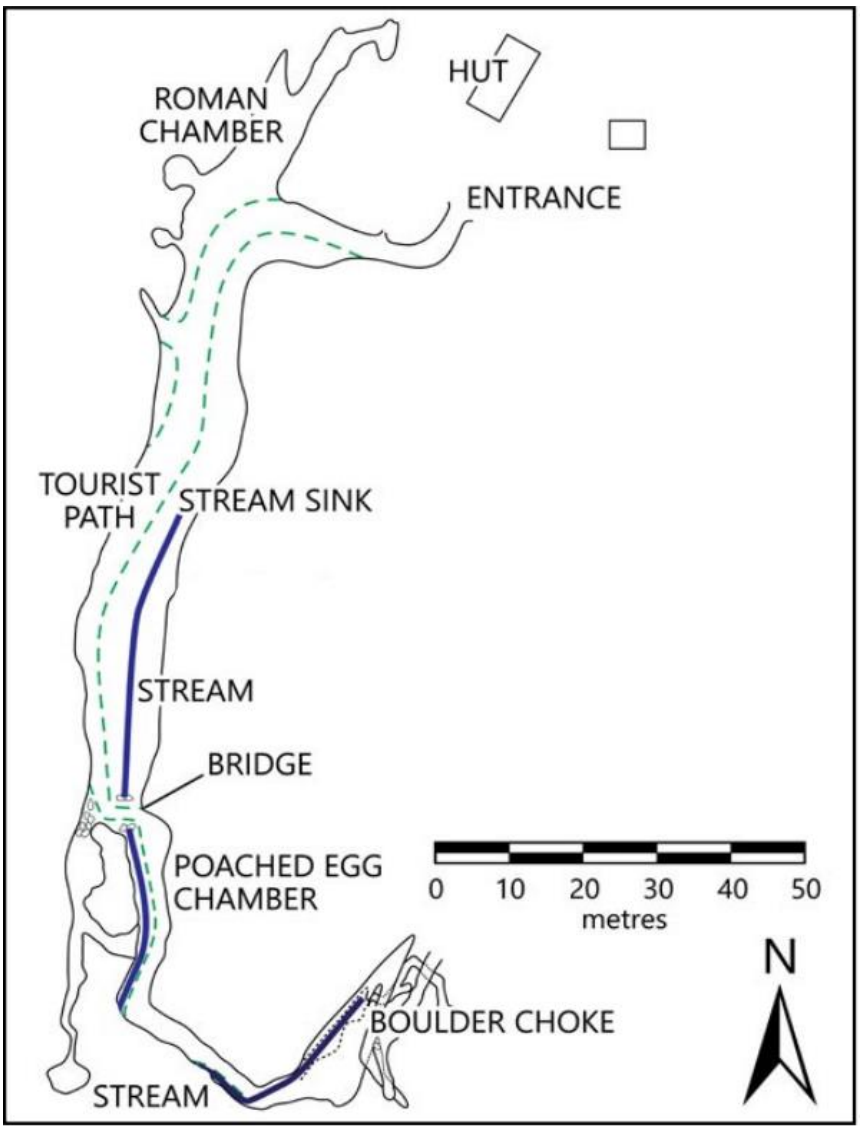

Figure 3.1: Plan of Poole's Cavern (from Rowberry et. al., 2020).

3.1.1 Vegetation & Soil

The cave resides below the deciduous woodland of Grin Low Wood, which was reclaimed and planted following use as a site of lime production in the 19th century. The soil above Poole's Cavern consists of leaf litter and a thin (10 cm), but organic rich, topsoil (Hartland, 2010). Lime-kiln waste is close to the surface (30 cm), as with other sites in the immediate area (Charles et. al., 2015), confirmed by soil sampling. As the CaO and carbonate enriched waters are exposed to air, tufa deposits rich in metal hydroxides can form near the surface. Soil pH in these regions is about 12.3 (Burke et. al., 2012).

3.1.2 Local hyperalkaline biogeochemistry

Within local soils, there is some evidence for distinct hyperalkaline microbial communities. Burke et. al., 2012 has profiled a distinct obligate, anaerobic alkaliphilic community in the lime kiln deposits in Buxton. Following a decreasing redox potential with soil depth, the soil horizon stratifies microbial nitrate reduction over microbial iron reduction with increasing anoxia. This is typical for most soil communities, where energy production becomes less favourable with depth. There is no change on sulphates, suggesting a lack of sulphate reducing bacteria. The dominant community seems to be *Comamonadaceae sp.* that taps into soil organic matter.

A later study, Charles et. al., (2015), looked at harnessing a microcosm of these microbes to treat hyperalkaline nuclear-power waste by digesting isosaccharinic acid, produced from waste cellulose breaking down at high-pH (Basil et. al., 2015). This has since been trialled and deployed in nuclear power stations (Basil et. al., 2020). He found evidence of *Clostrida* forming biofilms as a protective mechanism, to stabilise the community

against high pH. *Clostridium formicaceticum* seemed to be the dominant species, exhibiting hydrogen respiration and methanogenesis. The bacteria utilise extracellular polysaccharides and transport proteins to maintain a neutral cytoplasmic pH, protecting against the external environment (Burke et. al., 2012).

There is also evidence of communities surviving in a non-karst hyperalkaline spring in Buxton. Smith et. al., 2016 sequenced the community in pH 7.3 to 13 waters. At pH 13, the sequence library was dominated by *Gammaproteobacteria* of the families *Pseudomonadaceae* and *Enterobacteriaceae*, with low overall diversity. Fe(III) was not respired under these conditions, but was at lower pH. At pH 13 microbes were likely 'surviving' and not metabolising effectively. Fe(III) reduction and sulfate reduction was exhibited at pH 11.4, and the communities were able to colonise porous sandstone in a column experiment. This suggests that communities can survive in a hypothetical karst aquifer and are able to function between pH 11 and 12.

Importantly, there seems to be some evidence that a 'cave' or 'karst aquifer' community exists in Poole's Cavern itself. Blyth et. al., (2014) conducted a study looking at glycerol dialkyl glycerol tetraethers (GDGTs), biomarker lipids for certain microbes, as a potential TEX_{86} palaeothermometer. Evidence shows two distinct profiles between the subsurface soils above the cave and in the PE speleothem drip waters. The drip waters are dominated by branched GDGTs, suggesting a bacterial source and the soils are dominated by isoprenoid GDGTs, suggesting an aquatic archaea source. This difference suggests evidence of in-situ production within the cave, or within the overlying karst vadose zone. Considering the high calcite precipitation rates in PE, this puts a greater precedence on a vadose/epikarst community existing at Poole's Cavern.

3.1.3 In-cave speleothems

Roman Chamber (RC), named after its archaeological findings (Bramwell et. al., 1983), is nearer to the entrance and host to numerous speleothems, including stalactite straws, stalagmites, flowstones, and columns (Rowberry et. al., 2020). The drip waters here are of mild alkalinity, typical of UK caves, constituting more typical speleothem formations. Smithson, 1991 investigated internal Vs. external temperatures at the site, whereas Smithson, 1993 investigated vertical temperature gradients. It was found that the cave largely has a uniform temperature, close to mean annual temperature, and that temperature increases with height. Temperature is most uniform in summer, whereas the lower or entrance regions can get substantially colder in winter. When it is very warm outside, it is possible for warm air to get above the cold/dense outflow of air coming out the cave. This leads to a significant rise in temperature at upper parts of the cave such as RC (Smithson, 1993). TinyTag loggers within the cave now provide a continuous dataset to review these effects (cave-science.org.uk).

Poached Egg (PE) Chamber, so named due to several unusual stalagmites with bright orange tops (Newton et. al., 2015), is found towards the south end of the cave (Figure 3.2). Here, calcite precipitation is dominated by hyperalkaline waters (pH 10-13), seeded by 19th century lime waste deposits in Grin Low Wood above the cave (Hartland et. al., 2009). As previously described, oversaturated hyperalkaline drip waters facilitate rapid growth rates of around 10 mm/yr. This has led to large but low-density speleothems, with morphology like other hyperalkaline stalagmites found in train tunnels (Figure 3.4). It is thought that the orange colour comes from co-precipitated organic matter coming from the surface, exhibiting annual winter banding of humic/fulvic compounds and fluorescing layers in cross-section (Figure 3.3, Hartland, 2010). Samples from PE seem to

fluoresce more than samples from non-hyperalkaline waters (pH 8), due to the high pH forcing deprotonation of functional groups, causing intermolecular repulsion, exposing organic matter to light (Hartland, 2010). This annual banding suggests rapid, fracture flow source from the surface, as slower matrix flow, or aquifer mixing, would smooth such a distinct banding signal.

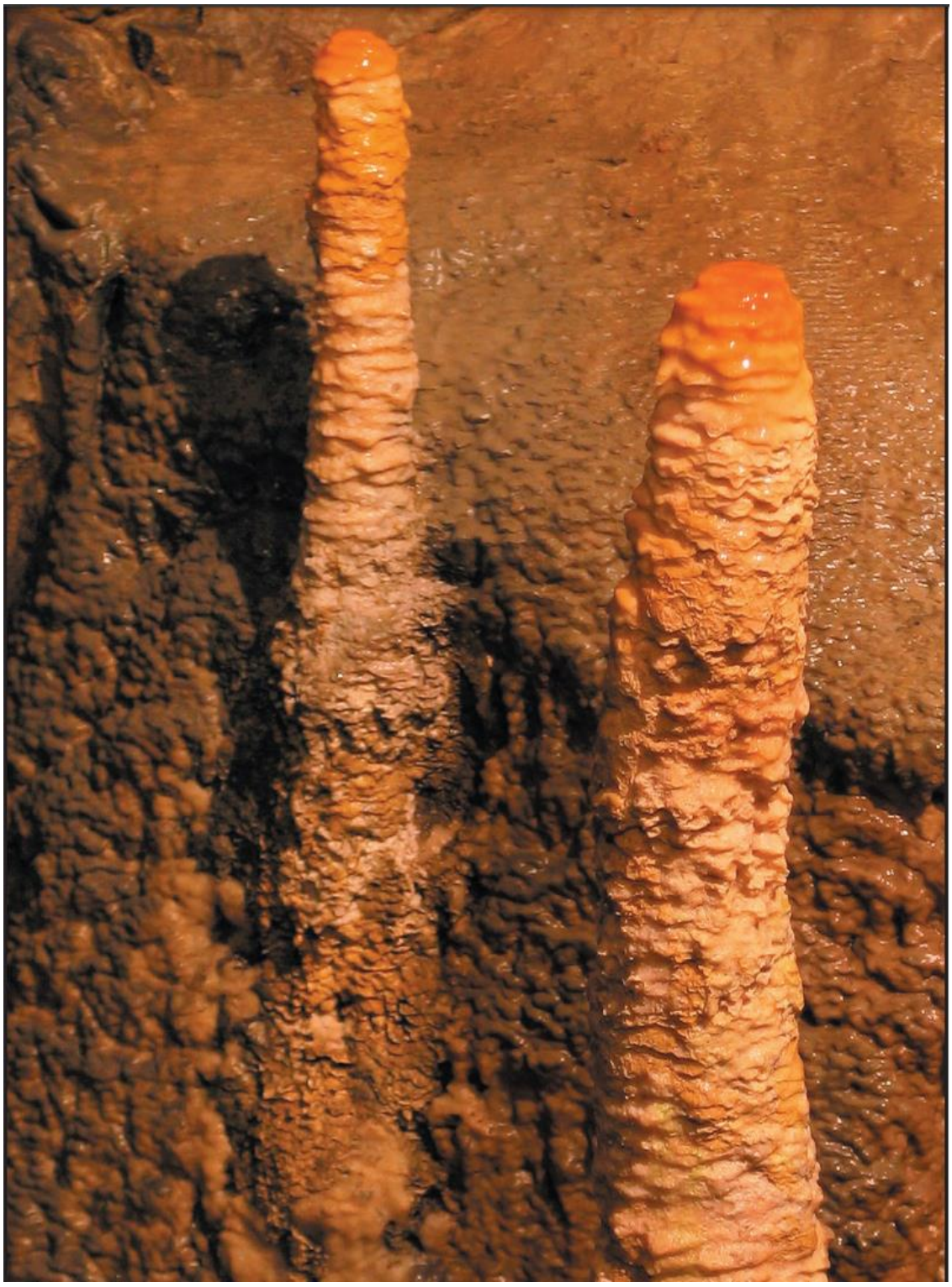

Figure 3.2: ''Poached-egg'' stalagmites, Hyperalkaline speleothems from Poole's Cavern (approx. 1m tall) (Photo by I. Fairchild) - Hartland, 2010.

Figure 3.3: Re-growth sectioned and polished, showing annual laminae (Photo, A. Hartland).

Figure 3.4:''Array of hyperalkaline speleothems in a disused railway tunnel. Note the similar morphology of these speleothems but distinct difference in colour'' (*Photo by J. Gunn*) - Hartland, 2010.

3.1.4 Hydrology

A stream enters the cave from the bottom of this choke, flowing 100m through the cave to a sink (Pitty, 1996). The stream is sourced from sinks on Stanley Moore and resurges 500m further north at Wye's Head (Glennie, 1953), as confirmed by dye tracing experiments (Ford & Gunn, 1992). This water flows below the speleothems in PE chamber and has no effect on the speleothem geochemistry.

In PE chamber, rapid calcite precipitation is driven by hyperalkaline waters (pH 10-13), seeded by the 19th century lime waste deposits in Grin Low Wood above the cave (Hartland et. al., 2009). No literature of the exact morphology of the epikarst above the cave currently exists, and the exact residence time has not been calculated. However, annual banding of organic matter in the speleothem material (Hartland, 2010) suggests a prevalence of rapid fracture flow, rather than slower matrix flow, or aquifer mixing, which would smooth such a distinct banding signal.

3.2 WHITE SCAR CAVE SITE DESCRIPTION

White Scar Cave (259 m a.s.l.) is a carboniferous limestone show cave just north of Ingleton, N. Yorkshire. A 12m vadose canyon has formed as water drains the western flank of Ingleborough Hill to a resurgence in Chapel-le-Dale at 247m a.s.l. (Gascoyne, et. al., 1983). The cave is overlain by grass moor land and sheep grazing, typical for many caves in Yorkshire.

Using TinyTag loggers, temperature fluctuations at the stream are ±1.69°C with an average of 8.52°C (White, 2019). On the day of visit, water temperature inside the cave was between 8.3 and 8.4 °C (n=2), closely matching average cave air temperature. Average pH at the pools where water was collected was 8.42 ±0.04 (n=2). Average $\delta^{18}O$ at the sites collected was -7.95 ±0.2 (n=3).

The cave was chosen as a good comparator to Poole's Cavern drip waters as a representation of more 'usual' karst drip waters: alkalinity sourced from carbonate, rather than CaO, and pH around 8 rather than the 9-13 hyperalkaline range.

3.3 POOLE'S CAVERN FIELD-METHODOLOGY

3.3.1 Cave Water collection sites

Sampling and in-cave analysis was conducted at or near Poached Egg (PE) chamber, ~100m south from the entrance (Figure 3.1). This location was chosen due to its hyperalkaline drip-waters, facilitating rapid calcite precipitation.

5 speleothems in PE chamber were chosen for water collection, all were established as hyperalkaline and with sub-30-second drip rates. These are labelled PE1-5, from right to left if facing the streamway and from highest to lowest points (Figure 3.5).

Water was collected using funnels and tubing, supported by a 1Lt HDPE bottle cut out to fit the speleothem top (Figure 3.6). This allowed drip waters to bypass the speleothem surface. Various container sizes (5-20Lt) were used to collect the drip waters over a period of 2-3 weeks, rinsing in triplicate before use. In this period, drip rates were consistent enough to almost fill the containers completely and yielding 30-45 L of speleothem drip water in total.

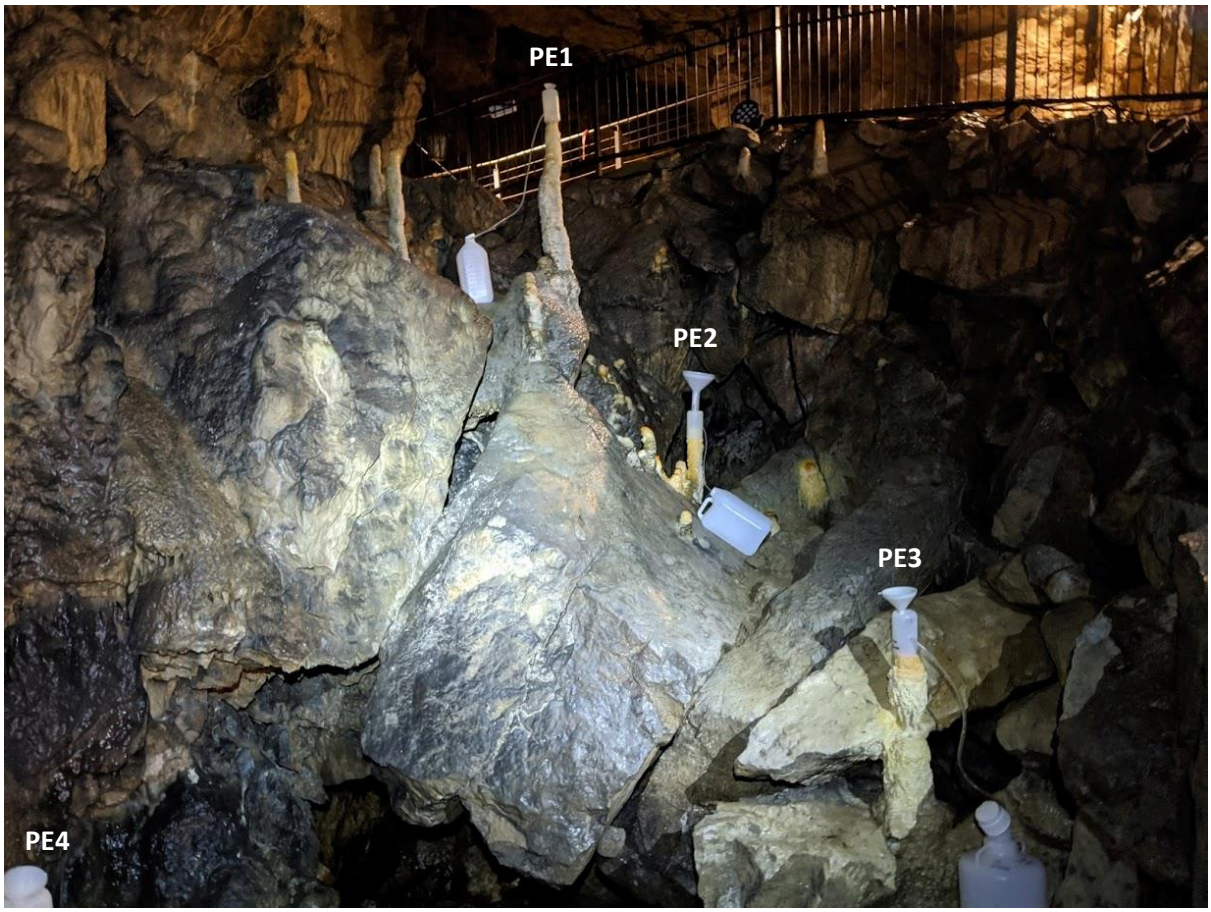

Figure 3.5: Placement of drip water collectors PE1-4 in Poole's Cavern.

Figure 3.6: Drip water collector setup consisting of a funnel, tubing and a 1-litre water bottle cut to the size of the speleothem.

3.3.2 Water storage

Drip waters were then bulked together and decanted into 4-litre collapsible jerry cans for storage or immediate use. All headspace volume in each container was removed to minimise the opportunity for CO_2 exchange and thus calcite precipitation during storage. Samples were then transported back to the laboratory and stored at 7 °C, coincidently similar to in-cave temperatures found in February 2021. To minimise microbial degradation, consideration was made to minimise the time between water removal from the cave and subsequent usage.

3.3.3 In-cave sub-sampling of collected waters

Sub-samples of 50 ml volume were taken from each individual water collection site, as well as the bulked water sample. This included:

a) 50 ml unfiltered for inorganic orthophosphate colourimetry and alkalinity titrations, filled to the brim to remove headspace that might facilitate calcite precipitation.
b) 50 ml filtered at 0.2 µm to remove cells and colloidal fractions, filled to the brim
c) ~25 ml unfiltered for total phosphate colourimetry, leaving headspace to allow for expansion during subsequent freezing.

Samples for a) and b) were stored in a clean fridge at LEC, with as short as time as possible (1-3 days) between removal from the cave and analysis. This minimised effects such as phosphate sorption to the container material. Samples for c) were frozen to prevent sample degradation whilst allowing a large sample number to be accrued for acid digestion.

A further 2ml sample was collected and stored within a chromocol vial for oxygen and deuterium isotope analysis.

3.3.4 pH, Conductivity, Temperature

pH, conductivity (µS/cm) and immersion temperature (°C) were measured using a WTW Multi 340i handheld device. pH was calibrated on arrival to Poole's Cavern using two buffer solutions. Readings were taken from aliquots of each of the speleothem drip waters and the homogenised bulk water. Air temperature readings can be validated using the Tiny-tag array installed in the cave.

3.3.5 Alkalinity

Total alkalinity was recorded using a Hach Digital Titrator, determined by titration to specified end points using phenolthalein and Bromocresol Green indictors with a 0.16M sulphuric acid titrant. Hydroxide alkalinity was calculated by titrating a phenolphthalein sample solution with H_2SO_4 until pink and multiplying the number of units administered by 0.4. Bicarbonate alkalinity was calculated by titrating a bromocresol sample solution with H_2SO_4 until green and multiplying the number of units administered by 0.4. Total alkalinity is the sum of these values.

3.4 WHITE SCAR – FIELD METHODOLOGY

The sampling and testing procedure in White Scar largely followed the same protocol to that in Poole's Cavern. Please refer to the details in methodology section 3.3.

10 Lt of water was respectively collected from calcite pools in two locations: Pool 1 to the north-west, just after the calcite squeeze, and Pool 2 to the south after Stream Aven (Figure 3.7). Approximately 8Lt of drip water was also collected over a period of 2 weeks from a speleothem just above Pool 1, using the sample funnel setup as in Poole's Cavern.

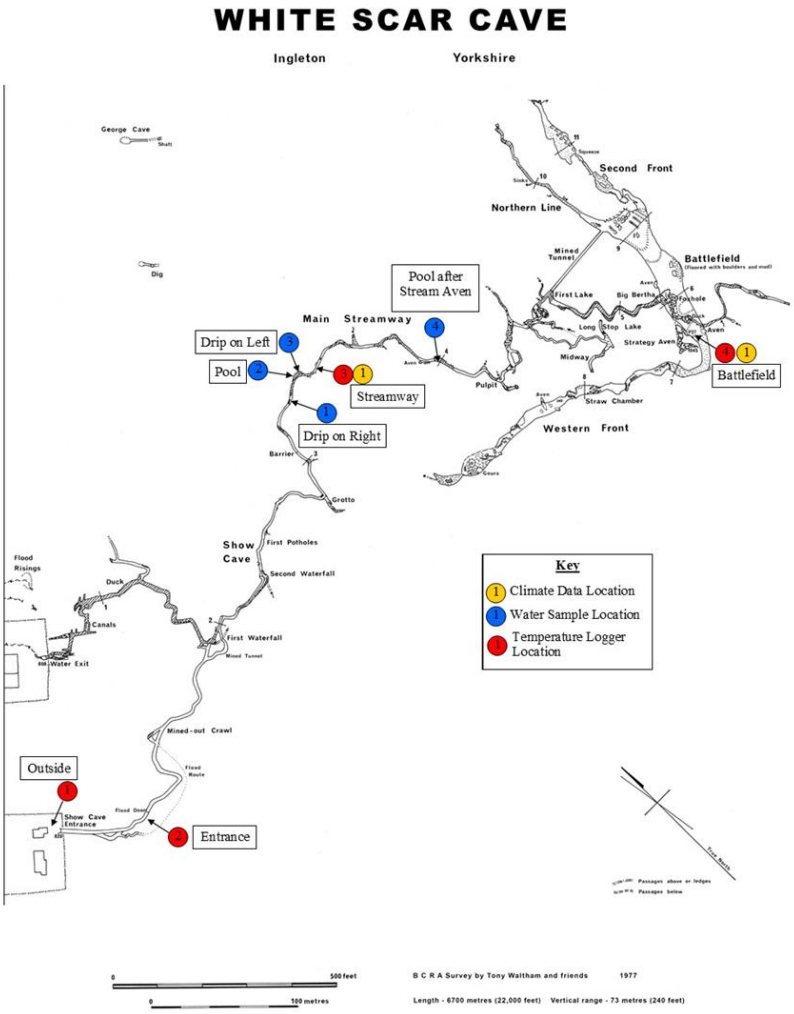

Figure 3.7: Topological map of White Scar Cave, Ingleton, Yorkshire. Water was collected from Pool on the left (2) and the pool on the right after Stream Aven (4). White, J., 2021.

3.5 LABORATORY METHODOLOGY – CAVE WATERS

Cave waters which were known to be low, or devoid of natural phosphorous concentrations were spiked with laboratory grade potassium dihydrogen orthophosphate and left to equilibrate at a range of temperatures and natural pH values to facilitate determination of the phosphate-O isotope – temperature relationship by pyrophosphatase enzymes.

We use two different concentrations of Potassium Dihydrogen Orthophosphate (100-ppb and 400-ppb) to provide a phosphate source for the experiments and to test the capacity of enzymes to process phosphate. Cave waters spiked with this phosphate were left to equilibrate at 4 °C, 7.2 (±0.34) °C, 16°C, 21-22.6 (±0.89) °C and 30 °C. We use cave waters from Poole's Cavern and White Scar to investigate the effects of pH on this relationship.

We also undertake a time-controlled experiment, to establish the rapidity with which isotopic equilibrium is reached, across a range of temperatures and P concentrations. This was repeated with an emphasis on the first 24hrs, at 0, 4, 8, 12, 24 hrs and 3, 7, 11 days.

3.5.1 Phosphate dosing of cave water samples

As the drip waters in PE chamber were largely devoid of natural phosphate, P was added and dissolved to known concentrations. This provided a definitive starting concentration and isotopic value, as well as ensuring sufficient phosphate for subsequent experimental work and analysis.

Potassium Dihydrogen Orthophosphate H_2KO_4P (Fischer Scientific P/4800/63, CAS: 7778-77-0, molecular weight 136.084, Batch 1091771 - 09/08/2010) was weighed using a micro balance (Mettler Toledo XP6 ±0.001 mg) to make up concentrations of 100-ppb and 400-ppb of P. For example, stoichiometrically 6.976 mg H_2KO_4P equates to 400 ppb of P in 4Lt of water.

Weighed aliquots were stored in 1ml Eppendorf tubes before dosing the 4Lt collapsible jerry cans at the start of experimental work. The sample tube was triple rinsed with pipetted drip-waters to ensure full dissolution.

3.5.2 Water Incubation procedure

Jerri cans containing 4-litres of collected drip waters were moved to temperature-controlled locations a minimum of 12hrs before addition of Potassium Dihydrogen Orthophosphate. At LEC this included a walk-in cold store (7.2 ±0.34 °C), lab-temperature (21-22.6 ±0.89 °C) and a temperature-controlled cabinet (30 °C).

After equilibrating to the controlled temperature environment each jerrican was dosed with phosphate and left to reach chemical equilibrium with constituent pyrophosphatase enzymes for 3-5 days. Following the literature, this allows more than enough time for isotopic equilibration to take place (Chang & Blake, 2015). A greater duration of isotopic equilibration causes loss of orthophosphate from solution by adsorption to the container walls (Jarvie et. al., 2002). The phosphate in the water is then precipitated as brucite, terminating the isotopic exchange by microorganisms.

3.5.3 Concentration Tests

Samples were taken to assess P concentrations before and after dosing, and at the end of the chemical equilibration period. This would usually include 2x6ml samples, both

unfiltered and at 0.2 µm filtered, for inorganic orthophosphate colourimetry and a frozen 20ml sample for digested total phosphate colourimetry. These concentration values could be used to calculate the expected yield in silver phosphate.

3.5.4 Cave water processing to silver phosphate

1Lt aliquots were removed from the 4Lt jerry cans, removing all headspace in the container before re-storing.

Brucite precipitation was derived from the MAGIC method for soluble reactive phosphorus extraction from freshwaters (Tamburini et. al., 1992). Per 1Lt sample, 20ml of 3M Mg brine was added and shaken well, before adding a further 5ml of 1M NaOH. After leaving to settle in a fridge for 1 hour, the supernatant was poured off to centrifuge the residual phosphate-containing brucite precipitate at 3000 rpm for 15 mins.

Brucite was then stored in a fridge before further preparation, deeming that no isotopic alteration of phosphate-oxygen could take place in this bound-state.

Brucite was then re-dissolved into solution using minimal volumes of 1M HNO_3.

3.5.4.1 Purification of extracts to silver phosphate (Ag_3PO_4)

The following method is adapted from Tamburini et al., 2010 by Samantha Coyle, University of Nottingham and Andi Smith at the NERC Isotope Geosciences Laboratories, British Geological Survey.

3.5.4.2 Ammonium phospho-molybdate (APM) precipitation

Solutions of dissolved brucite in HNO_3 were added to a 250ml conical flask with 25ml of 4.2M ammonia nitrate, 1ml concentrated sulfuric acid to acidify to pH 1 and 40ml of ammonium heptamolybdate solution 10% w/v. Flasks were sealed with pierced foil and put in a rotating shaker at 50 ^oC overnight producing yellow APM precipitate.

The APM precipitate was subsequently vacuum filtered with 0.2 µm nylon filters, supported with a glass microfiber filter, and washed through with 300ml 0.6M NH_4NO_3 (5% solution). Filtered crystals were then added to a 100ml glass beaker.

3.5.4.3 Magnesium Ammonium Phosphate (MAP) precipitation

In a fume cupboard the APM was dissolved off the filter using a minimum quantity (25ml) of citric acid-NH_4OH solution and set to magnetically stir. Each filter was carefully removed ensuring full dissolution of APM. 7ml of magnesia solution along with 7ml of 1:1 NH_4OH/DDW solution was slowly added, thereby raising the pH to 8-9. Samples were covered and left to sit at 50 ^oC overnight to produce a white struvite (MAP) precipitate.

The MAP precipitate was vacuum filtered using 0.2 µm nylon filters and rinsed with 100ml of 1:20 v/v NH_4OH/DDW solution. Filter papers were transferred back into a clean 100ml beaker and MAP dissolved using 20ml 0.5M nitric acid, carefully removing the filter.

3.5.4.4 Cation removal

Resin columns were prepared using DOWEX 1X8 100-200 mesh cation exchange resin slurried in 6 ml of de-ionised water. Each resin column was left to settle and conditioned with 7-10ml of 7M HNO_3 followed by 20ml of DI water.

Samples of dissolved MAP were added to the resin column, set to drip as slow as possible, and collected into 50ml centrifuge tubes.

3.5.4.5 Ag_3PO_4 precipitation

7mL of Ag-ammine solution was added to the resin eluant, noting the yellow flash that indicates good probability for silver phosphate precipitation. 1ml of concentrated

NH_4OH was then added to lower the pH, bringing the solution back to colourless. Samples were left uncovered at 50 ^oC to allow Ag_3PO_4 precipitation as ammonia evaporation facilitated establishment of optimum pH 7. pH can be corrected towards pH 7.0 using either HNO_3 or NH_4OH.

After 1-2 days, Ag_3PO_4 precipitate was vacuum filtered using 0.2 µm nylon filters and rinsed with plenty of DI water, scraping the sides of the container to ensure minimal losses. Resulting papers were placed on a glass evaporating dish and left in a drying cabinet overnight.

3.5.4.6 Ag_3PO_4 preparation for analysis

Ag_3PO_4 was scraped of the dry filter papers and stored in 1ml sample tubes.

Approximately 200µg of silver phosphate was weighed into small silver capsules for isotope analysis. Sample weights are recorded to enable %O yield to be calculated and all samples are weighed in triplicate.

3.6 LABORATORY METHODOLOGY – CALCITE MATERIAL

The aim of the following was to test if the phosphate-O isotope-temperature relationship experienced in the drip waters, from Poole's Cavern, was translated into calcium carbonate. Cave waters amended with 100 & 400 ppb of P using laboratory grade potassium dihydrogen orthophosphate were dripped at a constant rate using a peristalitic pump, onto an upturned watch-glass (Figure 3.8). A few drops of water were left to dry on the glass beforehand to promote calcite nucleation. Experiments were performed at room temperature (21-25°C) and at a constant drip rate of 1 drip every 20-30 seconds until a total of 4 litres of cave water had passed over the precipitation plate (typically over a period of 3-4 weeks).

The GILSON MINIPULS 3 peristaltic pump was set to 0.20 to 0.25 to achieve the 1 drip (approx. 0.1 ml) every 20-30 seconds. This drip rate was like that found within Poole's cavern.

3.6.1 Collection of precipitated calcites

After the cave drip water supply had been exhausted (approx. 4 litres), the plates were left to air dry overnight and were re-weighed to calculate calcite yield. This was around 300-400 mg for 4Lt of Poole's Cavern Water (Figure 3.9). Plates were then scraped using a clean scalpel onto weighing paper and stored in 5ml Eppendorf tubes prior to further analysis.

Figure 3.8: Setup for the precipitation of calcite at room temperature in LEC.

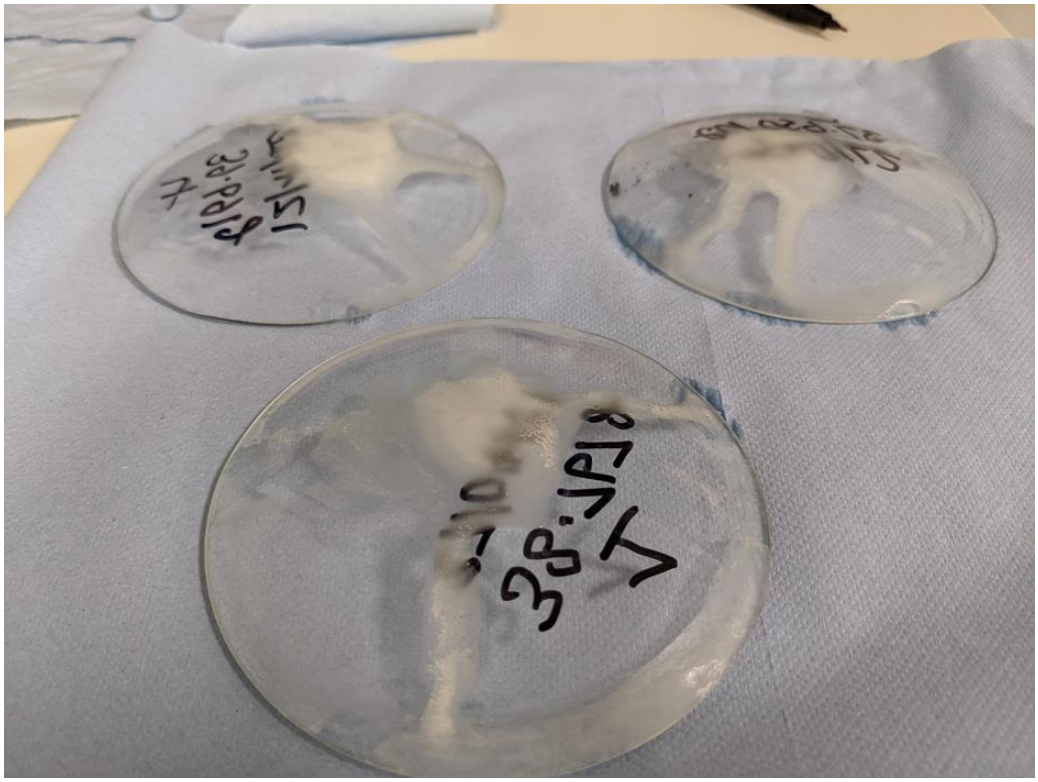

Figure 3.9: 300-400 mg of precipitated calcite from 4Lt of Poached Egg drip-waters collected from Poole's Cavern.

3.6.2 Extraction of silver phosphate from calcite plates

The section 3.5.4 method for the extraction of P from water was followed, except skipping the brucite precipitation and dissolution stage. Instead, 400-500 mg of calcite was dissolved in minimum quantity (~20 ml) of 1M HCl before moving onto APM precipitation.

3.7 LABORATORY METHODOLOGY – DRILLED SPELEOTHEMS

Calcite material was drilled and analysed from two speleothems grown over the past 100 years, to test the transfer of contemporary phosphate-18O - temperature relationships into stalagmite deposits: MERC-1 from Rukiesa Cave, Ethiopia (18.93 ±0.61 °C) and BFM-96-2 Brown's Folly Mine, UK (10 °C ± 0.4 °C). Both cave sites have been well constrained for temperature, $\delta^{18}O\text{-}H_2O$ and pH, thus allowing assessment of the palaeothermometer across a range of environmental conditions.

3.7.1 RUKIESA CAVE, ETHIOPIA: MERC-1

Rukiesa Cave is a Jurassic Limestone cave intercalated with marl and mudstone, approximately 1.3 km long and 192 m deep. Since the 1930s, the cave has been overlain by ploughed agricultural fields, including maize, millet, coffee, and chat (Baker et. al., 2007., Wynn et. al., 2021). Thin soils of <1 m thickness have developed over the sandy limestone that constitutes the roof of the cave (Baker et. al., 2007). Phosphate sources are likely to be agricultural in origin, backed up by high phosphate and nitrogen concentrations in drip waters and calcite (Wynn et. al., 2021) and $\delta^{15}N\text{-}NO_3$ isotopic compositions which place the nitrogen source at the boundary between manure and inorganic fertiliser (Wynn et. al., 2021).

Mercury chamber is found ~25m below the surface in Rukiesa Cave. The drip waters within the chamber have a pH of 7.81, HCO_3^{2-} alkalinity of 6.17 mM and water $\delta^{18}O$ of -0.35‰. (Wynn P; Unpublished data). This fits within the reported range of dripwater $\delta^{18}O$ for the cave, (-2.3 to -0.3‰; n=7; Asrat et. al., 2008). Cave air or water temperature has not been recorded in Mercury Chamber. However, the cave air temperature from nearby Asfa Chamber (~30m below surface) has an average of 18.93 ±0.61 °C recorded

at 30 minutes intervals from October 2005 to March 2007 (Baker et. al., 2007., Asrat et. al., 2008). The temperature at the cave entrance, 2m below the surface, was 18.03 ±1.2 °C between June 2006 to September 2007 (Asrat et. al., 2008). As Mercury chamber is between these two locations, it can be assumed that temperature is also around 18-19 °C and not too dissimilar to Asfa chamber.

Speleothem MERC-1, (Figure 3.10), collected in 2004, from Mercury chamber contains around 130-375 ppb of PO_4-P, sourced from the overlying agricultural land (Baker et. al., 2007). Samples were extracted from date of collection in 2004 to laminae age 1950 (based on laminae counting and verified with ^{14}C dating (n=6), (Baker et al., 2007)). Based on the sample size, precipitation rate is around 0.2 mm/yr on average.

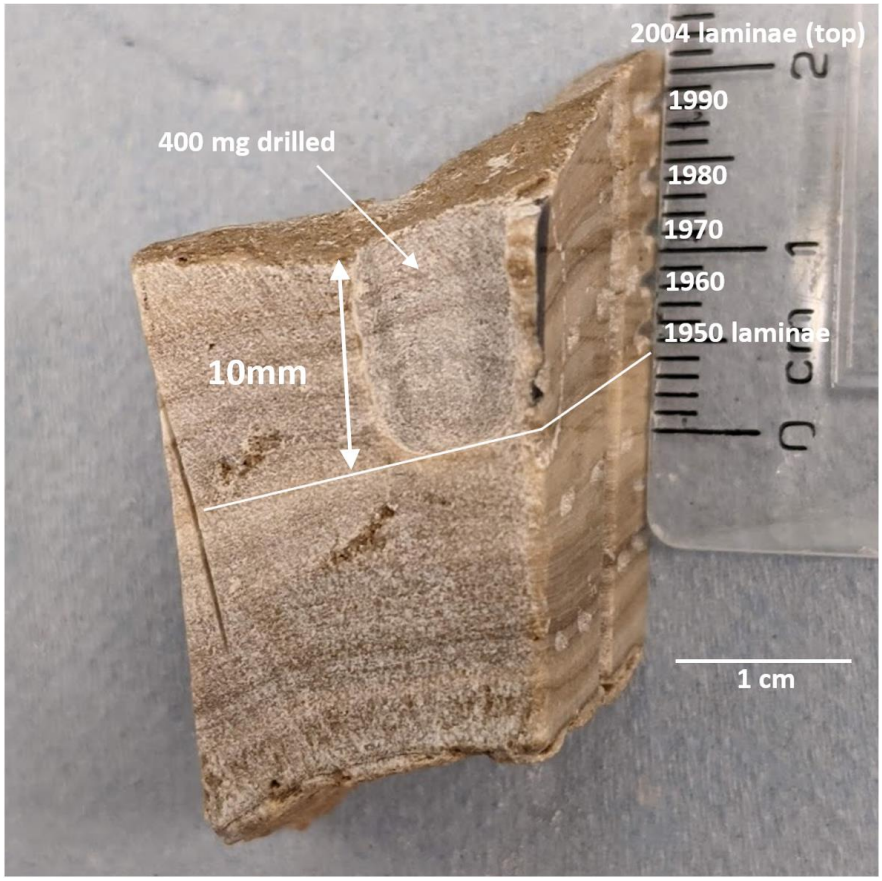

Figure 3.10: MERC-1 speleothem from Rukiesa Cave, Ethiopia collected in 2004. Post-drilling photo showing the drill location (left) perpendicular to the polished and dated drill face (right). 2004 to 1950 dating model (n=6), as described in Baker et. al., 2007, shown to the right.

3.7.2 BROWN'S FOLLY MINE, UK: BFM-96-2

Brown's Folly Mine is a disused limestone excavation that was worked between 1836 and 1904, residing 5-15m below the surface, (Baker et. al., 1999. Baldini et. al., 2001). The mine is located at the crest of Bathford Hill at ~150 m asl (Baldini et. al., 2001). Speleothem material has been growing in the cave since the 1900s, but the precipitation rates have been greatest since the 1980s: 4 times the rate than between 1940 and 1975 (Baldini et. al., 2001). This is thought to be due to the steady reclamation of vegetation above the cave since 1886, allowing CO_2 concentrations to rise high enough in the soil to facilitate carbonate saturation (Baldini et. al., 2005). The presence of vegetation has had a profound effect on $\delta^{18}O$, and $\delta^{13}C$ in the Brown's Folly Mine speleothem calcite, creating a magnitude of isotopic variation that would be expected from a glacial-interglacial transition (Baldini et. al., 2001). The vegetation above the cave is primarily deciduous forest of mixed ash, sycamore and oak (Baldini et al., 2005), with a 25cm thick clay soil containing leaf litter, rootlets, and root macropores (Fairchild et. al., 2006). Vertical fractures ('gull rifts') allows fissure flow into the cave, with slower flow through the limestone matrix (Fairchild et. al., 2006). pH ranges between 7.57 and 8.04 within the cave between 16 sites (Wynn, 2021 – unpublished data).

BFM-96-2 (Figure 3.11), collected in 1996, was precipitated with an in-cave water temperature of 9.9 ◦C ± 0.1 °C (Baker et. al., 1998., Baldini, et. al., 2001). Average growth rate was around 0.12 mm/yr at the primary drip spot to 0.07 mm/yr at the secondary precipitation site flowing down the side. $\delta^{18}O_{H2O}$ data is not available for Brown's Folly Mine, however the average rainfall $\delta^{18}O_{H2O}$ taken from Wallingford, UK between 1979 and 1996 through the GNIP database was -6.7‰ (IAEA/WMO, 2021). P-sources are likely to be natural in origin, as opposed to an agricultural source, from the deciduous

woodland above the cave. This is similar to Poole's Cavern, which also experienced vegetation re-establishment following the cessation of industrial activity in a similar period. Sample integration was between the date of collection in 1996 to the base of the speleothem formation which started growing around 100 years ago (Wynn et. al., 2008).

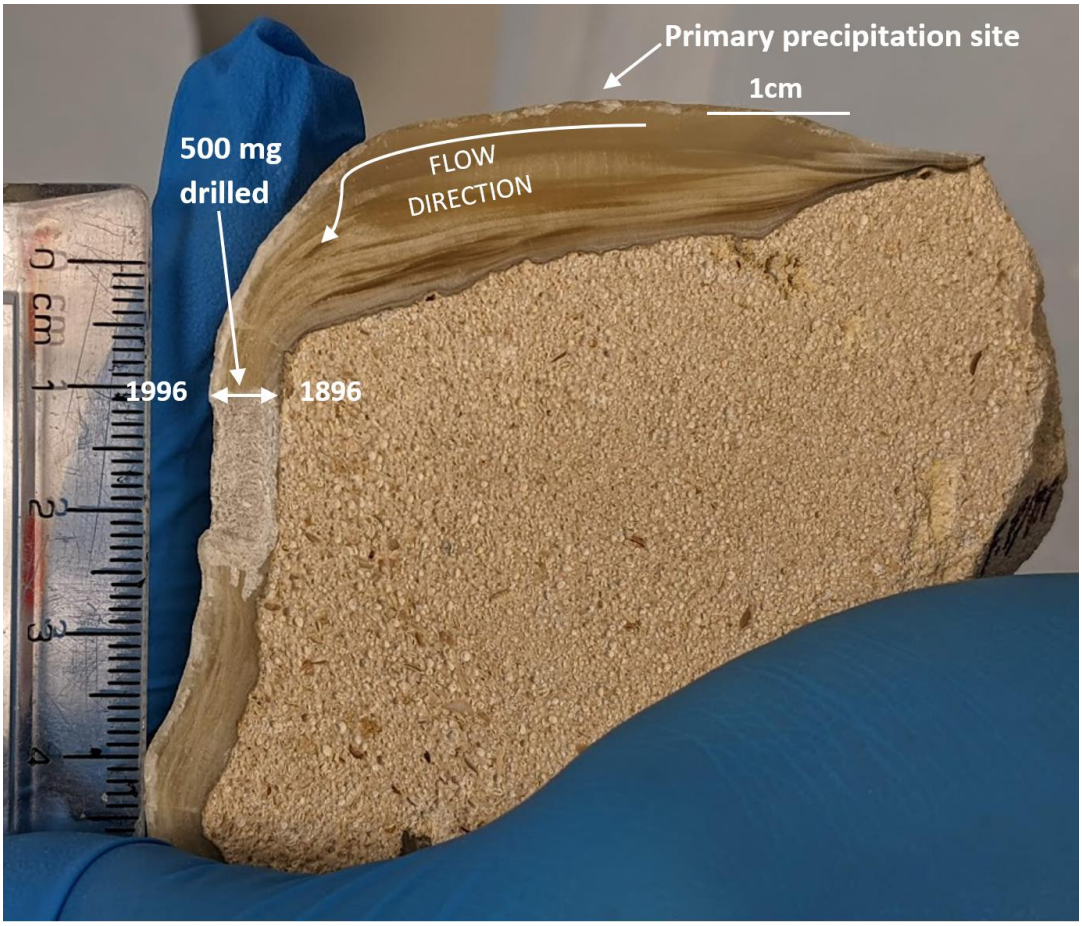

Figure 3.11: BFM-96-2 from Brown's Folly Mine, UK. Post drilling photo showing the drilling location perpendicular to the primary precipitation site at the top of the speleothem. Water would have dripped from above and flowed over the host rock to the left.

3.7.3 DRILLING PROCEDURE

400-500 mg of speleothem material was hand drilled from both speleothem samples for $\delta^{18}O\text{-}_{PO_4}$ analysis. Samples were burred perpendicular to laminations using an MFA Como Drills 399DPLUS. Each sample's chronology covered the time from sample collection to a dated laminae.

Before collection each surface was lightly drilled to clear potential contamination, disposing a small amount of calcite material. The drill-bit was cleaned with 1M HCl and de-ionised water between samples.

3.7.4 EXTRACTION OF SILVER PHOSPHATE FROM SPELEOTHEM MATERIAL

The section 3.5.4 method for the extraction of P from water was followed, except skipping the brucite precipitation and dissolution stage. Instead, 400-500 mg of calcite was dissolved in minimum quantity (~20 ml) of 1M HCl before moving onto APM precipitation.

3.8 ANALYTICAL METHODOLOGY

3.8.1 Colourimetry

Colourimetric analysis was performed on aliquots of raw and phosphate-amended drip waters to yield phosphate concentrations in ppb (micrograms per litre). Samples 2ml in volume were repeated in triplicate, using a Seal AQ2 autoanalyzer, following the phosphomolybdenum blue method (EPA-118-A Rev.3, analytical range of 5 to 1,000 ppb of P per litre and limit of detection of ±1 ppb P/L).

Total phosphate concentrations could be calculated by first digesting 8.2 ml of sample/blank/standard with 1.6 ml of potassium persulphate and 0.2 ml 11N sulphuric acid in a sample tube and autoclaving. This lyses all organic phosphate sources to be measured in conjunction with orthophosphate (EPA-119-A Rev 4, analytical range of 10 to 1,000 ppb of P per litre and a limit of detection of ±4 ppb P/L).

The analyser was calibrated using automated dilutions of a 1mg/L P standard before every run, noting low variance in the generated calibration plot, and comparing to previous calibrations. Further check standards were made up from two phosphate sources, checked at regular intervals: 0.5, 0.1 and 0.05 mg/L and WRX100 0.15 mg/L and WRX400 0.0375 mg/L.

3.8.2 Trace Element Analysis

Trace element analysis on unfiltered Poole's Cavern and White Scar waters was conducted at Lancaster Environment Centre using a Thermo Scientific iCAP 6000 series ICP-OES. 1 % Nitric acid was added to each sample at a ratio of 0.1ml/10ml. To ensure the sample was digested completely, and to accommodate for any trace elements associated with precipitates or sorption to the walls of the container, the entire sample bottle that was collected from the cave site was digested. In this case each sample was weighed, and the correct volume of acid was added stoichiometrically.

Diluted standards were prepped to calibrate the machine at the start of the run, splitting analysis into two separate groups. Check standards were all prepped from a secondary source:

i. Group 1: Ca, K, Mg, Na
    a. Calibration Standard 1: Ca at 0, 10, 25, 50, 100, 150 ppm
    b. Calibration Standard 1: K, Mg, Na at 0, 0.5, 1, 2, 5, 10 ppm
    c. Check Standard 1: Ca, Fe, Mg, K, Na at 1 ppm
ii. Group 2: Ag ,Al, B, Ba, Cd, Ca, Cr, Co, Fe, K, Mg, Mn, Na, N, Pb, Zn
    a. Calibration Standard 2: 0, 25, 100, 200, 500, 1000 ppb (Certipur solution IV 1.11355.0100)
    b. Check Standard 2: 50 ppb (High Purity Standards ICP-AM-3 Lot. 1502329)

3.8.3 Isotopic Analysis

3.8.3.1 Water Isotopes ($\delta^{18}O$ & δD)

Aliquots of cave drip waters were analysed for oxygen and hydrogen isotopes in H_2O at NIGL Keyworth. Oxygen isotope ($\delta^{18}O$) measurements were made using the CO_2 equilibration method with an Isoprime 100 mass spectrometer plus Aquaprep device. 200 µl of water was loaded into Labco Limited exetainers and placed in a heated sample tray at 40°C. The exetainers were then evacuated to remove atmosphere, flushed with CO_2, and left to equilibrate for between 12 (first sample) - 37 (last sample) hours. Each individual gas sample was then admitted to the cryogenic water trap where any water vapour is removed. The dry sample gas is then expanded into the dual inlet mass spectrometer for analysis. Two laboratory standards (CA-HI and CA-LO) were analysed in each run. The value of these laboratory standards has been determined accurately by comparison with international calibration and reference materials (VSMOW2, SLAP2 and GISP), allowing expression as $\delta^{18}O$ (‰). Errors are typically ±0.05‰.

Hydrogen isotope (δD) measurements were made using a continuous flow EA-IRMS (EuropyrOH-Isoprime) with liquid autosampler. Each sample (0.5 µl) was injected into a heated septa-sealed injector port (160°C). The resulting water vapour is flushed through into a chromium-packed reactor (980°C) by helium carrier gas. The chromium reduces the water, resulting in the quantitative conversion to hydrogen gas:

$$2Cr_{(s)} + 3H_2O_{(l)} \rightarrow Cr_2O_{3(s)} + 3H_{2(g)}$$

The hydrogen gas entered the IRMS generating simultaneous peaks for H_2 at m/z 2 and HD at m/z 3. The peaks were integrated and corrected for H^{3+} contribution, and the areas compared to those of a reference H_2 pulse introduced prior to the arrival of the sample

peak. Each sample is analysed in triplicate. In each run two laboratory standards (CA-HI and CA-LO) were run several times. These standards were compared with international calibration and reference materials (VSMOW2, SLAP2 and GISP) and so the D/H ratios (versus VSMOW2) of the unknown samples were calculated. Errors are typically ±1.0‰.

3.8.3.3 Phosphate-oxygen Isotopes

Oxygen isotope analysis of Ag_3PO_4 ($\delta^{18}O_{PO_4}$) was undertaken on an ELEMENTAR PYROCUBE elemental analyser (EA) coupled to a GEOVISION Isotope Ratio Mass Spectrometer (IRMS) at the NERC Isotope Geosciences Laboratories (NIGL), Keyworth, UK.

Prior to analysis the EA-IRMS was checked for stability through a series of reference (CO) gas injections and tuned to achieve optimum sensitivity. Ag_3PO_4 samples are introduced to the EA via the built-in autosampler in a flow of lab grade (99.9%) helium. The sample is pyrolysed at 1450°C in the presence of graphite, carbon black and glassy carbon. Oxygen from phosphate combines with available carbon forming CO gas. Residual liquid silver is captured in a graphite crucible for disposal. The sample gas is retained in a CO trap and released to the MS by thermal programmed desorption (TPD©) throughout a total run time of 13 minutes.

Raw isotope values were processed on the ELEMENTAR IONOS software by comparing the sample peak area to that of a standard material of known isotope composition (USGS 80, 81, Alfa2 and B2207). Standards were treated the same way as the samples, i.e. weighed into silver caps and pyrolysed during the same run as the samples.

Raw isotope values were corrected offline for blank, drift and linearity issues if necessary, before correction using a two-point calibration, based on the externally

calibrated values of USGS 80 and B2207, with Alfa 2 and USGS 81, acting as check standards: chosen as they most closely cover the natural range of 'expected' isotope values.

Oxygen isotope values were corrected to the international VSMOW scale and reported. Typical precision is ±0.3‰ for $\delta^{18}O_{PO_4}$ based on within run replication of reference materials, with standard deviations aimed to be <1.0‰ between triplicates.

4 - RESULTS 1: PHYSICO-CHEMICAL CHARACTERISTICS OF COLLECTED SPELEOTHEM DRIP-WATERS

The following provides a summary of chemical characteristics for the speleothem drip-water collections. This covers 6 visits to Poole's Cavern, UK (13/11/2020 to 26/04/2021) and one visit to White Scar Cave, UK (20/05/2021). Data recorded in-situ includes water temperature, conductivity, and pH. $\delta^{18}O$ and δD isotopes, and alkalinity, were recorded with collected aliquots in the laboratory.

This data aims to provide an overview of factors that might influence microorganisms to overturn phosphate, and therefore impact a $\delta^{18}O_{PO4}$-temperature relationship. For the Poole's Caverns waters in particular, pH and alkalinity is key to understanding how CaO driven hyperalkalinity facilitates the rapid precipitation of synthetic calcite in the laboratory. $\delta^{18}O_{H2O}$ data is essential for calculating predicted $\delta^{18}O_{PO4}$ for any given temperature. P concentration data also describes seasonal change in the phosphate geochemistry of Poole's Cavern.

4.1 POOLE'S CAVERN DRIP-WATER CHARACTERISTICS

4.1.1 Drip Rate:

Ranged from 1 drip every 13s at PE2 to 1.2s at PE3. During water collection, the fast drip rate at PE3 facilitated the greatest water yield. For this reason, the largest container available (30 Lt) was often placed at PE3.

4.1.2 Drip-water Temperature:

Average for PE1-5 (Table 4.1) was 7.37 (±0.04) °C, ranging from 8.2 °C (25/11/20) to 6.8 °C (03/03/21). The temperature of 'bulked water' represents the weighted mean of water volumes collected from PE1-5. The average from all three bulked collections (7.03 ±0.25 °C) is similar to the total average for PE1-5 (6.97 ±0.12 °C), suggesting the bulking process has little influence on temperature. Between December 2020 and April 2021, average annual air temperature at the bridge near Poached Egg Chamber (Tiny tag probe 840308) was 8.05 ±0.08 °C (n=23,567), with the coldest temperature of 7.92 °C between 09/12/2020 and 11/12/2020. This suggests that the drip-waters coming from the cave roof are around 0.69 °C cooler than air temperature.

4.1.3 Conductivity:

A wide range exists between PE1-5 in Poole's Cavern: 470 (±11.31 1SD) µS/cm in PE1 to 1216.5 (±115.04 1SD) µS/cm in PE3 (Table 4.1). These are similar values to that in Hartland et. al., 2010 (600 µS/cm in PE1 and 1340 µS/cm in PE3). Over the collection periods between Winter and Spring, each drip site generally increased in conductivity, with the greatest increase at site PE4 (+804.00 µS/cm). Bulked waters are biased high (954.33 ±41.20 1SD µS/cm) due to it volumetrically containing primarily PE3.

4.1.4 pH:

Hyperalkaline drip-waters in Poole's Cavern ranged from pH 9.35 (PE2 13/11/20) to 12.37 (PE3 03/03/21) with an average of 11.62 (±0.37 1SD) over the collection period (Table 4.1). This is comparable to the average of Hartland et. al., 2010 (pH 11.8). pH of bulked water (12.06 ±0.17 1SD) is greater than the average PE1-5 value due to volumetric bias of PE3 which averaged 12.16 (±0.18 1SD). Moreover, bulk-water mixing would have led to aeration causing the pH to rise as CO_2 is absorbed.

4.1.5 Drip-water $\delta^{18}O$:

There was little variation between PE1-5 or collection date. Averages ranged from -7.62 (±0.05 1SD)‰ in PE4, to -7.66 (±0.15 1SD)‰ in PE2 (Table 4.1). Bulked waters are similar at -7.64 (±0.10 1SD)‰.

4.1.6 Drip-water dD:

There was little variation throughout. Averages ranged from -49.50 (±0.99 1SD)‰ in PE2, to -50.07 (±0.57 1SD)‰ in PE5 (Table 4.1). Bulked waters are similar at -49.79 (±0.72 1SD)‰.

Site	Average Temp °C	n=	Range	SD	Average Conductivity µS/cm	n=	Range	SD	Average pH	n=	Range	SD	Average $d^{18}O$ VSMOW2 (‰)	n=	Range	SD	Average dD VSMOW2 (‰)	n=	Range	SD
Bulked water	7.03	3.00	0.50	0.25	954.33	3.00	82.00	41.20	12.06	3.00	0.34	0.17	-7.65	2.00	0.12	0.09	-49.38	2.00	2.12	1.50
Bulk stored in Roman Chamber	7.70	2.00	0.80	0.52	531.00	1.00	n/a	n/a	11.52	2.00	0.73	0.52	-7.56	2.00	0.05	0.03	-49.13	2.00	0.38	0.27
PE1	7.65	2.00	0.90	0.64	470.00	2.00	16.00	11.31	11.57	3.00	0.28	0.15	-7.65	2.00	0.22	0.15	-49.53	2.00	1.40	0.99
PE2	7.28	4.00	1.20	0.57	508.00	5.00	565.00	255.04	11.10	5.00	2.66	1.05	-7.66	4.00	0.30	0.15	-49.50	4.00	2.20	0.99
PE3	7.30	4.00	1.20	0.55	1216.50	4.00	233.00	115.04	12.16	5.00	0.47	0.18	-7.64	4.00	0.11	0.05	-49.85	4.00	0.71	0.34
PE4	7.30	4.00	1.40	0.62	760.75	4.00	804.00	350.66	11.81	5.00	1.03	0.50	-7.62	4.00	0.13	0.05	-49.98	4.00	1.70	0.73
PE5	7.30	4.00	1.30	0.61	502.40	5.00	529.00	250.88	11.48	5.00	0.77	0.33	-7.63	4.00	0.17	0.08	-50.07	4.00	1.21	0.57
Average PE1-5	7.37	5.00	0.50	0.04	691.53	5.00	788.00	133.30	11.62	5.00	2.38	0.37	-7.64	5.00	0.19	0.10	-49.79	5.00	1.44	0.72
Roman Chamber	9.25	1.00	n/a	n/a	600.00	1.00	n/a	n/a	9.25	1.00	n/a	n/a								

Table 4.1: Average data collected from Poole's Cavern during 6 site visits between 13/11/2020 and 26/04/2021. PE = Poached Egg Chamber. Bulked Water is a mix of PE1-5 collections, but primarily made of PE3. 'Bulk stored in Roman Chamber' is water from the first site visit where drip-waters were mixed into a vessel and stored/equilibrated in Roman Chamber. This differs from the usual bulked waters, which were mixed in a vessel and immediately emptied into smaller containers for storage. Water was also collected from Roman Chamber during this first visit. Drip-water Temperature (°C), conductivity (µS/cm) and pH were recorded using a WTW Multi 340i handheld device. Water Isotope data was collected on all site visits except 13/11/20 and analysed at NIGL Keyworth. Water temperatures for 13/11/20 were retracted as they were 11.7 °C; far higher than the air temperatures recorded that day in-cave (8.2 °C) and the average/range for subsequent collections.

4.1.7 POOLE'S CAVERN - ALKALINITY

4.1.7.1 Hydroxide alkalinity:

80.3-92.5 % of alkalinity in Poole's Cavern drip-waters is present as hydroxide (Table 4.2), sourced from the dissolution of CaO in lime kiln waste. This facilitates the rapid precipitation mechanisms of calcite in Poole's Cavern. Hydroxide concentrations range from 40.8 mg/L in PE1 to 150.9 mg/L in PE3. The alkalinity in the bulk water (108.9 ±5.7 mg/L) is again volumetrically biased towards the high hydroxide alkalinities in PE3. The wide variation between drip sites (±110.1 mg/L) suggests that drip-waters are exposed to varying degrees of CaO dissolution, despite being within a few meters of each other within Poached Egg Chamber. This suggests a complex hydrological connection between the soil system, epikarst and speleothem drip site.

4.1.7.2 Carbonate alkalinity:

7.5-19.7 % of the alkalinity in Poached Egg drip-waters is made up of carbonate, ranging from 9.3 mg/L (PE5) to 12.3 mg/L (PE3) (Table 4.2). This is atypical for more conventional cave waters, such as at White Scar Cave, where most of the alkalinity saturation comes from carbonate dissolution of the limestone bedrock. The variation in data here is much tighter than hydroxide, suggesting the exposure of water to limestone substrates and/or prior calcite precipitation between drip sites is less variable.

4.1.7.3 Total Alkalinity:

Average Total Alkalinity varies from 50.8 (n=1) mg/L in PE1 to 163.2 mg/L in PE3 (Table 4.2). Again, this suggests different hydrological regimes despite the drip sites being only a few meters apart. The high alkalinity in PE3 suggests a hydrological reservoir that has high exposure to lime deposits, allowing for increased dissolution.

Site	Average Hydroxide mg/L	% of total	n=	Range	SD	Average Carbonate mg/L	% of total	n=	Range	SD	Average Total alkalinity mg/L
Bulked water	108.9	90.5	3.0	10.8	5.7	11.5	9.5	3.0	3.2	1.7	120.4
PE1	40.8	80.3	1.0	n/a	n/a	10.0	19.7	1.0	n/a	n/a	50.8
PE2	61.9	85.0	3.0	75.6	41.1	10.9	15.0	3.0	1.6	0.8	72.8
PE3	150.9	92.5	3.0	18.0	10.0	12.3	7.5	3.0	1.6	0.8	163.2
PE4	104.3	90.3	3.0	42.4	21.7	11.2	9.7	3.0	2.0	1.1	115.5
PE5	45.3	82.9	3.0	53.2	29.7	9.3	17.1	3.0	4.0	2.3	54.7
Average PE1-5	80.6	88.2	5.0	110.1	46.6	10.7	11.8	5.0	2.9	1.1	91.4

Table 4.2: Average results of phenolphthalein alkalinity (hydroxide) mg/L, bromocresol alkalinity (carbonate) mg/L and total alkalinity (hydroxide + carbonate) mg/L in Poached Egg drip-waters of Poole's Cavern from 3 collections between 08/03/21 and 26/04/21. PE = Poached Egg. Logged using a Hach Digital Titrator by multiplying the recorded units by 0.4 to convert to mg/L.

4.1.8 POOLE'S CAVERN – PHOSPHORUS GEOCHEMISTRY

4.1.8.1 Inorganic Orthophosphate:

Average natural orthophosphate ranged from 15.3 (±0.6) ppb in PE4 to 23.3 (±1.4) ppb in PE2 (Table 4.3). This equates to an overall average of 19.2 (±3.7) ppb between PE1-5, with the Bulk water averaging slightly higher at 24.4 (±1.7) ppb. Inorganic phosphate concentrations are around 8.1 ppb higher in Winter (Bulk 1), when there was more rainfall, than Spring (Bulk 2). These results suggest that a sizeable fraction of phosphate exists in Poole's Caverns waters, and certainly enough to influence phosphate-oxygen isotope values even with additional orthophosphate. For example, even after adding 100-ppb of further orthophosphate, 30.4 % of the silver phosphate product used for isotopic analysis could theoretically be made up of this natural-background source.

4.1.8.2 0.2 µm filtered Orthophosphate:

There is a seasonal difference between orthophosphate pre and post filtering at 0.2 µm. In Spring, there is a loss of 0.6 ppb between the unfiltered and filtered average of PE1-5 (Table 4.3). This suggests that forms of P are likely dissolved inorganic orthophosphate by being small enough to pass through filtration. Spring P is not likely to be in large forms, such as colloidally bound. The Spring bulked collections (Bulk 2) compliment this, with 4.2 ppb difference between unfiltered (30.1 ±5.8 ppb) and 0.2 µm filtered (15.8 ±0.2 ppb).

Conversely, the loss of 21.6 ppb when filtering Winter collections (Bulk 1) could suggest evidence of P being present in larger forms than 0.2 µm. The forms of P are changing seasonally likely due to changes in precipitation and surface runoff.

4.1.8.3 Total Phosphate:

Spring collections yielded net 0 readings for total phosphate, suggesting it was around the limits of detection for the methodology (±10 ppb). Conversely, Winter collections (Bulk 1) were 40.5 ±13.9 ppb (Table 4.3). Taking this value away from inorganic orthophosphate in that period, yields a potential 10.4 ppb from organic phosphate sources. This is good evidence of winter vegetation dieback introducing organic P into Poole's Cavern as suggested in Hartland et. al., 2010.

Sample	N=	Average Inorganic Orthophosphate ppb	SD	N=	Average Inorganic Orthophosphate 0.2 µm ppb	SD	N=	Average Total P ppb	SD
PE1	1	22.7	0.6	1	21.3	0.6			
PE2	2	23.3	1.4	2	22.2	0.7			
PE3	2	18.2	0.2	2	17.0	1.4			
PE4	2	15.3	0.6	2	15.0	1.9			
PE5	2	16.3	2.8	2	17.7	1.4			
Average PE1-5	**5**	**19.2**	**3.7**	**5**	**18.6**	**3.0**			
Bulk 1 - Winter	3	30.1	5.8	3	8.5	4.1	3	40.5	13.9
Bulk 2 - Spring	2	22.0	2.4	2	15.8	0.2	1	1.4	
Average Bulk 1 & 2	**2**	**24.4**	**1.7**	**2**	**12.2**	**2.1**	**2**	**17.0**	**22.0**

Table 4.3: Colourimetric phosphate concentrations (ppb) of Poole's Cavern. Includes inorganic orthophosphate from unfiltered and 0.2µm filtered water, and total phosphate yields after acid digestion and autoclaving. PE= Poached Egg Chamber. Each sample was tested in triplicate from PE1-5 collected during between 26/03/2021 and 26/04/2021 (This is apart from PE1 which was only collected on 26/03/21). Bulked waters of PE1-5 were tested in Winter 25/11/20, 09/12/20 and 02/03/21 (Bulk 1) and Spring 26/03/21, 26/04/21 (Bulk 2).

4.2 WHITE SCAR CAVE DRIP-WATER CHARACTERISTICS

4.2.1 Drip rate:

Was 1 drip/8s for the speleothem above the left-hand pool (LHP).

4.2.2 Water temperature:

Average was 8.35 ±0.1 °C (n=2) for LHP and right-hand pool (RHP), with little variation being 100m apart in the main streamway. The water collected from the speleothem was measured after removal from the cave and therefore the temperature is not included here.

4.2.3 Conductivity:

Ranged from 309 (RHP) to 376 (speleothem) µS/cm**,** with an average of 336 µS/cm (n=3). This is lower than that found in Poole's Cavern, suggesting a lower overall presence of ionic species.

4.2.4 pH:

Ranged from 7.95 (speleothem) to 8.46 (RHP) with an average of 8.26 (n=3). This mild alkalinity is typical for speleothem waters, and lower than hyperalkaline Poole's Cavern.

4.2.5 Drip-water $\delta^{18}O_{H2O}$:

There was little variation, ranging from -7.75‰ in RHP to -8.04‰ in LHP, averaging at -7.94‰ (n=3). This is a similar, but slightly higher, range than Poole's Cavern.

4.2.6 Drip-water δD_{H2O}:

There was little variation, ranging from -52.5‰ in the RHP to -54.5‰ in the LHP speleothem, averaging at -53.80‰ (n=3) overall. This is slightly higher than Poole's Cavern.

Site	Volume Collected Lt	n=	Conductivity µS/cm	Temp °C	pH	$\delta^{18}O$ VSMOW2 (‰)	δD VSMOW2 (‰)	Notes
Left Hand Pool LHP	10	1	324	8.4	8.37	-8.04	-54.4	
Right Hand Pool RHP	10	1	309	8.3	8.46	-7.75	-52.5	
Speleothem by Left Hand Pool	8	1	376	n/a	7.95	-8.01	-54.5	*Readings taken at LEC 03/06/21.
Average		**3**	**336**	**8.9**	**8.26**	**-7.94**	**-53.80**	

Table 4.4: Data collected from White Scar Cave, Yorkshire on 20/05/2021. Water was collected from two calcite pools, as well as an active speleothem above the Left-Hand Pool (LHP). Water Temperature (°C), conductivity (µS/cm) and pH were recorded using a WTW Multi 340i handheld device. Water Isotope data was collected and later analysed at NIGL Keyworth. Measurements of pH and conductivity in the speleothem drip-water were made upon returning to Lancaster.

4.2.7 White Scar - Alkalinity:

Unlike Poole's Cavern, the alkalinity in White Scar Cave is entirely carbonate derived with no detectable hydroxide. Ranging 150.4 mg/L in RHP to 157.6 mg/L of in LHP (Table 4.5). Average alkalinity (154 mg/L, n=2) is higher than Poole's Cavern (91.4 mg/L, n=5) despite the difference in pH.

Site	n=	Hydroxide mg/L	Carbonate mg/L	Total alkalinity mg/L
Left Hand Pool LHP	1	0	157.6	157.6
Right Hand Pool RHP	1	0	150.4	150.4

Table 4.5: Results of phenolphthalein alkalinity (hydroxide) mg/L, bromocresol alkalinity (carbonate) mg/L and total alkalinity mg/L from water collected in White Scar on 20/05/2021. Logged using a Hach Digital Titrator by multiplying the recorded units by 0.4 to convert to mg/L.

4.2.8 White Scar – Phosphorus Geochemistry:

White Scar speleothem-waters contain only trace amounts of natural P, only just above the limits of detection for the auto-colourimeter (±1 ppb) with an average of 5.0 (±0.4) ppb of inorganic orthophosphate, and 2.8 ppb orthophosphate that passed through the 0.2 µm filter (Table 4.6). This suggests low probability of background P significantly influencing the phosphate-oxygen isotopes. Total P values were measured at or near 0 ppb in LHP and RHP. This can be explained by the 10-ppb minimum detection level of the methodology, and a range of detection of ±4 ppb, as orthophosphate for LHP (3 ppb) and RHP (2.7 ppb) fit below this limit.

Sample	Ortho-phosphate (ppb)	SD	Ortho-phosphate 0.2 µm (ppb)	SD	Total P (ppb)	SD
LHP White Scar 200521	3.0	0.0	0.3	1.5	-2.1	1.9
RHP White Scar 200521	2.7	0.6	-0.3	0.6	-3.7	1.2
Speleothem Drip-water	9.3	0.6	8.3	0.6		
Average	5.0	0.4	2.8	0.9		

Table 4.6: Phosphate concentrations (ppb) analysed from aliquots of water collected from White Scar Cavern on 20/05/2021. Includes inorganic orthophosphate concentrations from unfiltered and 0.2 µm filtered water, and total phosphate yields after acid digestion and autoclaving. LHP = Left Hand Pool, RHP = Right Hand Pool. Each sample was tested in triplicate.

5 - RESULTS 2: PHOSPHATE CONCENTRATION AND PHASE CHANGE DURING SAMPLE EQUILIBRATION

The following data is derived from experiments designed to evaluate how the different phosphate phases present in the drip-waters may evolve over time in sealed containers, and at different temperatures. This is significant as different phosphate phases are metabolised at different rates by microbes, therefore impacting their potential to overturn phosphate to a temperature-isotopic-equilibrium. P existing as dissolved inorganic phosphate is the most easily overturned by microbes as it requires the least activation energy.

Phosphate phases that can be distinguished include inorganic phosphorus, as orthophosphate P, and organic phosphate as the difference between this value and the total P value.

The size of phosphate pools can also be evaluated by filtering the samples at 0.2 and 0.45 μm. This differentiates between dissolved inorganic phosphate, which should fit through the filter, and larger forms such as colloidal or organic P.

The experiments were conducted by adding 100-ppb and 400-ppb of potassium dihydrogen orthophosphate (PDOF) in Poole's Cavern drip-waters. A control check was also made with DI water at 100-ppb to check for losses independent of cave water chemistry.

5.1 POOLE'S CAVERN P PHASE AND CONCENTRATION CHANGE 400-ppb

5.1.1 Inorganic Orthophosphate change at 400-ppb (Figure 5.1)

Concentration declined over a period of 72hrs, becoming stable thereafter. This loss from solution suggests conversion of a portion of added PDOF into a phase which is inaccessible to this analysis. This becomes more profound with increase in temperature, with 137 ppb being lost at 36°C in 72hrs compared to 81 ppb at 21.9 °C and 60 ppb at 7.2°C (a).

5.1.2 0.2 µm filtered orthophosphate change at 400-ppb (Figure 5.2)

During filtration the majority of P is being removed. This equates to a 92.5 % loss, with 30-ppb remaining from 400-ppb originally added at 7.2°C (b). Over time, the loss of P stabilises after 24 to 72 hours. Prior to this, P is immediately sequestered from the orthophosphate phase, with minor redissolution events. Whilst the precise mechanisms of P loss are uncertain, data from the 100-ppb tests suggest sequestration of added PDOF into a colloidal phase larger than 0.2 µm in the first 24hrs.

5.1.3 Total-P change at 400-ppb (Figure 5.3)

At t=0, total-P values are comparable to Ortho-P concentrations. This suggests there is no significant extra source of P (such as organic-P) that has not already been picked up in the orthophosphate method. The loss of Total-P through time again suggests that PDOF is moving into a phase which is inaccessible to this analysis. This could include losses to the container walls. However, over the experiment's duration, variation between Total P and Ortho-P suggests subtle movement between phases. This could describe the redissolution of colloids,

precipitated solids, or movement between organic pools. This observation becomes most profound towards the end of the experiment and increases with temperature. For example, the total-P sample in the incubator at 36 °C is 23 ppb higher than the ortho-P at 72hrs (c), suggesting 9 % of total phosphorus has potentially been sequestered into organic forms.

5.2 POOLE'S CAVERN P PHASE AND CONCENTRATION CHANGE 100-ppb

5.2.1 Inorganic Orthophosphate change at 100-ppb (Figure 5.4)

PDOF was dissolved in Poole's drip-waters to an aimed value of 100-ppb. However, initial measurements undertaken at t=0 appear to be lower than that theoretical value. The is due to a combination of factors including the slight over-filling of containers above 4Lt, leading to increased dilution, and loss of P to forms that are not captured in the methodology, including immediate adhesion to the container walls.

Inorganic orthophosphate does not significantly drop over the incubation period, with most values within error of each other. For example, orthophosphate is 74 ppb at 0hrs and 68 ppb at 504 hrs with overlap at ±1 SD (d). Only at 696 hrs does orthophosphate substantially drop from 74 ppb to 56 ppb. This contrasts with 400-ppb PDOF, at the same temperature, which dropped steadily over 264 hrs (a).

5.2.2 0.2 & 0.45 µm filtered orthophosphate-P change at 100-ppb (Figure 5.4)

As with the 400-ppb data (b), 69 % of orthophosphate is being filtered out at 0.2 µm. This is likely to the orthophosphate being sequestered into large colloidal fractions, common in Poole's waters stabilised by the high pH (Hartland et. al., 2010). These colloidal forms are also mostly larger than 0.45 µm, with only an extra 6 ppb (8 %) able to pass through 0.2 & 0.45 µm.

5.2.3 Total-P change at 100-ppb (Figure 5.4)

Total-P is lower than ortho-P. The 4hr value shows high variation, close to the orthophosphate concentration, but is otherwise lower throughout the experiment. Unlike the samples at 400-ppb, 100-ppb total-P aliquots were frozen prior to analysis. It is possible that cryo-precipitation is causing this loss.

5.3 DI-WATER CHECK FOR P LOSSES

A control check was made using de-ionised water to evaluate where P losses might exist that are independent of cave water chemistry (including pH, microbes, and particulates including colloids), as well as to check the robustness of colourimetry methods at low P concentrations. This leaves potential losses limited to the container walls, independent of pH and filtration.

Over a 3-day period no losses in P were observed in both methodologies (Table 5.1). This suggests no losses to the plastic container, at least at a neutral pH. The orthophosphate method alone was able to pick up all the PDOF that was added in the water, and the Total P method was successful in mirroring this. This suggests method repeatability, despite the Total-P method containing extra digestion prep stages that might have promoted P losses.

All dissolved PDOF seems pass through 0.45 µm filter successfully. This gives weight to the hypothesis that P in Poole's drip-waters is being sequestered into colloidal forms larger than 0.45 µm. However, at 0.2 µm, 12 ppb (11.67 %) of the PDOF is being filtered out. This suggests that the 0.2 µm filtering process alone can account for sizeable losses, and should be considered when interpreting results.

Sample Name	Date	P ppb	SD
100-ppb-DI Total P	17/02/2021	98.77	6.37
100-ppb-DI orthophosphate	16/02/2021	100.00	1.73
100-ppb-DI ortho-P 0.2 µm	16/02/2021	88.33	0.58
100-ppb-DI ortho-P 0.45 µm	16/02/2021	100.67	2.52

Table 5.1: Colourimetry data of a control check for P losses. 4Lt of DI water was dosed with 1.827 mg of potassium dihydrogen orthophosphate (PDOF), yielding around 100-ppb of P, and left for 3 days at 7°C. The same container type and material was used as with previous experiments. Tested for unfiltered, as well as 0.2 & 0.45 µm filtered, orthophosphate P, as well as total phosphate. 1SD from triplicate results.

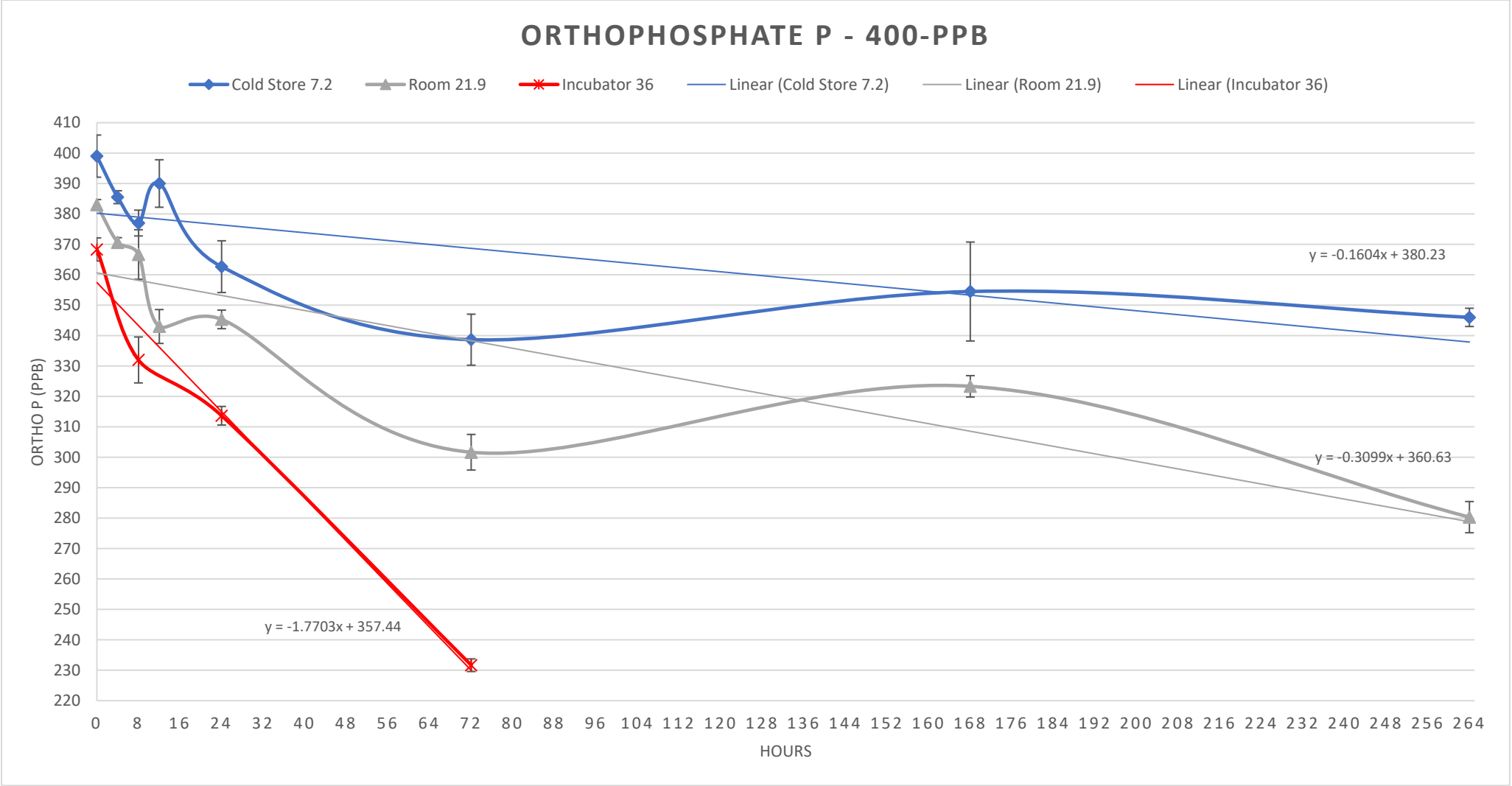

Figure 5.1: Orthophosphate P colourimetry of Poole's Cavern water spiked to 400-ppb, incubated at 7.2 °C, 21.9 °C and 36 °C for 11 days. Poole's Cavern water naturally contained 20 ppb of Ortho-P before dosing. 1 SD error bars from triplicate results.

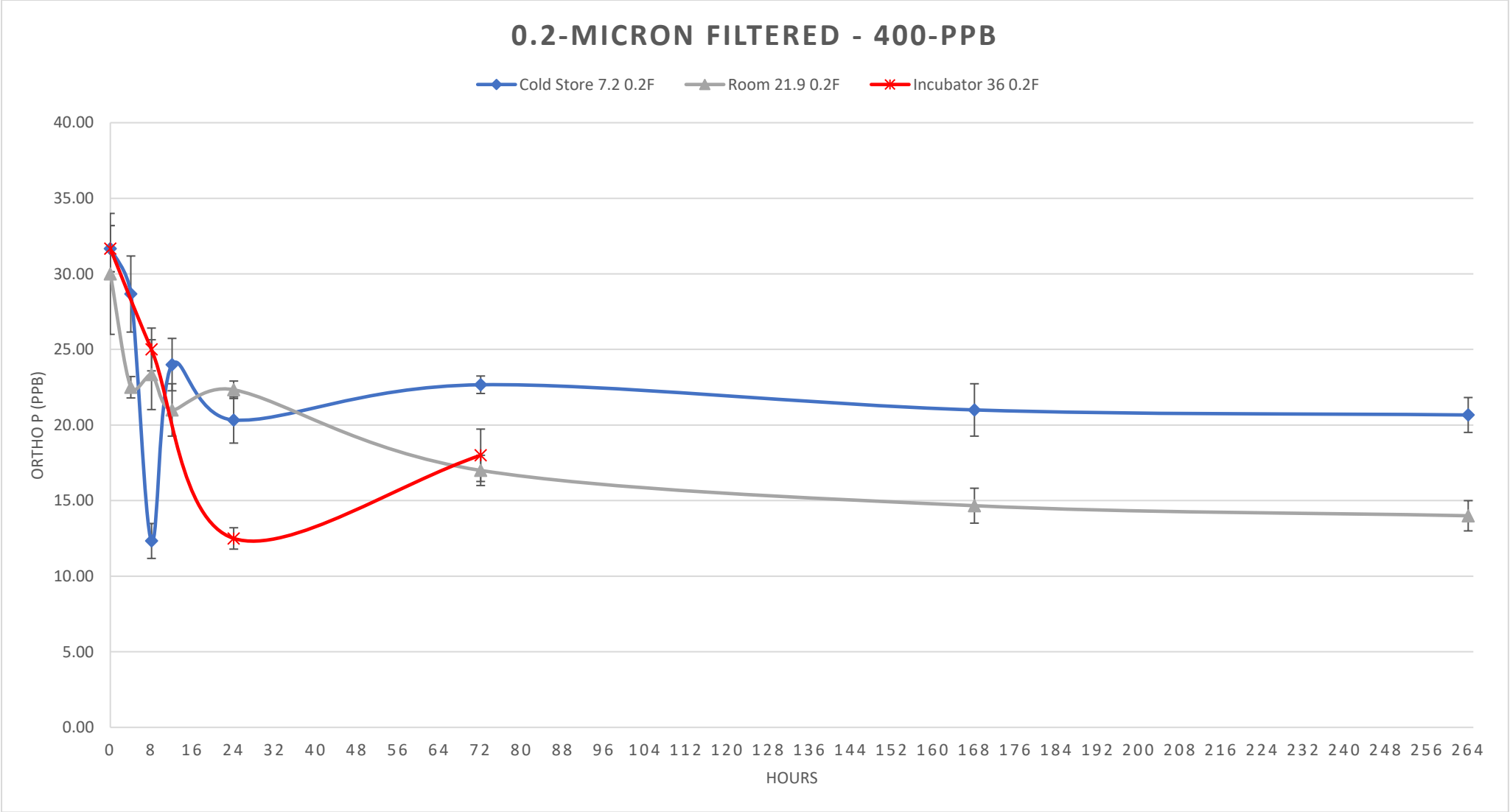

Figure 5.2: Orthophosphate P colourimetry of Poole's Cavern water spiked to 400-ppb, incubated at 7.2 °C, 21.9 °C and 36 °C for 11 days. Poole's Cavern water naturally contained 20 ppb of Ortho-P before dosing. Filtered at 0.2-µm. 1 SD error bars from triplicate results.

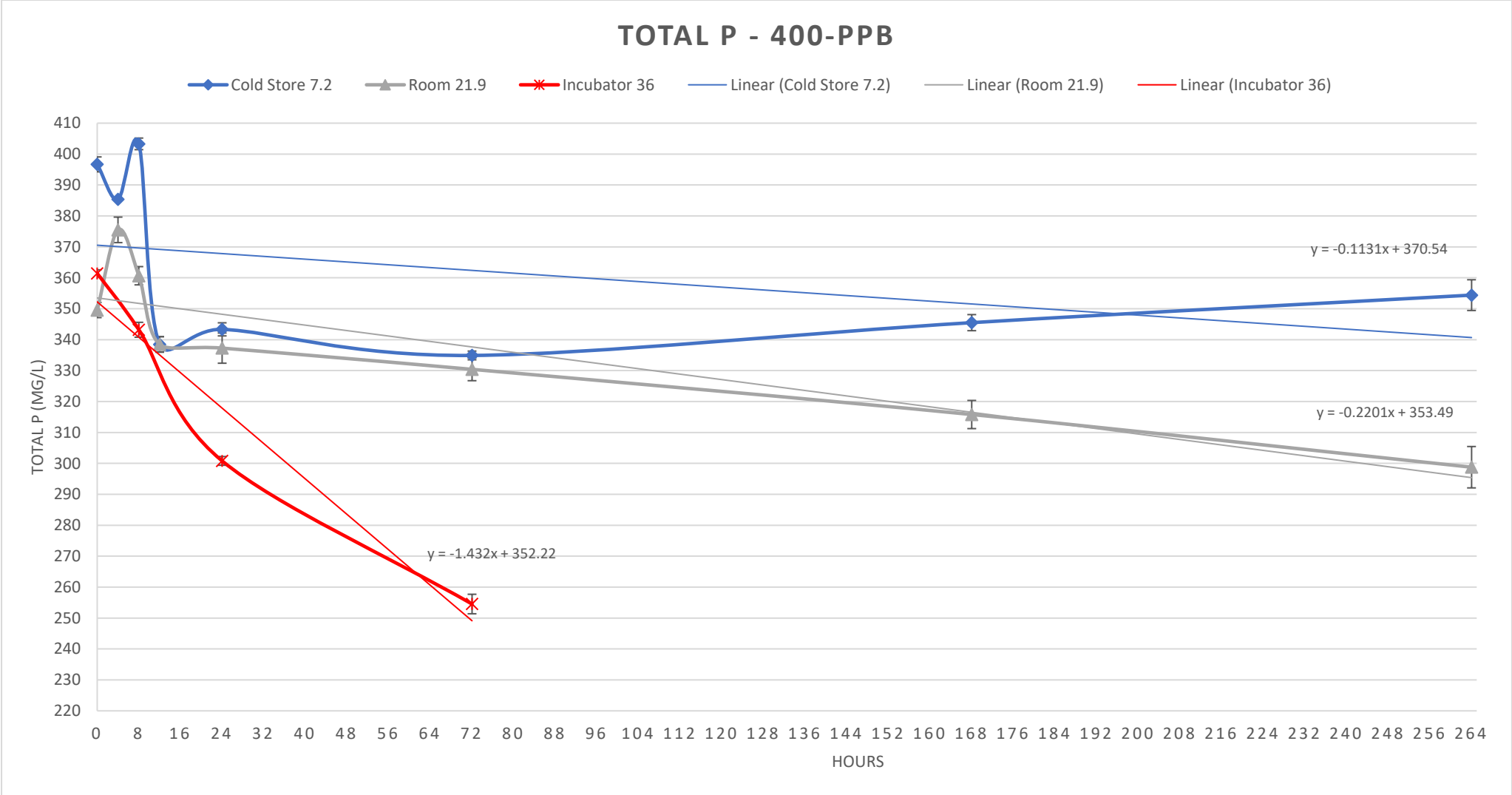

Figure 5.3: Total P colourimetry of Poole's Cavern water spiked to 400-ppb, incubated at 7.2 °C, 21.9 °C and 36 °C for 11 days. Poole's Cavern water naturally contained 20 ppb of Ortho-P before dosing. 1 SD error bars from triplicate results.

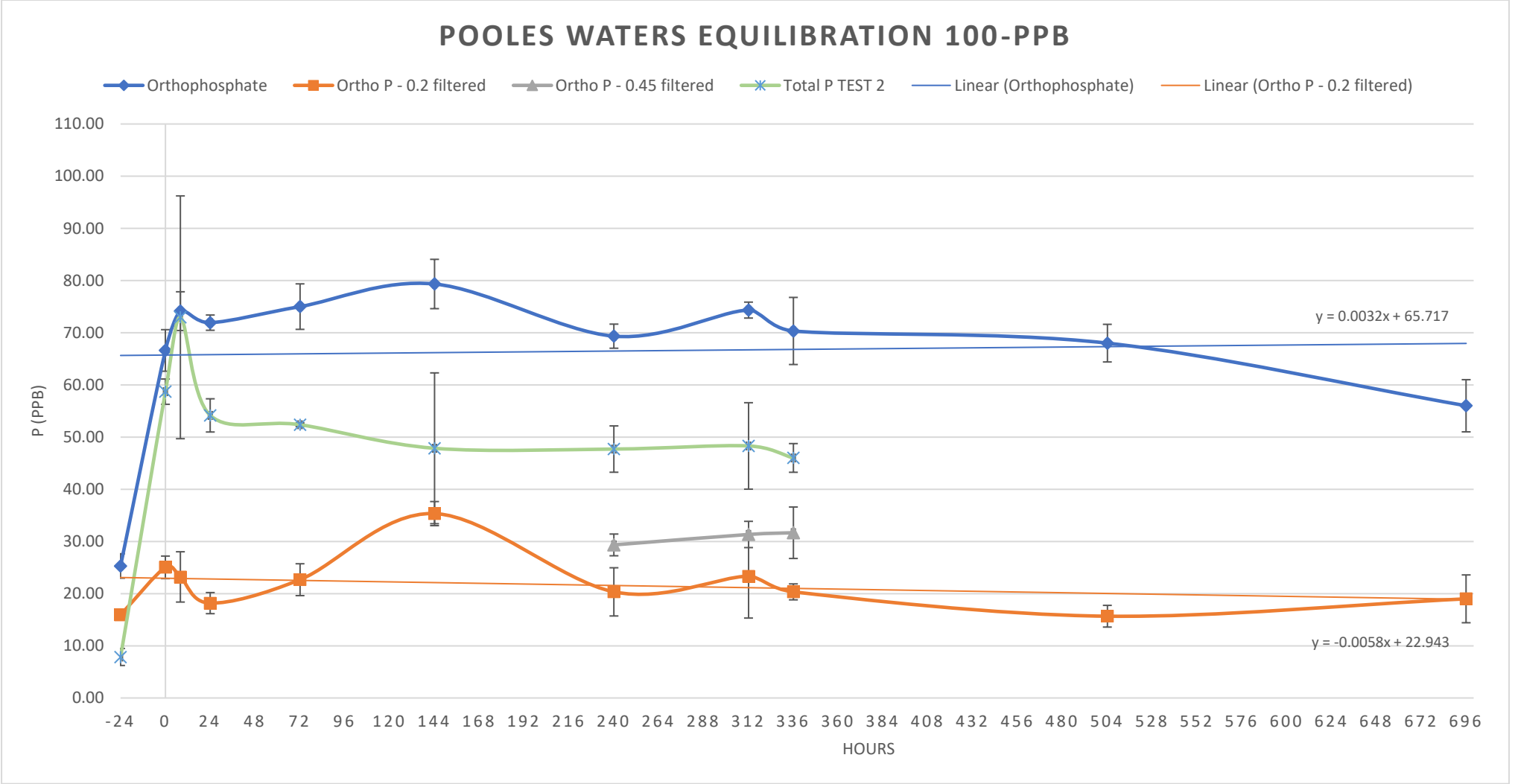

Figure 5.4: Phosphate colourimetry data for Poole's Cavern waters dosed with 100-ppb of PDOF and incubated for 29 days (02/02/21 to 03/03/21) at 7°C. Data collected includes inorganic orthophosphate, both unfiltered and filtered at 0.2 & 0.45 µm, along with total phosphate. 1 SD error bars from triplicate results.

6 - RESULTS 3: PHOSPHATE OXYGEN ISOTOPE DATA

6.1 POOLE'S CAVERN DRIP-WATER PHOSPHATE-OXYGEN-TEMPERATURE RELATIONSHIP AT 100-ppb

The following describes the phosphate-oxygen-temperature relationship of Poole's Cavern drip-waters, collected between 13/11/2020 and 26/04/2021, after adding 100-ppb of P in the form of potassium dihydrogen orthophosphate (PDOF) and equilibrated to different temperatures. Data is compiled from experiments conducted at the NERC isotope Geosciences Laboratories and Lancaster Environment Centre, as well as a reading from 'natural 'P in unadulterated drip-waters.

The aim of this data is to assess the efficacy of phosphate-oxygen-isotopes as a chemical thermometer in speleothem drip-waters, and to derive an equation that describes this relationship.

6.1.1 RELATIONSHIP BETWEEN TEMPERATURE AND $\delta^{18}O_{PO4}$ IN POOLE'S CAVERN WATERS AT 100-ppb

A statistically significant negative relationship (r=-0.96, p <0.001) exists between temperature and phosphate-oxygen-isotopes ($\delta^{18}O_{PO4}$) in Poole's Cavern drip-waters between 30 °C and 7 °C. As temperature increases, $\delta^{18}O_{PO4}$ decreases at a rate of -0.2‰/°C deviating from the $\delta^{18}O_{PO4}$ of PDOF. This relationship persists even when accounting for ±1 SD error between triplicate readings (Figure 6.1).

Statistics 1 - Pearson's r correlation:

r = -0.964 (p <0.001, n=8). This describes a statistically significant correlation between increasing temperature and decreasing $\delta^{18}O_{PO4}$ values. This is as per other findings in the literature.

Statistics 2 – Regression analysis:

R^2=0.928 (p <0.001, n=8). This test suggests that a linear relationship between temperature and phosphate-oxygen-isotopes can account for 92.8 % of variation in our dataset.

The dataset is 'bookended' at 30 °C and 7 °C by reproduced $\delta^{18}O_{PO4}$ readings from separate experiments, different batches of Poole's Cavern water and different P sources:

a. At 30 °C, a single reading of +16.15‰ (25/01/2021) was successfully repeated with triplicate results of +16.2 ±0.8‰ from a fresh batch of Poole's Cavern drip-water at a later date (30/07/2021).
b. At 7.2 ±0.34 °C, two separate readings that were taken 6 days apart (+20.11 ±0.31‰, and +20.61 ±0.06‰) correlate to $\delta^{18}O_{PO4}$ of P naturally occurring in 8Lt of Poole's Cavern drip-waters collected on 26/03/2021 (+20.2 ±0.5‰). The in-cave temperature at the time the

brucite precipitation was 7.2 ±0.2 °C, and coincidently the same as the cold-store temperature in LEC during the previous equilibration experiment.

The range of $\delta^{18}O_{PO4}$ between 30 °C and 7 °C (±5.1‰) presented in Figure 6.1 is strikingly comparable to that expected for the same temperature range as presented in the literature: ±6.1‰ (McLaughin et., 2004) to ±4.4‰ (Chang et. al., 2015). This gives good justification that the range of data we are seeing is realistic and indicative of PPase turnover of orthophosphate to equilibrium with temperature.

However, compared to the literature, $\delta^{18}O_{PO4}$ values are consistently more positive. Ranging from +15.5‰ to +20.61‰, where they would have been expected to range from +13.5‰ to +18.0‰ according to Chang et. al., 2015. This could be due to:

a. A fraction of the PDOF not being fully turned over to equilibrium with temperature, meaning a portion of the phosphate-oxygen pyrolysed is being biased towards the starting value of PDOF (+18.2 ±0.4‰).
b. Other O sources being pyrolysed (e.g. calcite, sulphate, nitrate) that is biasing the data.
c. Or, more likely, the high pH chemistry of Poole's Cavern drip-waters is biasing the data positively compared to other literature which has been undertaken at neutral pH (e.g., Chang & Blake, 2015).

There is a poor relationship $\delta^{18}O_{PO4}$ and temperature at 4 °C, which does not conform to the linear relationship observed between 7 to 30 °C. This is likely related to the low temperature reducing the ability for enzymes to turnover phosphate to equilibrium with temperature.

6.1.2 TRENDLINE BETWEEN TEMPERATURE AND $\delta^{18}O_{PO4}$ IN POOLE'S CAVERN WATERS AT 100-ppb:

A linear trendline was used to display the relationship between $\delta^{18}O_{PO4}$ and temperature (Figure 6.1). This allows the relationship to be represented as an equation, mirroring existing equations in the literature (Longinelli & Nuti, 1973., McLaughin, et. al., 2004., Pucéat et. al., 2010., Chang et. al., 2015).

6.1.2.1 Results retracted from the trendline

Out of the dataset, the following readings were deducted from this trendline for the following reasons:

a) **4°C Fridge Temperatures (Keyworth Fridge 4°C 25/01/21 and LEC Lab Fridge 4°C 30/07/21):** The incubations taken at 4°C consistently produced data that didn't plot along the linear trend of warmer temperatures. This was likely due to the temperature causing unfavourable enzymatic conditions, meaning that phosphate is not readily being overturned by microbes to equilibrium with temperature. Temperatures around 4°C in caves are limited to high-altitude (e.g. Alpine) and polar environments, and not commonly found in many terrestrial caves including those in the UK. For this reason, while the 4°C data cannot be dismissed for being unrepresentative of a typical cave environment, the results represented in this study may define a phosphate-oxygen-temperature relationship that is true for temperate or tropical cave systems.

b) **Keyworth incubator 16 °C 25/01/21 (+15.50‰):** Only enough silver phosphate could be obtained to provide one reading in this instance. For this reason, the range of potential error could not be evaluated. A repeat of these experiment yielded triplicate results that fit the expected relationship to temperature.

c) **Poole's In Cave Temp 1 25/01/2021 (22.60 ±2.30) and Poole's In-Cave Temp 2 18/02/21 (22.03 ±3.27):** These are repeat readings from the same silver phosphate sample of 100-ppb of P stored in a container that was left in Roman Chamber over the Christmas period at 8.1 ±0.85 °C. The results showed 1 high O % reading from 25/01/2021, which was retracted, leaving 2 sets of 2 data-points that exhibit a very wide analytical range in $\delta^{18}O_{PO4}$ value: ±3.2‰ (25/01/2021) and ±4.63‰ (18/02/2021). This much isotopic variation would only be expected over a ±23.15 °C change in temperature and is likely being caused by the pyrolysis of contaminant oxygen sources. Moreover, due to the Coronavirus pandemic, the water was left to equilibrate for much longer than other experiments (8 weeks). There was also poor temperature control between the time when the water was removed from the cave and Brucite precipitation in the lab. In later in-cave experiments, the Brucite was precipitated in the cave to mitigate this.

POOLE'S CAVERN PHOSPHATE-OXYGEN ISOTOPES 100 PPB

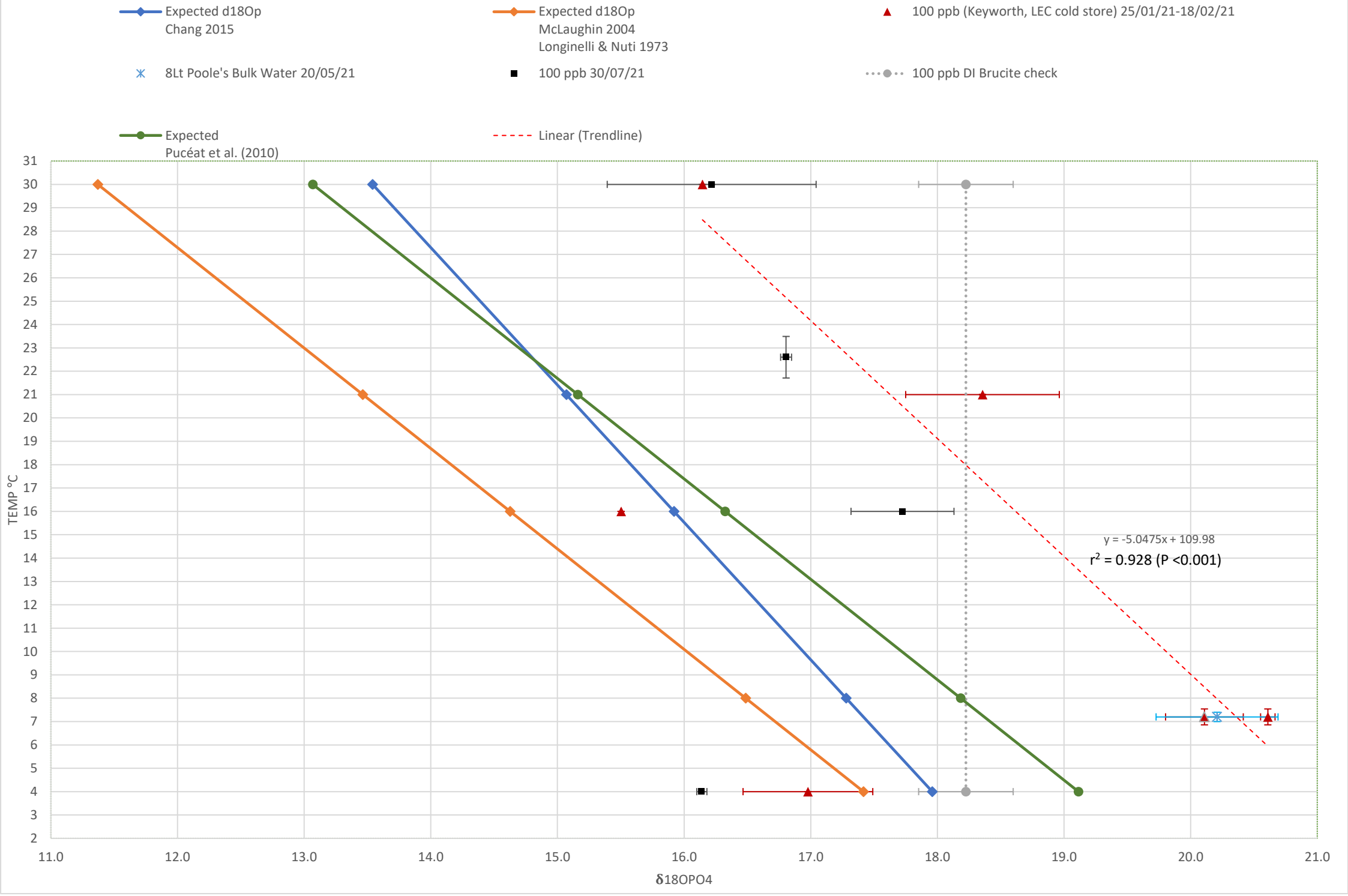

Figure 6.1: Phosphate-oxygen-isotope temperature relationship of Poole's Cavern waters spiked to 100-ppb. Data obtained from experiments undertaken at BGS Keyworth (25/01/21, 18/02/21), repeats at LEC (30/07/21) and two results from spiked waters left sealed in Poole's Cavern. Included is a result for 8Lt of un-spiked Poole's Cavern water, thought to represent in-cave temperature composition. Control data shows values for 100-ppb of potassium dihydrogen orthophosphate (PDOF) dissolved in boiled DI water and processed to silver phosphate (+18.2 ±0.4‰). Error bars added for ±1 SD phosphate-oxygen and temperature range. Solid lines denote the phosphate-oxygen-temperature relationship expected results, as calculated from equations in Chang & Blake., 2015, Longinelli & Nuti, 1973., and Pucéat et. al., 2010.

6.2 POOLE'S CAVERN PHOSPHATE-OXYGEN-ISOTOPE TEMPERATURE RELATIONSHIP WITH 400-ppb P

Due to low silver-phosphate yields in preliminary 100-ppb P experiments, it was decided to increase the potassium dihydrogen orthophosphate (PDOF) concentration being dosed into the Poole's Cavern drip-waters to 400-ppb P. The aim was to guarantee that adequate silver-phosphate was being precipitated to allow triplicate isotopic readings. This was justified as P concentrations >400-ppb are often found within cave environments, and it was thought that microbes would still be able to overturn this concentration of P to equilibrium with temperature.

A large series of experiments were made using 400-ppb P with several repeat tests to ensure repeatability. This was done at the following temperatures: 4°C, 7.2 to 8 °C, 16 °C, 20 to 23 °C and 31 to 38 °C. Bulked-water was also dosed and left inside Poole's Cavern at 7.2 °C.

Unfortunately, while 400-ppb P yielded adequate silver phosphate volumes, the isotopic results suggest a perturbed relationship to temperature. This is shown in Figure 6.2, using the raw data, and Figure 6.3 as a moving average of this data grouped by temperature. This suggests that there is an upper concentration limit for dissolved orthophosphate in cave drip-waters, after which the phosphate-oxygen-temperature relationship ceases to exist.

6.2.1 RELATIONSHIP BETWEEN TEMPERATURE AND $\delta^{18}O_{PO4}$ IN POOLE'S CAVERN WATERS AT 400-ppb

Nearly all $\boldsymbol{\delta}^{18}O_{PO4}$ results at 400-ppb are near to the initial value of +18.2 (±0.4)‰, that represents PDOF in boiled DI water and the likely starting value for $\boldsymbol{\delta}^{18}O_{PO4}$ to deviate from (Figure 6.2). This is contrast to 100-ppb, where the results significantly deviate both sides of PDOF according to temperature.

There is no statistical relationship between $\boldsymbol{\delta}^{18}O_{PO4}$ and temperature at 400-ppb (Figure 6.2). Most values are within ±1 SD of each other, with a generally wide range at each incubation temperature.

Statistics 1 – Pearson's r Correlation:

r = 0.27 (p >0.05 n=45) suggesting there is no correlation between $\delta^{18}O_{PO4}$ and temperature.

Statistics 2 – Regression analysis:

R^2 = 0.074 (p >0.05 n=45) suggesting that only 7.4 % of our data can be explained by a correlation between $\delta^{18}O_{PO4}$ and temperature.

The likely reason for this is due to the higher concentration of P exceeding the processing capacity of PPase and microbe needs. These leads to a portion of PDOF that is in excess and does not get overturned by microorganisms, meaning that equilibrium to temperature is never reached. In this case, enzymatic activity which drives isotopic equilibration according to temperature will not be detected given the large pool size of phosphate-oxygen available to measure.

POOLE'S CAVERN PHOSPHATE OXYGEN ISOTOPES 400PPB

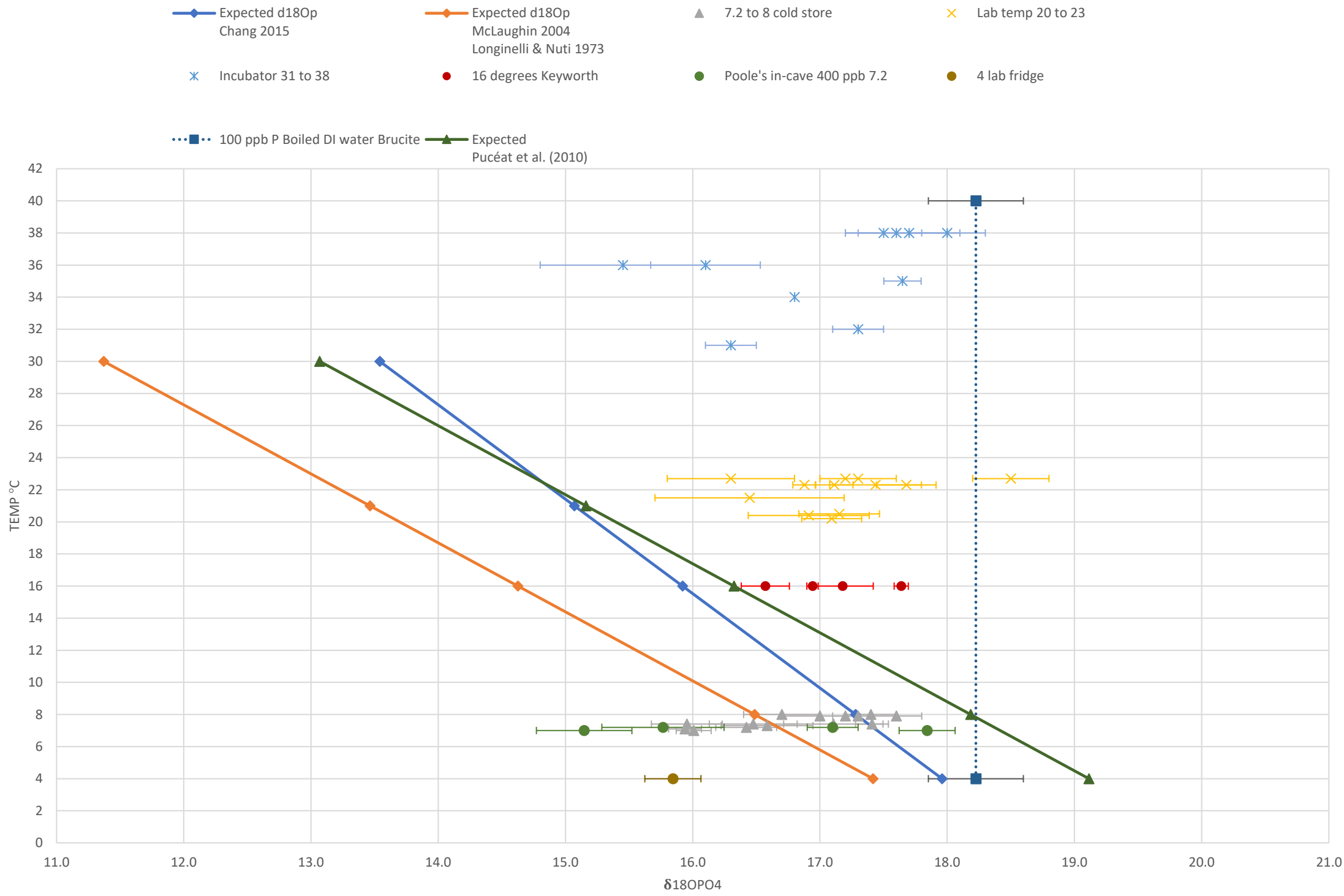

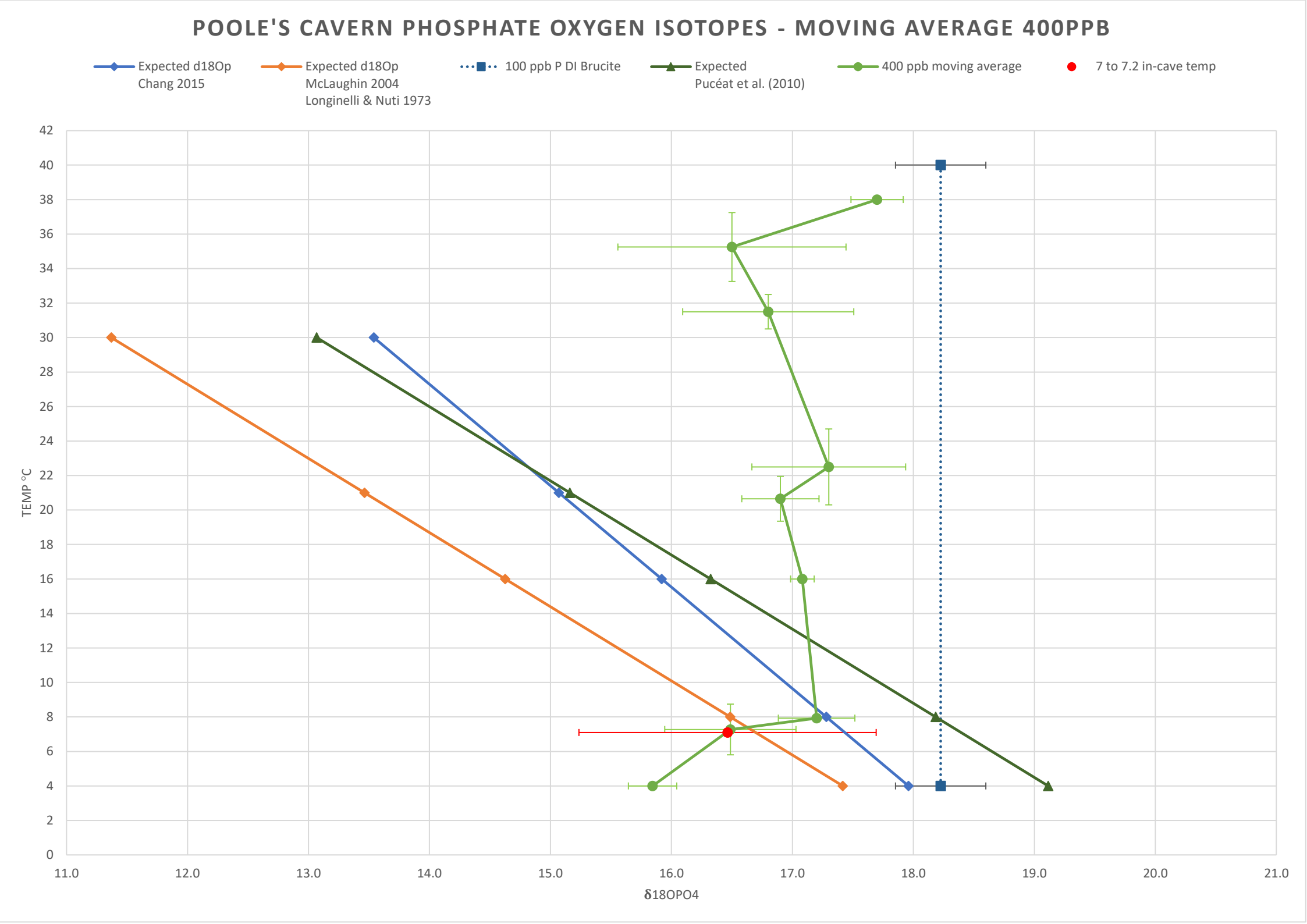
POOLE'S CAVERN PHOSPHATE OXYGEN ISOTOPES - MOVING AVERAGE 400PPB
Expected d18Op Chang 2015
Expected d18Op McLaughin 2004 Longinelli & Nuti 1973
100 ppb P DI Brucite
Expected Pucéat et al. (2010)
400 ppb moving average
7 to 7.2 in-cave temp
TEMP °C
δ18OPO4
0
2
4
6
8
10
12
14
16
18
20
22
24
26
28
30
32
34
36
38
40
42
11.0
12.0
13.0
14.0
15.0
16.0
17.0
18.0
19.0
20.0
21.0

Figure 6.2: Phosphate-oxygen-temperature relationship of Poole's Cavern waters spiked to 400-ppb and left to equilibrate for 0-11 days over a grouped range of temperatures: 4°C, 7.2 to 8 °C, 16 °C, 20 to 23 °C, 31 to 38 °C, and an in-cave temperature of 7.2 °C. Error bars denote ±1 SD. Mixture of results conducted at LEC on 08/03/21 to 06/06/21 and 30/07/21. Control line shown for 100-ppb brucite from boiled DI water (+18.2 ±0.4‰). Solid lines denote the phosphate-oxygen-temperature relationship expected results, as calculated from equations in Chang et. al., 2015, McLaughin et. al., 2004 and Pucéat et. al., 2010.

Figure 6.3: A moving average of the phosphate-oxygen-temperature relationship of Poole's Cavern waters, spiked to 400-ppb and left to equilibrate for 0-11 days over a range of temperatures, with datapoints (n=9) grouped by temperature: 4°C, 7.0-7.4 °C, 7.9-8 °C, 16.0 °C, 20.2-21.5 °C, 22.3-22.7 °C, 31.0-32.0 °C, 34.0-36.0 °C, 38°C and an in-cave temperature of 7.0-7.2 °C. Error bars denote ±1 SD. Mixture of results conducted at LEC on 08/03/21 to 06/06/21 and 30/07/21. Control line shown for 100-ppb brucite from boiled DI water (+18.2 ±0.4‰). Solid lines denote the phosphate-oxygen-temperature relationship expected results, as calculated from equations in Chang et. al., 2015, McLaughin et. al., 2004 and Pucéat et. al., 2010.

6.3 WHITE SCAR CAVE DRIP-WATERS PHOSPHATE-OXYGEN-ISOTOPE TEMPERATURE RELATIONSHIP

As a comparison to Poole's Cavern, drip-waters from White Scar Cave were also equilibrated under similar conditions, but over a shorter period (72 hrs). This was done because, unlike the hyperalkaline drip-waters of Poole's Cavern, the drip-waters of White Scar are of mild alkalinity, and therefore represent the more typical speleothem chemistry found in most cave environments. Enough water was collected for several experiments at 400-ppb P (4, 8, 22, 31-32 ^{o}C), and two triplicate readings at 8 ^{o}C and 16 ^{o}C. The shorter incubation time was chosen based on the initial results of 100-ppb Poole's Cavern waters, and the fact that microbial overturn of orthophosphate often occurs in <3 days (Chang & Blake, 2015).

6.3.1 THE RELATIONSHIP BETWEEN TEMPERATURE AND $\delta^{18}O_{PO4}$ IN WHITE SCAR AT 400-ppb P:

Other than at 4 °C, most phosphate-oxygen isotope ($\delta^{18}OPO_4$) results are within error of the initial PDOF value of +18.2 (±0.4)‰.

There is no evidence for a statistical relationship between $\delta^{18}OPO_4$ and temperature at 400-ppb in White Scar drip-waters. Most values are within error (±1 SD) of each other.

Statistics 1 – Pearson's r correlation:

r = 0.37 (p >0.05 n=13) suggesting there is a no correlation between phosphate-oxygen and temperature.

Statistics 2 – Regression analysis:

R^2 = 0.14 (p >0.05 n=13) suggesting that only 14 % of our data can be explained by a correlation between phosphate-oxygen and temperature.

Again, the likely reason for this lack of a relationship between $\delta^{18}OPO_4$ and temperature is due to the higher concentration of P exceeding the processing capacity of PPase and microbial requirements. This leads to a portion of PDOF that is in excess and does not get overturned by microorganisms, meaning that equilibrium to temperature is never reached. In this case, enzymatic activity which drives isotopic equilibration according to temperature will not be detected given the large pool size of phosphate-oxygen available to measure.

At lower temperatures, $\boldsymbol{\delta}^{18}O_{PO4}$ hovers in a region that could be expected according to the literature (e.g. McLaughin et. al., 2004., Chang et. al., 2015 shown by the solid lines Figure 6.4). This creates a conflicting hypothesis, where the $\boldsymbol{\delta}^{18}O_{PO4}$ values are following what would be expected in the literature at low temperatures but being unable to overturn orthophosphate effectively at warmer temperatures. However, considering that the $\boldsymbol{\delta}^{18}O_{PO4}$

values have been shown not to deviate much with temperature, and the wide error (±1 SD), this overlap is most likely to be coincidental due to the PDOF value of +18.2 (±0.4)‰ overlaps the literatures regression lines.

6.3.2 WHITE SCAR RESULTS AT 100-ppb P:

As with 400-ppb, isotope values at 100-ppb P do not deviate far from the PDOF value. This suggests a lack of isotopic fractionation in general, which could be a sign of low microbial activity or at least poor turnover of orthophosphate.

There is no variation in $\boldsymbol{\delta}^{18}O_{PO4}$ between 400-ppb and 100-ppb at 8 °C. +17.8 ±0.3‰ is the same as the spectrum of values at 400-ppb (range +16.5 to +18.1‰). Again, this matches very nicely to what would be expected from the literature at this temperature (e.g. McLaughin et. al., 2004., Chang et. al., 2015 shown by the solid lines in Figure 6.4).

The 16 °C value at 100-ppb (18.7 ±0.2) is within error of the initial PDOF value of +18.2 (±0.4)‰. This suggests a lack of microbial fractionation of orthophosphate at 16 °C.

By averaging the data presented in Figure 6.4, the above observations can be summarised (Figure 6.5). All values are within error of each other (±1 SD), except for the 100-ppb value at 16 °C (+18.7 ±0.2), which is within error of PDOF. This suggests a poor relationship exists between $\boldsymbol{\delta}^{18}O_{PO4}$ and temperature in White Scar waters, complementing our statistical analysis.

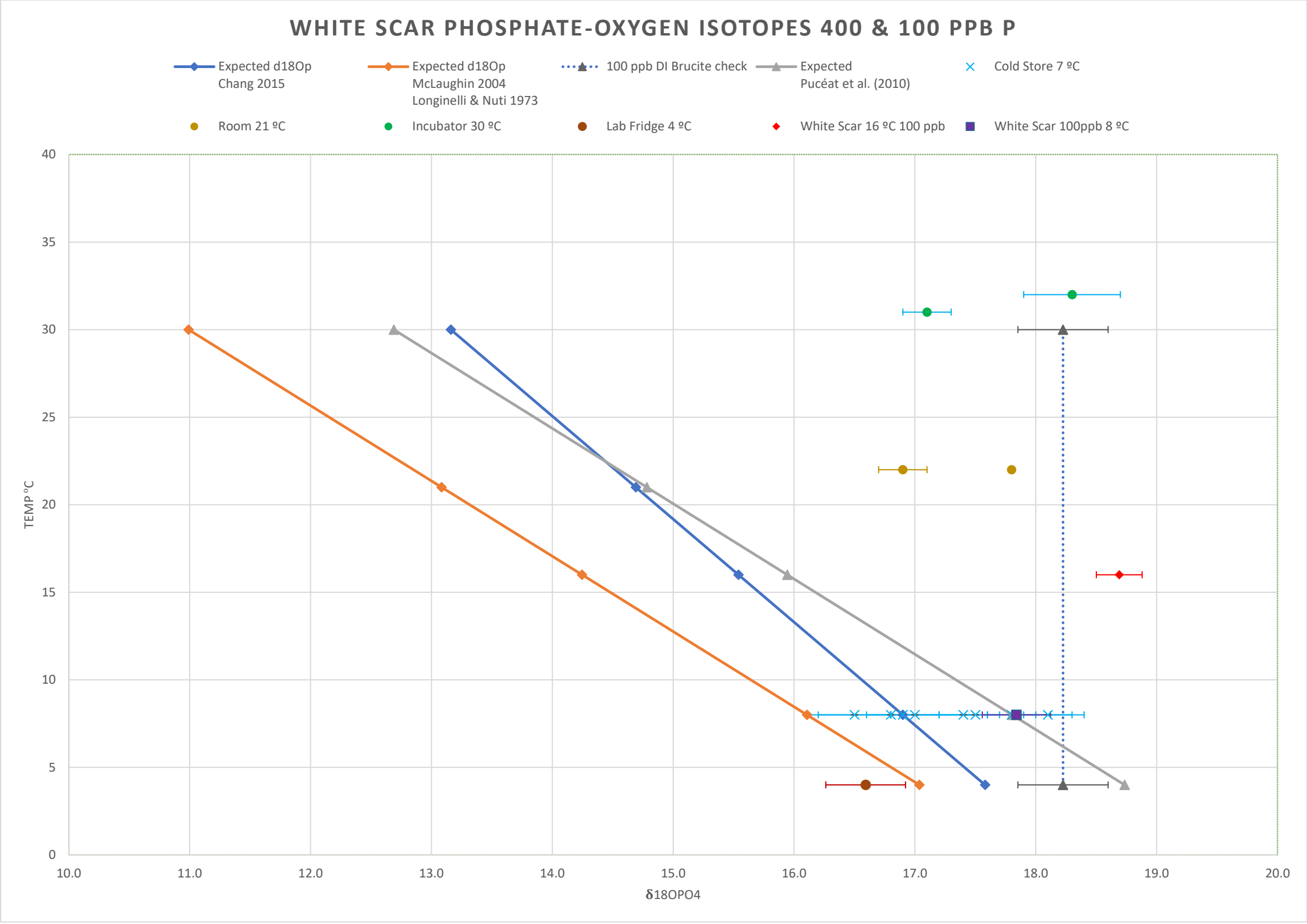
WHITE SCAR PHOSPHATE-OXYGEN ISOTOPES 400 & 100 PPB P
Expected d18Op Chang 2015
Expected d18Op McLaughin 2004 Longinelli & Nuti 1973
100 ppb DI Brucite check
Expected Pucéat et al. (2010)
Cold Store 7 ºC
Room 21 ºC
Incubator 30 ºC
Lab Fridge 4 ºC
White Scar 16 ºC 100 ppb
White Scar 100ppb 8 ºC
TEMP °C
δ18OPO4
0
5
10
15
20
25
30
35
40
10.0
11.0
12.0
13.0
14.0
15.0
16.0
17.0
18.0
19.0
20.0

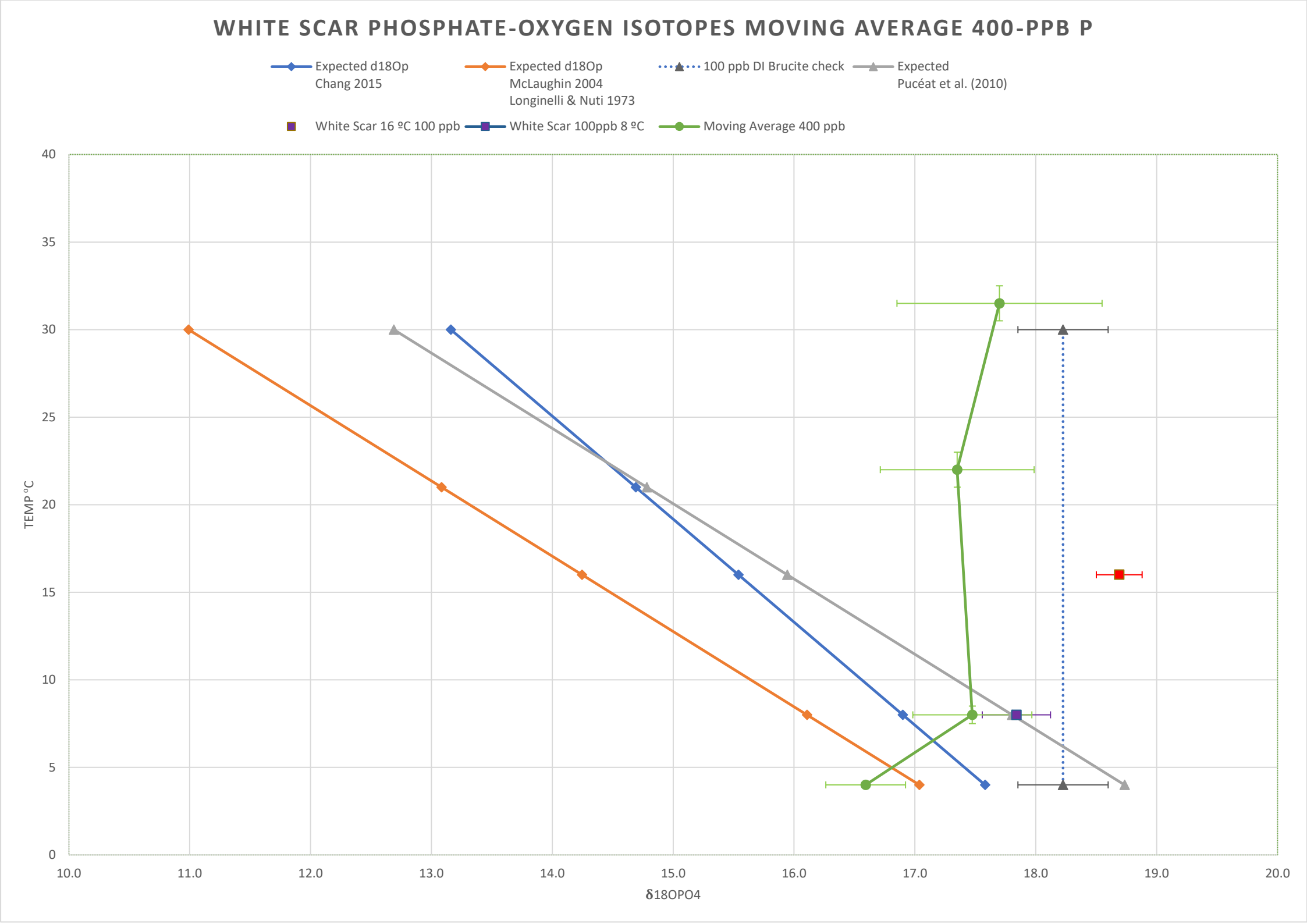
WHITE SCAR PHOSPHATE-OXYGEN ISOTOPES MOVING AVERAGE 400-PPB P
Expected d18Op Chang 2015
Expected d18Op McLaughin 2004 Longinelli & Nuti 1973
100 ppb DI Brucite check
Expected Pucéat et al. (2010)
White Scar 16 ºC 100 ppb
White Scar 100ppb 8 ºC
Moving Average 400 ppb
TEMP °C
δ18OPO4
0
5
10
15
20
25
30
35
40
10.0
11.0
12.0
13.0
14.0
15.0
16.0
17.0
18.0
19.0
20.0

Figure 6.4: Phosphate-oxygen temperature relationship of White Scar waters spiked to 400 & 100-ppb and left to equlibrate for 0-3 days. Mixture of results conducted at LEC on 17/06/21 and 30/07/21. Control line shown for 100-ppb brucite from boiled DI water (+18.2 ±0.4‰). Solid lines denote the phosphate-oxygen-temperature relationship expected results, as calculated from equations in Chang et. al., 2015, McLaughin et. al., 2004 and Pucéat et. al., 2010.

Figure 6.5: A moving average of the phosphate-oxygen-temperature relationship of White Scar waters, spiked to 400-ppb (n=4) and 100-ppb (n=2) and left to equilibrate for 3 days over a range of temperatures: 4°C, 7-8 °C, 16.0 °C, 22 °C and 31.0-32.0 °C. Error bars denote ±1 SD. Mixture of results conducted at LEC on 17/06/21 and 30/07/21. Control line shown for 100-ppb brucite from boiled DI water (+18.2 ±0.4‰). Solid lines denote the phosphate-oxygen-temperature relationship expected results, as calculated from equations in Chang et. al., 2015, McLaughin et. al., 2004 and Pucéat et. al., 2010.

6.4 PHOSPHATE OXYGEN ISOTOPE EQUILIBRATION EXPERIMENTS

Phosphate-oxygen isotopes ($\boldsymbol{\delta}^{18}O_{PO4}$) are known to take time to equilibrate to the ambient temperature via isotopic exchange between phosphate and water oxygen. Based on the literature, this equilibration period has been determined to range between 12 hrs to 5 days (Chang & Blake, 2015). However, those experiments were based on laboratory grade pyrophosphatase (PPase) under optimum psychochemical conditions. The equilibration experiments undertaken as a part of this project were designed to evaluate the change in $\boldsymbol{\delta}^{18}O_{PO4}$ over time with drip-waters from Poole's Cavern (pH 11-12) and White Scar Cave (pH 8), after the addition of 400-ppb P as potassium dihydrogen orthophosphate (PDOF). Incubation temperatures included 7.0-7.4 ^{o}C, 16 ^{o}C, 20.2-22.3 ^{o}C, and 34-36 ^{o}C, taking aliquots periodically with an emphasis on the first 24hrs (0, 4, 8, 12, 24, 48, 72, 264 hrs.). A repeat set of experiments was made at 30 ^{o}C and 8 ^{o}C for 24 and 72 hrs to duplicate some results.

It was hypothesised that 0hr $\boldsymbol{\delta}^{18}O_{PO4}$ would begin near PDOF (+18.2 (±0.4)‰) and deviate from this value over time as microbes metabolise PDOF. As this temperature-fractionation by PPase takes place, the final value for each sample was expected to slowly equilibrate to temperature.

6.4.1 EQUILIBRATION EXPERIMENTS IN POOLE'S CAVERN WATERS AT 400-ppb P:

All temperatures have 0hr $\boldsymbol{\delta}^{18}O_{PO4}$ values that deviate slightly from the expected starting value of +18.2 (±0.4)‰. This ranges from +16.0 (±0.3)‰ at 7.4 ^{o}C to +17.7 (±0.2)‰ at 22.3 ^{o}C (Figure 6.6).

The overall range of $\boldsymbol{\delta}^{18}O_{PO4}$ is very limited, with ±2.2‰ between the highest and lowest values recorded irrespective of temperature. According to the literature, a variation of ±6.5‰ (McLaughin et., 2004) to ±4.4‰ (Chang and Blake, 2015) would be expected in this temperature range. This contrasts with 100-ppb data presented in section 6.1, where total variation is ±5.1‰ and much more comparable to the literature.

There appears to be no consistent temperature control on $\boldsymbol{\delta}^{18}O_{PO4}$ throughout the equilibration phase with 400-ppb P additions. This suggests PPase activity is having an insignificant effect on the $\boldsymbol{\delta}^{18}O_{PO4}$ signature and likely stems from the replete 400-ppb pool size of available phosphate.

6.4.2 EQUILIBRATION EXPERIMENTS IN WHITE SCAR CAVE AT 400-ppb P

Most $\boldsymbol{\delta}^{18}O_{PO4}$ values do not deviate far from the initial PDOF value of +18.2 (±0.4)‰ over time, with many overlapping when considering ±1 SD (Figure 6.7). Moreover, at 72hr, $\boldsymbol{\delta}^{18}O_{PO4}$ at 8 ^{o}C, 22 ^{o}C, and 31-32 ^{o}C returns to this initial PDOF value. This suggests that temperature is having little to no effect on $\boldsymbol{\delta}^{18}O_{PO4}$ fractionation at 400-ppb, and that orthophosphate is not likely being metabolised in a significant way. Any fluctuations are more likely to be due to minor variability in environmental conditions, or processing variability between each sample.

In general, there is very small range of $\boldsymbol{\delta}^{18}O_{PO4}$ values recorded with ±1.8‰ between the highest and lowest values recorded irrespective of temperature. According to the literature, we would expect a variation of ±6.7‰ (McLaughin et., 2004) to ±4.4‰ (Chang et. al., 2015) in this temperature spectrum.

This lack of temperature or time control on equilibration at 400-ppb P indicates minimal impact of enzymatic activity on phosphate-oxygen equilibration with water. This is typical of a system where the phosphate is replete and thus the pool size prevents the expression of pyrophosphatase turnover to equilibrium.

POOLE'S CAVERN 400-PPB EQUILIBRATION 08/03/21 TO 19/03/21, 05/06/21 TO 06/06/21

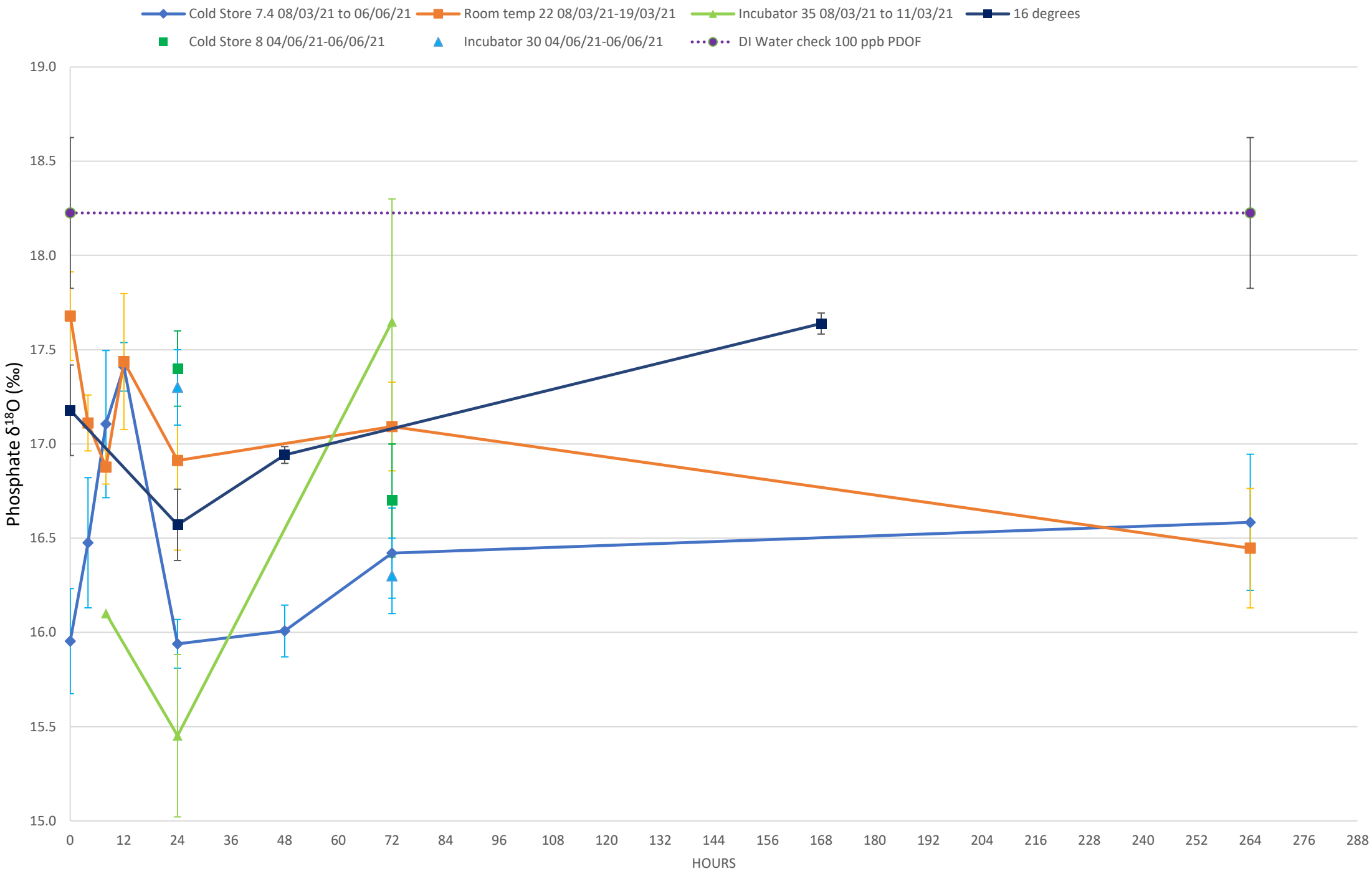

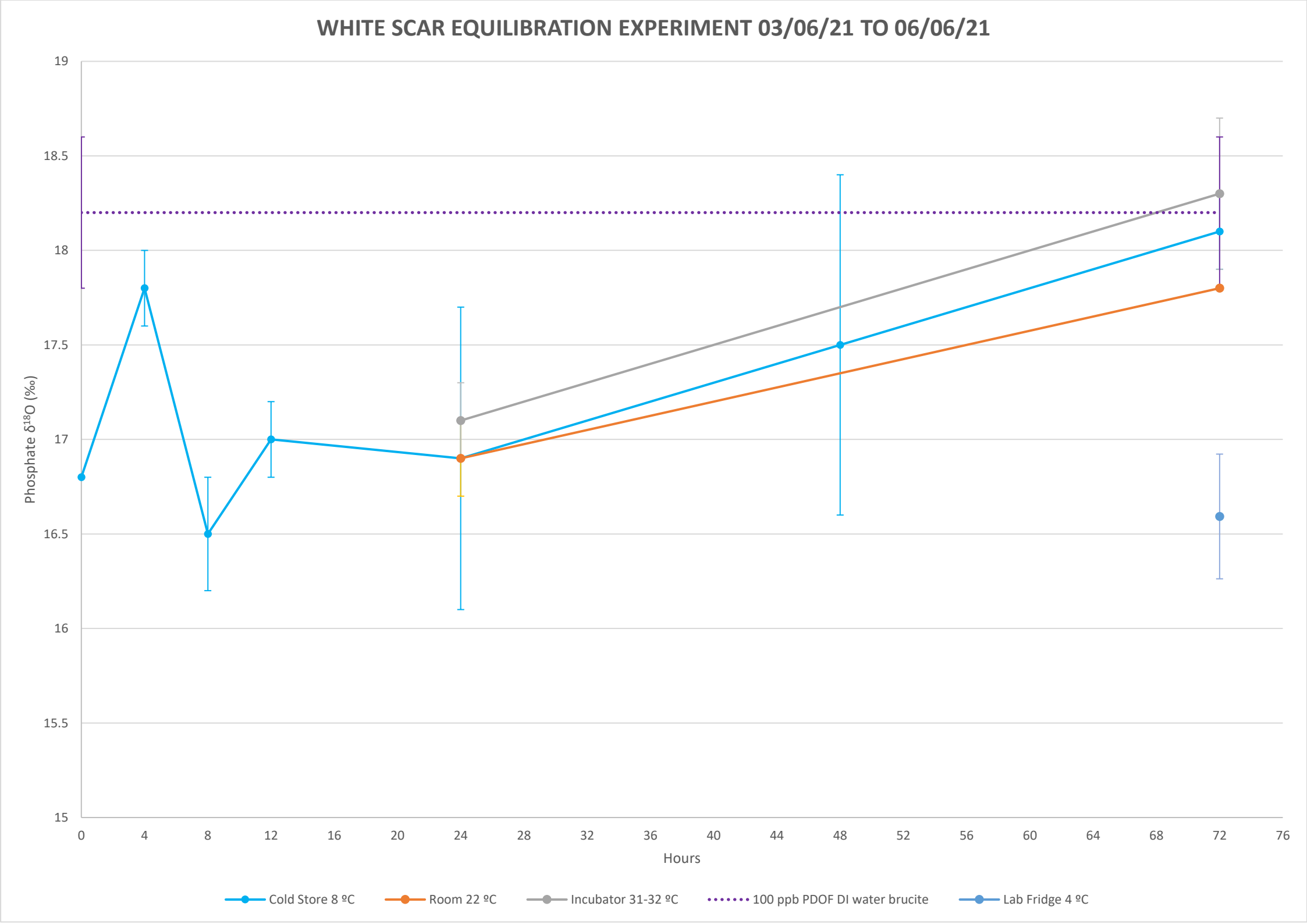
WHITE SCAR EQUILIBRATION EXPERIMENT 03/06/21 TO 06/06/21
Phosphate δ18O (‰)
19
18.5
18
17.5
17
16.5
16
15.5
15
0
4
8
12
16
20
24
28
32
36
40
44
48
52
56
60
64
68
72
76
Hours
Cold Store 8 ºC
Room 22 ºC
Incubator 31-32 ºC
100 ppb PDOF DI water brucite
Lab Fridge 4 ºC

Figure 6.6: Equilibration experiments conducted between 08/03/21 to 11/03/21 at 7.0-7.4 ºC, 16 ºC, 20.2-22.3 ºC, and 34-36 ºC. Also included is 24, 48hr repeats at 8 and 30 ºC on 04/06/21 to 06/06/21. Poole's Cavern drip-water was dosed with 400-ppb of potassium dihydrogen orthophosphate (PDOF) and incubated at different temperatures for up to 11 days, removing brucite aliquots at 0, 4, 8, 12, 24, 48, 72, 264 hr intervals. Error bars given in ±1 SD. Included is a control line for 100-ppb PDOF in boiled DI water (+18.2 ±0.4‰) representing the ideal starting value.

Figure 6.7: Equilibration experiments conducted between 03/06/21 to 06/06/21 at 8 ºC, 22 ºC, and 31-32 ºC. White Scar drip-water was dosed with 400-ppb of potassium dihydrogen orthophosphate (PDOF) and incubated at different temperatures for 72hrs, removing brucite aliquots at 0, 4, 8, 12, 24, 48 and 72 hr intervals. Error bars given in ±1 SD. Included is a control line for 100-ppb PDOF in boiled DI water (+18.2 ±0.4‰) representing the ideal starting value.

7 - RESULTS 4: ANALYSIS OF PHOSPHATE OXYGEN ISOTOPE DATA CONTAINED WITHIN CONTEMPORARY SPELEOTHEM CALCITE

As well as speleothem drip-waters, phosphate-oxygen-isotope ($\boldsymbol{\delta}^{18}O_{PO4}$) data was collated from calcite material. This includes in-lab grown calcite material from Poole's Cavern drip-waters dosed to 100 & 400-ppb with potassium dihydrogen orthophosphate (PDOF), natural calcite from Poole's Cavern and two contemporary speleothem samples grown in the last 100-yrs but in different climatic regions: Rukiesa Cave, Ethiopia (18.93 ±0.61 °C) and Brown's Folly Mine, UK (10 °C ± 0.4 °C).

The aim of these experiments was to see if a $\boldsymbol{\delta}^{18}O_{PO4}$ temperature signal could be successfully translated into calcite material without further alteration. This opens the potential for $\boldsymbol{\delta}^{18}O_{PO4}$ to be used as a novel speleothem palaeothermometer.

7.1 NATURAL CALCITE $\delta^{18}O_{PO4}$ DATA

7.1.1 Calcite $\delta^{18}O_{PO4}$ values

Data pertaining to natural calcite grown within three different cave sites with contrasting environmental conditions are presented within Table 7.1.

All measured $\delta^{18}O_{PO4}$ values are within ±1 SD of each other, showing no distinct variation with sample type, source, or temperature. On first assessment this suggests there is no distinct relationship between $\delta^{18}O_{PO4}$ and temperature and, more significantly, suggests there is mechanism that is fractionating all values in a similar way into the +21.1 to +21.4‰ range. The reason for this could be due to contamination from non-phosphate O sources during sample prep, including calcite, sulphate, and nitrate (Nisbeth et. al., 2019), all of which are present in these calcite samples. During brucite dissolution in acid, these contaminants are of particular concern and can become incorporated into silver phosphate (Nisbeth et. al., 2019).

7.1.2 Compared to estimated $\delta^{18}O_{PO4}$ values from the literature

However, when using the equations provided in the literature to calculate the predicted $\delta^{18}O_{PO4}$, we see that predicted values for Rukiesa Cave are close to those expected from the combination of temperature and $\delta^{18}O_{H2O}$ composition (Table 7.1). Predicted $\delta^{18}O_{PO4}$ by Longinelli & Nuti 1973 for Rukiesa Cave (+21.2‰) is identical to our measurement. Chang & Blake, 2015 and Pucéat et al., 2010 are +1.4 to +1.7‰ from the recorded value respectively. This correlation is good evidence to suggest that +21.2 (SD ±0.2)‰ is a valid reading for Rukiesa Cave. Conversely, the same cannot be said for Brown's Folly Mine where the recorded value of +21.2 (SD ±0.4)‰ is underrepresented in predictions from the literature. At best, Pucéat et al., 2010 estimates $\delta^{18}O_{PO4}$ as +18.6‰ for the in-cave temperature (10 °C ± 0.4) and estimated $\delta^{18}O_{H2O}$ (-6.7‰). This divergence is significant even when accounting for ±1 SD.

Unlike Poole's Cavern waters, pH is not a valid reason for this discrepancy as it is within range of Rukiesa Cave. This suggests there is no distinct relationship between $\delta^{18}O_{PO4}$ and temperature and, more significantly, suggests there is a mechanism that is fractionating all values in a similar way into the +21.1 to +21.4‰ range. Furthermore, this view would also negate the validity of $\delta^{18}O_{PO4}$ in Rukiesa cave expressing a genuinely 'correct' value.

However, the Brown's Folly Mine value may be suspect as it is not known how much phosphate concentration exists in the calcite. It is possible that very low concentrations of P exist, meaning that O is likely to be coming from alternative sources such as nitrate. This contrasts with Rukiesa Cave calcite which contains 130-375 ppb of PO_4-P (Baker et. al., 2007). Moreover, $\delta^{18}O_{PO4}$ was calculated without an in-cave $\delta^{18}O_{H2O}$ value. Instead, data was averaged from Wallingford, UK between 1979 and 1996 through the GNIP database at -6.7‰ (IAEA/WMO, 2021). This should provide a fair estimation for in-cave $\delta^{18}O_{H2O}$, but might not be exactly comparable.

7.1.3 Poole's Cavern $\delta^{18}O_{PO4}$ data

As with Brown's Folly Mine, the averaged in-cave calcite $\delta^{18}O_{PO4}$ value for Poole's Cavern (+21.4 ±0.4‰) differs to what would be expected in the literature (Table 7.1). However, when we take drip-water $\delta^{18}O_{PO4}$ into account (Table 7.2) we see that there is only a ±1‰ difference between drip-water, soil samples, laboratory incubations and in-cave calcite all at the 7.2 °C conditions found in Poole's Cavern. This is good evidence of a successful transfer of a phosphate-oxygen-temperature signal between drip-water and calcite phases with minimal (+1‰) fractionation following precipitation. Considering this, a pH fractionation mechanism is the most plausible reason for the over difference in recorded $\delta^{18}O_{PO4}$ and hypothesised $\delta^{18}O_{PO4}$ from the literature.

7.2 SYNTHETIC CALCITE FROM POOLE'S CAVERN DRIP-WATER

Synthetic stalagmite calcite was grown over 4-weeks to assess the impact of temperature on $\boldsymbol{\delta}^{18}O_{PO4}$ and its transfer into the calcite deposit. For this, drip-water from Poole's cavern dosed with PDOF was used to enable sufficient calcite to be precipitated over short a short experimental period. Data pertaining to experimental conditions at room temperature and concentrations of added PDOF to values of 400-ppb P and 100-ppb P are displayed below in Table 7.3.

All values are greater than the +18.2 ±0.4‰ PDOF value. This suggests a mechanism that is isotopically enriching $\boldsymbol{\delta}^{18}O_{PO4}$ from the expected starting value conversely to what was seen in the waters at the same temperature. For example, the Poole's lab-precipitated calcite plates are +4.3 to +4.8‰ compared to the corresponding drip-waters at similar temperatures (+16.8 ±0.04‰ at 22.6 ºC) which itself is significantly lower than PDOF. Secondly, the $\boldsymbol{\delta}^{18}O_{PO4}$ values from synthetic calcite are almost identical to those found in Poole's Cavern, despite a 14 ºC difference between in-cave and laboratory temperatures. There is also no discernible difference between the calcite plates grown with 400-ppb of PDOF (+21.4 ±0.14‰) and 100-ppb of PDOF (+21.1 ±0.36‰). This suggests that both temperature and phosphate concentration is having little effect on $\boldsymbol{\delta}^{18}O_{PO4}$ values.

This evidence suggests a complete disconnect from any biotic fractionation mechanism in our synthetic calcite plates. This, and knowing that inorganic fractionation of $\boldsymbol{\delta}^{18}O_{PO4}$ does not readily occur, gives weight to the argument that alternative O sources have been incorporated into silver phosphate during sample processing that must be biasing readings. Or that the dynamics of calcite precipitation (temperature, rate, humidity, CO_2 concentration) are affecting P incorporation into calcite between in-cave and laboratory environments.

7.3 CONCLUSION

While there has been good success finding evidence for PPase fractionation of temperature in Poole's Cavern drip-waters, the translation into calcite samples is not so clear cut. There are several lines of discussion moving forward.

On one hand the tight relationship between $\boldsymbol{\delta}^{18}O_{PO4}$ in Poole's Cavern in-cave calcite, natural P in drip-waters, equilibrated 100-ppb experiments and soil P is good evidence for a phosphate-oxygen-temperature signal of 7.2 ºC translating between the water isotope and calcite isotope phases. The overall positive offset compared to the literature is likely driven by a pH effect. Then there is compelling evidence that a bona-fide $\boldsymbol{\delta}^{18}O_{PO4}$ reading has been taken for Rukiesia Cave, as predicted by the literature. The inference here is that the literature becomes a good analogue for a typical cave environment, given the more neutral pH in contrast with Poole's Cavern.

However, there is then evidence to the contrary. For example, it would be expected that $\boldsymbol{\delta}^{18}O_{PO4}$ for Brown's Folly Mine would also follow the literature, as extreme pH is not a factor, however predicted $\boldsymbol{\delta}^{18}O_{PO4}$ is poorly represented in the literature. This then raises concerns that all the +21 calcite $\boldsymbol{\delta}^{18}O_{PO4}$ values are the same due to contaminant O-sources being incorporated during sample processing. However, without an in-cave measurement, there is poor $\boldsymbol{\delta}^{18}O_{H2O}$ control on for Brown's Folly Mine, and it is unknown how much P might naturally be in the sample in the first place. Finally, there seems to be a disconnect between expected $\boldsymbol{\delta}^{18}OPO_4$ for natural calcite and synthetic calcite in Poole's Cavern which have the same values despite forming at very different temperatures. This puts weight on the argument that non-PO_4 oxygen sources are being incorporated during sample preparation.

Cave	Sample	pH	Ambient Temperature °C	$\delta^{18}O_{H2O}$ ‰	$\delta^{18}O_{PO4}$‰	Predicted δ 18OPO4‰ Chang & Blake, 2015	Predicted $\delta^{18}O_{PO4}$ ‰ Longinelli & Nuti 1973	Predicted $\delta^{18}O_{PO4}$‰ Pucéat et al., 2010
Brown's Folly Mine	BFM-96-2	7.57 to 8.04	10 °C ± 0.4	-6.7	21.2 (SD ±0.4)	17.8	16.9	18.6
Rukiesa Cave	MERC-1	7.81	18.93 ±0.61	-0.35	21.2 (SD ±0.2)	22.6	21.2	22.9
Poole's Cavern	Calcite 1-5 Average	11.10 to 12.16	7.36 ±0.50	-7.56	21.4 (SD ±0.4)	17.4	16.6	18.3

Table 7.1: Measured $\delta^{18}O_{PO4}$ from Brown's Folly Mine, Rukiesa Cave and Poole's Cavern calcite samples compared to predictions from the phosphate-oxygen-isotope literature. References for pH, $\delta^{18}O_{H2O}$ and Ambient Temperature can be found in the retrospective methodology and previous result sections.

Sample	Type	Phosphate $\delta^{18}O$ (‰)	n=	SD (‰)
LEC Cold Store 24hrs 100-ppb	Lab incubation	20.11	3.00	0.31
LEC Cold Store 6 days 100-ppb	Lab incubation	20.61	2.00	0.06
8Lt Poole's Bulk Water 26/03/21	Natural Water	20.21	3.00	0.48
Poole's Soil	Soil sample	19.8	3	0.2
Poole's in-cave calcite average	Calcite sample	21.40	16.00	0.40

Table 7.2: Measured $\delta^{18}O_{PO4}$ from Poole's Cavern in-cave samples, including drip-waters, soil samples and natural calcite. All represent an in-cave temperature of around 7.2 °C. Also included is the water equilibration experiments made in the cold store at 7.2 °C after adding 100-ppb of PDOF.

Sample	Type	Phosphate $\delta^{18}O$ (‰)	n=	SD (‰)
Poole's Room calcite #1	400-ppb	21.3	3	0.40
Poole's Room calcite #2	400-ppb	21.6	3	0.20
Poole's Room calcite #3	400-ppb	21.3	3	0.10
Poole's Room calcite #4	400-ppb	21.4	3	0.30
Poole's 100-ppb-calcite room	100-ppb	21.1	3	0.40

Table 7.3: Synthetic calcite places dripped under laboratory conditions with an ambient temperature of 22 °C. Four plates were dripped following the addition of 400-ppb PDOF and one was dripped with 100-ppb PDOF. There is no discernible difference following a change in PDOF additions.

8 - DISCUSSION

This discussion evaluates the potential for phosphate-oxygen-isotopes ($\delta^{18}O_{PO4}$) to be used as a novel chemical thermometer in contemporary cave environments. By developing a new in-cave fractionation equation to describe this relationship, and predict temperature, it is envisioned that this can add another dimension to speleothem palaeothermometry and palaeoclimatology.

This work is built around the hypothesis that ubiquitous pyrophosphatase (PPase) enzyme hydrolysis overturns inorganic phosphate within cave drip-waters, rapidly exchanging all 4-oxygen atoms within the molecule. If this phosphate pool is overturned completely, $\delta^{18}O_{PO4}$ is expected to become at equilibrium with the temperature of the ambient water. This phosphate can then co-precipitate within speleothem calcite, preserving a record of temperature through time.

The following discussion explores the temperature fractionation of $\delta^{18}O_{PO4}$ in contemporary cave waters, allowing us to formulate a temperature fractionation equation comparable to those published in the literature. Consideration is also given to how well $\delta^{18}O_{PO4}$ translates into calcite precipitated under similar conditions and specifically addressing speleothems that have deposited within the last 100 years . Two archives from the Pleistocene and the Archean are also used to test our equation in a palaeoclimate context.

8.1 EXISTING $\delta^{18}O_{PO4}$ – TEMPERATURE RELATIONSHIPS IN THE LITERATURE

Measuring $\delta^{18}O_{PO4}$ as a temperature proxy was first developed in the archaeological and marine biology fields, using the variation of phosphate-oxygen species within biogenic appetite to suggest environmental conditions of growth for bone, teeth, and shells (Longinelli & Nuti, 1973). More recently, contemporary work has extended the principles of $\delta^{18}O_{PO4}$ to soils and waters, and establishing environmental specific temperature fractionation equations and moving towards the theory of enzymatic-temperature-fractionation by PPase (Chang et. al., 2021). However, it remains that in-cave temperature fractionation applicable to the formation of speleothem calcite currently not addressed within the literature, yet could provide one of the most important independent palaeotemperature records to date if applied successfully.

8.1.1 Longinelli & Nuti, 1973

$$\mathrm{T}(°\mathrm{C}) = 111.4 - 4.3(\delta^{18}\mathrm{O_P} - \delta^{18}\mathrm{O_{H2O}}) \quad (8.i)$$

Equation 8.i was developed from the apatite of 15 marine fish species, measuring $\delta^{18}O_{PO4}$ in 24 specimens that grew in different ocean temperatures between 3 and 30 ◦C. To date, this still acts as a cornerstone for $\delta^{18}O_{PO4}$ thermometry and is frequently cited in the literature. However, three major problems exist with this temperature fractionation relationship.

Firstly, the dynamics of phosphate cycling can be very different between marine and terrestrial systems (Jaisi & Blake, 2010., Chang & Blake 2015) as well as between source materials (Smith et. al., 2021). This could mean that a universal $\delta^{18}O_{PO4}$ equation may not translate well between environments. Secondly, Pucéat et. al., 2010 suggests that this model should be treated with suspect when comparing to modern analytical methods as bromination was used for sample processing, rather than the more contemporary silver phosphate method (Smith et. al., 2021). Thirdly, as the tenacity of PPase in overturning phosphate was not known at the time, samples were not frozen prior to analysis (Blake et al., 2005). This was because the samples were not originally meant for isotopic analysis but does mean that poor temperature control may exist in the archive.

8.1.2 Pucéat et. al., 2010

$$\mathrm{T}(°\mathrm{C}) = 118.7\ (\pm 4.9) - 4.3(\pm 0.20)(\delta^{18}\mathrm{O_P} - \delta^{18}\mathrm{O_{H2O}}) \quad (8.ii)$$

This study aimed to overhaul the work of Longinelli & Nuti, 1973 by introducing better temperature controls and use the silver phosphate method to extract orthophosphate. Using the apatite of fish raised in aquariums, the new equation (8.ii) offers a +2‰ offset compared with Longinelli & Nuti, 1971. Comparing to O'Neil et. al., 1994., equation 8.ii had the implication of recalculating temperature by 4 to 8 °C. However, this paper studies an isotopic equilibrium mechanism that addresses phosphate in a mineral as opposed to aqueous phase.

8.1.3 Chang & Blake, 2015

$$1000 \ln \alpha_{PO4-H2O)} = 14.43(\mp 0.39) \frac{1000}{\mathrm{T(K)}} - 26.54\ (\mp 1.33) \quad \text{(8.iii)}$$

This paper acts as the primary reference point for the research undertaken as a part of this thesis, offering the most expansive study for a phosphate-temperature relationship driven by microbes. Under laboratory conditions, and using laboratory-grade pyrophosphatase hosted in yeast, waters dosed with dissolved potassium dihydrogen orthophosphate (PDOF) were incubated and equilibrated under a range of controlled temperatures. These results were compiled to produce a precise $\delta^{18}O_{PO4}$-temperature equation (8.iii) to explain PPase driven fractionation between 3 and 37 °C. Equation 8.iii describes an offset of +0.5 to +0.7‰ compared to Pucéat et. al., 2010. The disadvantage of this method is that it was conducted under optimum conditions for PPase, as recommended by the manufacturer. While this describes the PPase fractionation mechanism in its purist form, this is not representative of in-situ conditions for many phosphate samples including speleothems in cave environments. Within caves, conditions are likely sub-optimal for PPase activity (eg. limited availability of enzymes, variable phosphate pool size, alkaline pH), meaning that orthophosphate may only partly equilibrate to temperature or be overturned more slowly (Shen et. al., 2020).

For this reason, it is suggested that the derivation of an in-cave phosphate-oxygen-temperature equation may provide a better analogue for interpreting a $\delta^{18}O_{PO4}$ speleothem palaeoclimate record.

8.2 $\delta^{18}O_{PO4}$ – TEMPERATURE RELATIONSHIP IN POOLE'S CAVERN DRIP-WATERS

8.2.1 $\delta^{18}O_{PO4}$ – TEMPERATURE RELATIONSHIP AT 100-ppb

After dosing Poole's Cavern waters with 100-ppb PDOF and leaving to equilibrate at different temperatures, a statistically significant negative relationship exists between temperature and $\delta^{18}O_{PO4}$ between 7 °C and 30 °C (Figure 6.1). $\delta^{18}O_{PO4}$ decreases at a rate of -0.2‰/°C which is comparable to the literature (e.g., Chang & Blake, 2015). This relationship persists even when accounting ±1 SD error, and between repeat experiments. A Pearson's r of -0.964 describes a statistically significant correlation, and an R^2 of 0.928 ($p < 0.01$, $n=8$) suggests that the relationship between the variables is unlikely to be random.

Justification is given to the dataset being 'bookended' at 7 and 30 °C by repeat readings from different batches of water, experiments and, in the case of 7 °C, phosphate sources. This gives us some assurance that the signal is genuine and repeatable, with our mid-temperature readings following this trend.

However, two key features of our relationship between $\delta^{18}O_{PO4}$ and temperature that are different to established relationships within the literature (e.g. Longinelli & Nuti, 1973., Chang & Blake 2015), concern a positive offset of data and limited representation of the phosphate starting value at extremes of temperature.

8.2.1.1 Comparisons to the literature

In equilibrated Poole's Cavern drip-waters, higher $\delta^{18}O_{PO4}$ was recorded than in previous research for the same incubation temperatures. At 7 °C for example, this equates to +2.0‰ compared to Pucéat et. al., 2010., +2.9‰ compared to Chang & Blake, 2015 and +3.7‰ compared to Longinelli & Nuti, 1973. This suggests differing environmental and microbiological conditions in Poole's Cavern compared to the literature.

However, the slope of our regression line (-5.05) is close to that derived by Chang & Blake, 2015 (-5.88). This equates to a comparable rate of change of -0.198‰/°C in our dataset compared to -0.170‰/°C in Chang & Blake, 2015. This comparable rate of change, along with evidence of viable microbial communities (GDGTs – Blyth et. al., 2014, cell counts and community analysis – Results in prep as of writing) , suggests that we are likely seeing phosphate-oxygen-temperature fractionation by PPase in Poole's Cavern drip-waters, as opposed to some other fractionation mechanism. This is taking place uniformly between 7 °C and 30 °C, despite the general positive fractionation of $\delta^{18}O_{PO4}$ in Poole's Cavern. This is considered, because enzyme-driven fractionation of orthophosphate was the only effect on $\delta^{18}O_{PO4}$ through the work of Chang & Blake, 2015.

The work of Chang & Blake, 2015 has shown that PPase-driven $\delta^{18}O_{PO4}$ temperature-equilibration usually takes place in the first 24 hrs of dosing between 37 and 9 °C. At 3 °C, equilibration to temperature took 3-5 days, slower due to decreased microbial activity. Moreover, Shen et. al., 2020 suggests that PPase can fully overturn P in seconds to minutes in optimum conditions. For this reason, we suggest that equilibrium in most cases took place in the first 24hrs and certainly in the first 72hrs to 5 days: the incubation length for most of our samples.

8.2.1.2 Reasons for positive fractionation of $\delta^{18}O_{PO4}$ in Poole's Cavern

As well as the previously mentioned standardisation issues associated with $\delta^{18}O_{PO4}$ analysis (Chang & Blake, 2015), there are several further possibilities for the consistent positive fractionation of $\delta^{18}O_{PO4}$ compared to the literature:

i. The impact of hyperalkaline pH on $\delta^{18}O_{PO4}$:

It is known in other areas of isotopic study that pH variation can induce isotopic fractionation. Stüeken et. al., 2020 for example describes a strong positive fractionation (+17‰) in nitrogen isotopes found in hyperalkaline lakes. This fractionation is so strong and consistent, that it has been suggested as a palaeo-pH and atmospheric CO_2 proxy (Stüeken et. al., 2020). No specific information on hyperalkaline fractionation of $\delta^{18}O_{PO4}$ could be found in the literature, however it is quite possible that it may be influenced in a similar way.

ii. Due to colloidally bound Iron Oxides

The presence of colloidally bound iron oxides in Poole's Cavern waters could also explain some of the positive fractionation of $\delta^{18}O_{PO4}$. These complexes are common in the drip-waters of Poached Egg Chamber, supported by the high pH of the water (Hartland, 2010., Fairchild & Hartland, 2010) and have a high number of reactive sites (Hartland, 2011) that can actively sorb orthophosphate (Jaise et. al., 2010., Nisbeth et. al., 2019).

Small colloids (<100 nm) are uncommon in Poole's Cavern because calcium is an effective coagulant, compressing charged colloids that are put in greater proximity (Hartland, 2010). This is because under DVLO (Derjaguin—Landau—Verwey—Overbeek) theory, Van der waal attraction exceeds repulsive forces, forcing aggregation and gravitational deposition of colloids at high pH (Buffel et. al., 1998). This is likely the explanation for why orthophosphate

is being sorbed into these colloidal phases. This might explain why our PDOF is largely being filtered out at 0.2 µm.

A study by Jaise et. al., (2010) suggests that the lighter isotopologues of dissolved phosphate are inorganically sorbed first into iron oxide phases, forcing a form of kinetic fractionation. Luckily this effect occurs uniformly independent of temperature (4 to 95 °C), meaning that any relationship to temperature is most likely still microbially driven (Jaise et. al., 2010). Only the rate of fractionation increases with temperature (Jaise et. al., 2010). As the lighter isotopologues are removed, this leaves the heavier isotopologues dissolved in the water column to be metabolised. Although hypothetical, this could positively bias $\delta^{18}O_{PO4}$.

The question raised is whether bacteria will be able to access these colloidal fractions to metabolise phosphate. Fitriatin et. al., 2014 suggests that bacteria can fix colloidal P to soluble P, accessible for plants, in alkali soils and Bollyn et. al., 2017 suggests these forms are bioavailable. However, Zhao et. al., 2014 suggests high organic matter, high pH and the presence of iron-oxides can limit bacteria adhesion to colloids. For this reason, it is quite possible that isotopically heavy dissolved orthophosphate is metabolised first, as more energy is required to access the isotopically lighter colloidal fractions.

The impact of iron oxide colloids may go some way to explain the consistent positive fractionation of $\delta^{18}O_{PO4}$ in Poole's Cavern waters. Yet a temperature-fraction signal remains, as the overall effect is uniform and acting independently of temperature.

iii. Due to alternative O-sources (Nitrogen, Sulphate and Calcite)

The review paper of Nisbeth et. al., 2019 describes issues that can be faced with the insufficient removal of O-bearing compounds during sample processing to silver phosphate for $\delta^{18}O_{PO4}$ analysis. Problematic compounds include DOM, nitrate (NO_3^-) and sulphate (SO_4^{2-}

), which can become occluded within the silver phosphate matrix along with the desired orthophosphate (Davies et. al., 2014). All O-sources are pyrolysed during isotopic analysis, meaning any true $\delta^{18}O_{PO4}$ signal may be altered.

The $\delta^{18}O$ of Nitrate in Poached Egg calcite is +28.4‰ (Wynn et. al., 2021). If these nitrate-oxygen species become occluded within silver-phosphate during sample processing, oxygen is pyrolysed from the nitrate as well as phosphate, causing a positive bias in the $\delta^{18}O_{PO4}$ result.

8.2.1.3 Difference from potassium dihydrogen orthophosphate (PDOF)

At extremes of temperature, enzyme activity is likely to be minimal due to either denaturing at high temperatures (Kunitz, 1952), or limited activity at cold temperatures (Chang & Blake, 2015). Under these scenarios, the incubated water samples would perhaps be expected to not differ significantly from the starting PDOF isotopic composition.

However, it was found that at extremes of temperature $\delta^{18}O_{PO4}$ deviates from our expected starting concentration of PDOF (+18.2 ±0.4‰). This suggests isotopic fractionation by microbial turnover, as inorganic fractionation does not readily occur (Chang & Blake, 2015). By dissolving 100-ppb of PDOF in boiled Milli-Q water and processing to silver phosphate, we deemed this the best method to both remove any microbes that may fractionate $\delta^{18}O_{PO4}$ and to ensure the standard is being pyrolysed comparatively to the samples. Colourimetry confirmed that the only sources of P in these procedural standards was from PDOF.

PDOF salts weighed into the spectrometer yield readings of around +14.2 ±0.2‰. This is consistent with previous readings of this same batch in 2019 at +14.01 ±0.60‰ (Wynn, unpublished data). The +4‰ increase between raw PDOF and PDOF in brucite/silver phosphate could be due to differences in pyrolysis, driven by matrix effects. This issue is outlined well in Chang & Blake 2015, which describes a lack of standardisation in $\delta^{18}O_{PO4}$ of control samples, and large inter-laboratory discrepancies. A common standard, NBS SRM 120c, shows a range of ±2.8‰ (+19.9 to +22.7‰) in the literature (O'Neil et. al., 1994, Pucéat et. al., 2010, Chang & Blake, 2015). For this reason, it is hard to say if our +4‰ increase between phases is a pyrolysis discrepancy or a preparation issue. Low standard deviations, oxygen percentage values of the correct quantity, and tight standardisation both between and within analytical sequences suggest that this is not an issue of isotopic measurement.

At 4 °C it was found that $\delta^{18}O_{PO4}$ tends to reduce away from the initial +18.2 (±0.4)‰ PDOF value. This is the inverse expected for PPase overturn of PDOF to equilibrium with temperature, as it should be higher than +20.6‰ at 7 °C. However, if there was a lack of microbial turnover $\delta^{18}O_{PO4}$ would be expected to trend towards the PDOF Di-water value of +18.2 (±0.4)‰, but it is instead trending downwards away from this value. This observation could suggest that some other fractionation mechanism is occurring at low temperatures that works the opposite to PPase fractionation, occurring over several samples with both 100 and 400 ppb of PDOF.

A sizeable portion of Alkaline Phosphatase (APase) can be found in Poole's Cavern drip-waters, almost to the same quantity as PPase (Shen, J., Barnett, M., Smith, A – Results in prep as of September 2021). This is significant as APase forces a strong negative fractionation (-25‰) in $\delta^{18}O_{PO4}$ (Liang & Blake, 2006., Shen et. al., 2020), but the current consensus is that the rapidity and perversive nature of PPase overwrites this signal, and any other fractionation signals, to temperature (Blake et. al., 2005). However, the rate for PPase to overturn phosphate significantly reduces at low temperatures (Chang & Blake, 2015) and psychrophilic forms of alkaline phosphatase are possible in the environment (Lee, et. al., 2015). For this reason, there is a possible scenario where APase might outcompete PPase at lower temperatures which could force a strong negative fractionation away from equilibrium with temperature.

8.2.2 JUSTIFICATION FOR MICROBIAL ACTIVITY IN POOLE'S CAVERN

Because the fractionation of $\delta^{18}O_{PO4}$ with temperature does not occur inorganically (Chang & Blake, 2015), any major change in $\delta^{18}O_{PO4}$ with temperature is good evidence for enzymatic fractionation. Nonetheless, these is some further evidence for viable microbial activity in Poole's Cavern's hyperalkaline drip-waters.

Firstly, Burke et. al., 2012 notes evidence of a distinct alkaliphilic extremophile community existing within lime kiln deposits in Buxton. Moreover, Smith et. al., 2016 traced similar communities within a hyperalkaline aquifer on Harpur Hill, Buxton. These communities have since been harnessed to process hyperalkaline nuclear reactor waste (Basil et. al., 2015., Basil et. al., 2020). Therefore, there is good evidence for a microbial source in the soil system that could later survive an epikarst water reservoir before entering the cave.

Secondly, Blyth et. al., 2014 shows that distinct glycerol dialkyl glycerol tetraethers (GDGTs) can be found in Poole's Cavern, that are distinct from the soil community. This suggests in-situ primary production within the cave environment itself, including on speleothem material.

Thirdly, recently unpublished data linked to this study has just been released from the University of St. Andrew's and the British Geological Survey. This shows good evidence for a viable community in Poole's Cavern waters that will very likely host PPase enzymes. Growth on plate count agar (PCA) suggests a viable community of 2.8 (±1.4) x 10^7 cells/g of drip-waters from Poached Egg Chamber. This contrasts with 1.8 (±0.8) x 10^8 cells/g in the soil directly above the chamber (Shen, J., Barnett, M., Smith, A – Results in prep as of September 2021). Furthermore, preliminary phylogenetic modelling suggests a less diverse microbial community in Poole's Cavern drip-waters rather than the soil environment (expected due to

the extremes of pH) that is dominated by *Betaproteobacteria, Alphaproteobacteria* and *Gammaproteobacteria* (Shen, J., Barnett, M., Smith, A – Results in prep as of September 2021). This compliments Smith et. al., (2016) which found high levels of *Gammaproteobacteria* in the hyperalkaline aquifer on Harpur Hill, Buxton, suggesting similar communities thrive in both environments.

8.2.3 $\delta^{18}O_{PO4}$ – TEMPERATURE RELATIONSHIP AT 400-ppb P

After adding 400-ppb of PDOF to Poole's Cavern waters and leaving to equilibrate for up to 11-days, we found a perturbed relationship to temperature. No statistical correlation could be found between $\delta^{18}O_{PO4}$ and change in temperature, and most values do not deviate far from PDOF $\delta^{18}O_{PO4}$.

The likely reason for this was due to this concentration of P exceeding the processing capacity of PPase or oversaturating the cells requirements for orthophosphate. In this replete system, only a portion of the total P pool would be overturned, forcing little variation away from PDOF $\delta^{18}O_{PO4}$. Temperature equilibration of the total pool is thus never reached. This is an observation often seen in agricultural systems where, for example, a fertiliser $\delta^{18}O_{PO4}$ signal is expressed as the high concentration of P oversaturates the ability for PPase to express a temperature equilibrium $\delta^{18}O_{PO4}$ signal (Blake et. al., 2005., Bi et. al., 2018). In a closed system, microbes are likely becoming nutrient limited in some way meaning little use for the excess phosphate (Shen et. al., 2020). This effect will become more profound at extremes of temperature, where microbes are limited by enzyme denaturisation above 36°C or reduced metabolism at 4°C (Chang & Blake, 2015).

8.3 DEFINING THE $\delta^{18}O_{PO4}$ EQUILIBRIUM FRACTIONATION EQUATION AT 100-ppb

The trend of $\delta^{18}O_{PO4}$ –temperature at 100-ppb in Poole's Cavern waters showed that there is a statistically significant relationship between the two variables (R^2 = 0.928 p <0.01) between 7 and 30 °C when the water isotopic composition is held constant. Change in $\delta^{18}O_{H2O}$ would be expected to bias $\delta^{18}O_{PO4}$ by influencing the pools of ^{18}O or ^{16}O available in H_2O that can be integrated into phosphate, but nevertheless would be a consistent effect and independent of temperature. Following the work of Chang and Blake (2015), a model can be generated to take account of $\delta^{18}O_{H2O}$ and $\delta^{18}O_{PO4}$ to facilitate the calculation of temperature at different cave sites.

8.3.1 CALCULATION OF A NOVEL $\delta^{18}O_{PO4}$ –TEMPERATURE MODEL FOR SPELEOTHEM DRIP-WATERS

By calculating the fractionation factor between $\delta^{18}O_{PO4}$ and $\delta^{18}O_{H2O}$, $(1000Ln \propto (PO_4 - H_2O))$, this can be plotted against temperature to describe the relationship between $\delta^{18}O_{PO4}$, $\delta^{18}O_{H2O}$ and temperature (K) at 100-ppb (Figure 8.1). There is no requirement to convert temperatures to kelvin, however it allows a direct comparison equation 8.iii by Chang & Blake, 2015.

$\propto (PO_4 - H_2O)$ is defined as (8.iv):

$$\propto (PO_4 - H_2O) = \left(\frac{\delta^{18}O_{PO4} - \delta^{18}O_{H2O}}{1000}\right) + 1 \qquad (8.iv)$$

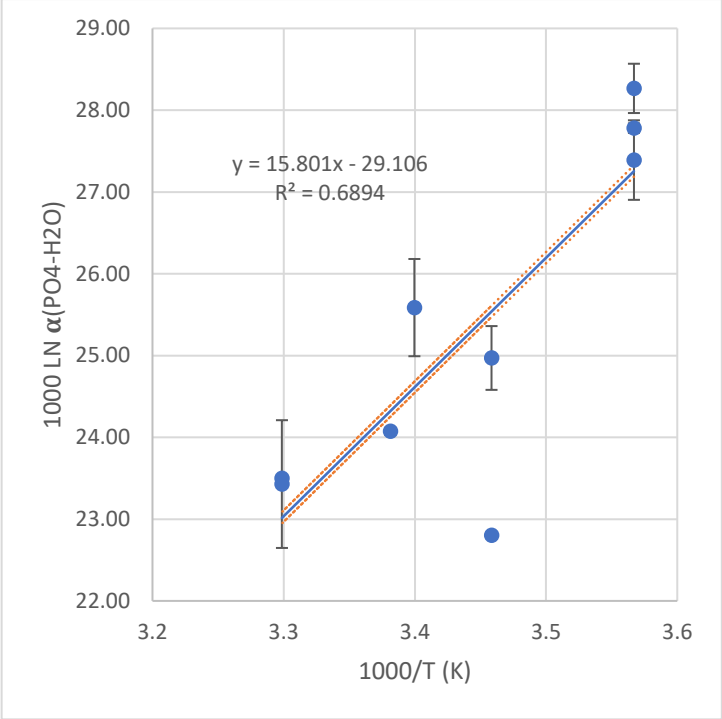

Figure 8.1: The temperature dependence of equilibrium PPase-catalyzed O-isotope fractionation between potassium dihydrogen orthophosphate (PDOF) and Poole's Cavern drip-water. This can be compared directly to Fig. 3. From Chang & Blake 2015. The solid line is a linear regression fit to the data (R^2 = 0.689 p <0.01). Dashed lines are 95% confidence intervals. Error bars represent ±1 SD‰ based on repeat readings of silver phosphate.

From the new linear regression model of the data from Graph 1 (R^2 = 0.69 n=9), the following equation can be derived to predict the relationship between $1000Ln \propto (PO_4 - H_2O)$ and temperature (1000/Kelvin) in Poole's Cavern drip-waters (Equation 8.v).

$$1000Ln \propto (PO_4 - H_2O) = 15.801 \cdot \left(\frac{1000}{T}\right) - 29.106 \qquad (8.v)$$

8.3.2 COMPARISONS TO OTHER STUDIES

Figure 8.2 better represents some of the observations discussed from Figure 8.1, compared directly with the literature. This describes an enriched O-isotope fractionation for orthophosphate–water in Poole's Cavern at 100-ppb, compared to the laboratory calibrations of PPase fractionation by Chang & Blake 2015 and biogenic phosphate minerals such as invertebrate shells (Longinelli and Nuti, 1973., Longinelli and Nuti, 1973b) and fish teeth (Pucéat et al., 2010).

The slope of the line plotted on Figure 8.1 & 8.2 (15.8 ±0.3), from the Poole's Cavern drip-water phosphate data, shows an offset of +0.9 compared to equation 8..iii by Chang & Blake, 2015 (14.4 ± 0.4) and is within error of Pucéat et al., 2010 (14.9 ± 1.0). This is surprisingly close, considering the very different experimental setups (i.e. a hyperalkaline cave environment to a lab-experiment in ideal conditions, and biogenic hydroxyapatite from fish-tooth enamel).

The Y-intercept of the Poole's Cavern equation 8.v (29.1) is +2.6 from the equation 8.iii of Chang & Blake, 2015 (26.5 ±1.3) but close to Pucéat et al., 2010 (28.8 ± 3.3) before correction. This corresponds to the +2‰ offset in $1000Ln \propto (PO_4 - H_2O)$ compared to Chang & Blake, 2015 or +1.2‰ compared to Pucéat et. al., 2010 before the -0.8‰ correction made by Chang & Blake, 2015. Again, this demonstrates the major issues in $\delta^{18}O_{PO4}$ standardisation when comparing between the literature.

The wider distribution of data (R^2 = 0.69) compared to Chang & Blake 2015 (R^2 = 0.99) can be justified due to our experiment using natural cave waters, as opposed to lab-grade PPase hosted in yeast being equilibrated under optimum manufacturer conditions. In a natural environment greater variation would be expected.

In all, the calibration for Poole's Cavern waters describes a similar rate of change between $1000Ln \propto (PO_4 - H_2O)$ and change in temperature (1000/K) compared to the literature but with greater overall $1000Ln \propto (PO_4 - H_2O)$ values that are distinct even when including standard error.

The greater magnitude of $1000Ln \propto (PO_4 - H_2O)$ values is likely due to hyperalkaline pH forcing the presence of iron oxide colloidal materials, the pyrolysis of secondary oxygen sources, and/or standardisation issues between laboratories as discussed within discussion sections 8.2.1.2 and 8.2.1.3.

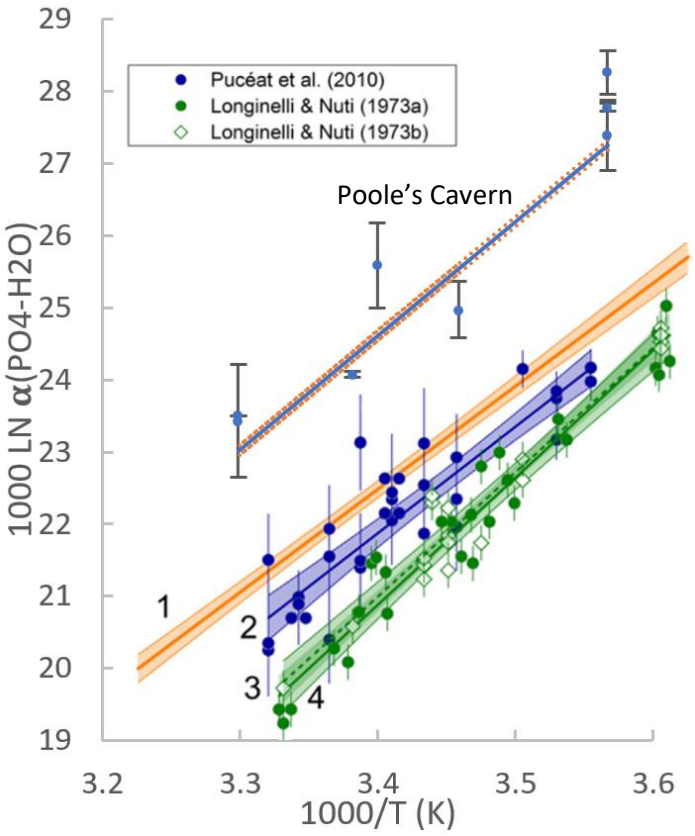

Figure 8.2: Comparison of equilibrium O-isotope fractionation for orthophosphate–water in Poole's Cavern (top, as in Figure 8.1) overlayed against Fig. 4 in Chang & Blake 2015. This shows laboratory calibrations of dissolved PO_4 (1; Chang & Blake, 2015) and empirical fractionations for biogenic phosphate minerals; invertebrate shells (4; Longinelli and Nuti, 1973a) and fish teeth (3; Longinelli and Nuti, 1973b, 2; Pucéat et al., 2010). Error bars on symbols represent 1 standard deviation for total analytical error. Shaded regions of regression lines represent 95% confidence intervals. It is noted that both Chang & Blake, 2015 and Pucéat et al., 2010 used a similar Ag3PO4 method to this study, however Figure 8.2 displays the −0.8‰ correction made by Chang & Blake, 2015 to the δ18OPO4 data of Pucéat et al., 2010. This was due to the reported differences between SRM 120c used as an isotopic standard (Chang & Blake, 2015).

8.3.3 IMPLICATIONS FOR CAVE SCIENCE

This novel phosphate-oxygen-temperature fractionation equation (8.v) for Poole's Cavern demonstrates the first evidence for a $\delta^{18}O_{PO4}$-temprature relationship existing in speleothem drip-waters, and the second evidence in any cave environment. This observation includes laboratory incubations with orthophosphate additions, and in natural occurring phosphate within the cave.

Critically, this evidence, backed up with preliminary microbiological data, suggests high probability for viable microbes with active pyrophosphatase enzymes within speleothem drip-waters, that can overturn and fractionate $\delta^{18}O_{PO4}$ to equilibrium with temperature between 7 and 30 ◦C.

In a speleothem and palaeoclimate context, this finding seems to be inherently linked to the concentration of phosphate in the system. Replete systems can readily oversaturate enzymatic activity meaning any fractionation cannot be seen in the large pool of drip-water phosphate. However, this experimental work was undertaken within a closed system where microbes were likely becoming nutrient limited in some other respect (Chen et. al., 2020).

Section 8.4 addresses whether the $\delta^{18}O_{PO4}$-temperature signal can be translated into speleothem material without alteration which has implications as a novel palaeothermometer for cave environments.

8.3.4 FURTHER WORK

Some repeat readings should be made using Poole's Cavern water in the same conditions as presented. The data set at 100-ppb is necessarily limited due to time and logistical constraints, thus leaving the central portion of the calibration line constrained by only a limited number of data points. Despite strong confidence in the upper and lower extremes of temperature, it is desirable to include more mid-temperature data. Equilibration experiments should also be made at this concentration to evaluate the rate of P turnover compared to Chang & Blake, 2021. Frustratingly most of our experiments were conducted using 400-ppb PDOF, which likely exceeded the capacity for PPase to overturn the entire orthophosphate pool.

We have also seen a difference in P-species between spring and winter through our colourimetry analysis (Results D1.8). For example, there is an increase in P_{org} (10-ppb) in the winter. This is likely linked to vegetation dieback and increased rainfall infiltration drawing these P sources into the cave (Huang et al., 2001; Fairchild and Treble, 2009; Fairchild et al., 2010). This seasonal influence could affect the ability for microbes to metabolise phosphate to isotopic equilibrium or introduce a seasonal isotopic bias and should therefore be investigated.

Finally, it would be useful to repeat 100-ppb PDOF experiments using more typical speleothem drip-waters. We did attempt this with White Scar drip-waters, however there are only 2 sets of readings at 100-ppb. Moreover, this preliminary data suggests a poor $\delta^{18}O_{PO4}$-temperature relationship. Although calcite material could not be grown in short periods, this study would isolate pH as the primary contender for the positive equilibrium fractionation in Poole's Cavern. Moreover, as most cave environments are not hyperalkaline, this would provide a better indication to fractionation equation to use for a palaeoclimatic study.

8.4 $\delta^{18}O_{PO4}$ – TEMPERATURE RELATIONSHIP IN POOLE'S CAVERN CALCITE MATERIAL

Speleothem archives have proven to be an invaluable resource in palaeoclimate studies, benefiting from an independence from 'orbitally-tuned' archives such as deep sea sediment-cores (McDermott et. al., 2004., Rasmussen et. al., 2006), exhibiting geographical diversity in terrestrial environments while supported by a robust ^{234}U-series dating system (Fairchild & Baker, 2012) that has been invaluable in temporally correcting existing records (e.g. Svensson et. al., 2008 and Cheng et. al., 2016). However, palaeotemperature interpretation from traditional archives (e.g. calcite $\delta^{18}O$) suffer from numerous effects that perturb a clear signal (Fairchild et. al., 2006). While alternatives such as clumped isotope measurements (Ghosh et al., 2006., Bajnai, et.al., 2020) or GDGT distributions (Baker et. al., 2019) show promise, there is currently no unambiguous palaeothermometer in speleothems. Considering that cave environments often represent average annual air temperature (McDermott et. al., 2004., Fairchild, et. al., 2006) there is value in pursuing this avenue of study to test and validate boundary conditions of general circulation models (GCMs) (McDermott, et. al., 2004).

As previously discussed, $\delta^{18}OPO_4$ thermometry has been effectively demonstrated in the literature (Longinelli and Nuti, 1973a., Longinelli and Nuti, 1973b., Pucéat et al., 2010., Chang & Blake, 2015., Shen et. al., 2020., Chang & Blake, 2021) and has now been demonstrated in the speleothem drip-waters of Poole's Cavern. This section now serves to discuss the translation of a drip-water $\delta^{18}OPO_4$ – temperature relationship into speleothem material. If successful without further fractionation, this would have implications for $\delta^{18}OPO_4$ to be a valuable tool in building multi-proxy palaeoclimate records.

8.4.1 TRANSLATION OF $\delta^{18}O_{PO4}$ BETWEEN PO_4 IN NATURAL DRIP-WATERS AND SPELEOTHEM MATERIAL IN POOLE'S CAVERN AT 7.2 °C

$\delta^{18}O_{PO4}$ from the natural P found in the drip-water of Poole's Cavern (+20.2 ±1SD 0.48‰) at 7.2 °C and from samples of 100-ppb PDOF incubated at the same temperature (average of +20.35‰ n=2) fits the prediction of our 100-ppb regression model (+20.36‰) built between 7 and 30 °C, thus suggesting that PPase equilibration has likely taken place. Between speleothem drip-water and speleothem calcite phases we would expect to see similar values if no further fractionation has taken place.

$\delta^{18}O_{PO4}$ was recorded from calcite samples of drip-plates that were placed on top of speleothems in Poached Egg chamber between July 2020 and April 2021 by Dr. Andi Smith of the British Cave Science Centre. Average $\delta^{18}O_{PO4}$ of this speleothem material was +21.4 (±0.48)‰ with a total range of +20.8 (±0.2) to +21.8 (±0.5)‰. Assuming similar drip-water temperatures over this period, this suggests a slight positive +1‰ fractionation between drip-water and calcite phases.

In all, this is good evidence to suggest that a $\delta^{18}O_{PO4}$-cave temperature signal can be incorporated into natural speleothem material without significant isotopic alteration.

8.4.2 TRANSLATION OF $\delta^{18}O_{PO4}$ BETWEEN EQUILIBRATED POOLE'S CAVERN DRIP-WATERS AND SYNTHETIC CALCITE AT 22 °C

The observations made in natural calcite did not seem to translate into synthetic calcite. In-lab experiments determined a $\delta^{18}O_{PO4}$ for Poole's Cavern drip-water to be +16.8 ±0.04‰ at 22.6 °C, or an estimated +17.3‰ according to our regression line for the same temperature. Without further fractionation, it would be expected to see similar values in calcite precipitated at this temperature assuming the water $\delta^{18}O_{PO4}$ had been fully equilibrated by PPase.

However, calcite that was precipitated under laboratory conditions at 22°C using 100 and 400 ppb PDOF produced $\delta^{18}O_{PO4}$ readings between +21.1 ±0.4‰ and +21.6 ±0.2‰. These values are potentially concerning, as it is like other calcite values from different temperatures and cave systems. This evidence suggests a deviation from the expected PPase driven fractionation in our synthetic calcite plates.

This observation might suggest that acid hydrolysis is occurring during sample dissolution, exchanging water-oxygen into anionic species such as phosphate. The probable reason for this is due to over acidification during calcite dissolution (McLaughlin et al., 2006). The altered O signal can be incorporated in the Ag_3PO_4 crystals, subsequently altering the $\delta^{18}O_{PO4}$ signature of the sample (Nisbeth et. al., 2019). One method to mitigate this would be to weigh the calcite sample and slowly add the stochiometric amount of hydrochloric acid to ensure calcite dissolution while maintaining a neutral pH (as per Wynn et. al., 2021). Here, the exact volume of 1M HCl was added to dissolve the calcite by weight, and the variation in $\delta^{18}O_{NO3}$ was wider (+12.3‰ to +32.3‰) than the consistent values expected with acid hydrolysis.

8.5 $\delta^{18}O_{PO4}$ – TEMPERATURE EQUATION FROM POOLE'S CAVERN WATERS

In this section the derived equation (8.v) from Section 8.3.1 (describing the phosphate-oxygen-temperature relationship of Poole's Cavern waters) can be rearranged to take $\delta^{18}O_{H2O}$ and $\delta^{18}O_{PO4}$ values to hypothesise temperature.

By rearranging equation 8.v, we can solve for T (K) as equation 8.vi, allowing us to make temperature predictions using $1000Ln \propto (PO_4 - H_2O)$:

$$T(K) = \frac{15801}{1000Ln\propto(PO_4-H_2O)+29.106} \quad (8.vi)$$

Converting T(K) to T(^{o}C), we get equation 8.vii:

$$T\ (°C) = \left(\frac{15801}{1000Ln\propto(PO_4-H_2O)+29.106}\right) - 273.15 \quad (8.vii)$$

We can now test equation 8.vii against the literature by making predictions for environmental temperature: from two contemporary records grown over the last 100 yrs (Section 8.6), to a 10,000 yr speleothem record from Australia and an estimate for ocean temperatures during the Archean (Section 8.7).

8.6 $\delta^{18}O_{PO4}$ SPELEOTHEM THERMOMETRY FROM RECENT STALAGMITE DEPOSITS IN THE UK AND ETHIOPIA

8.6.1 Brown's Folly Mine, UK

The $\delta^{18}O_{PO4}$ measurement for calcite taken from BFM-96-2, Brown's Folly Mine was +21.2 ±0.4‰. This value is +3.4 to +2.6‰ heavier than predictions by Chang & Blake 2015 and Pucéat et al., 2010. Once rearranged, this $\delta^{18}O_{PO4}$ suggests unrealistic sub-zero temperatures from the literature (Table 8.1). Equation 8.vii from this article predicts more 'realistic' temperatures in this case, but as the pH of the water in Brown's Folly Mine is 7.57 to 8.04 (n=16, Wynn, 2021 – unpublished data) it is unlikely that the model from Poole's Cavern can be justifiably applied.

As with the Poole's Cavern synthetic plates (processed on the same day), it is likely this is due to over acidification during calcite dissolution that is hydrolysing anionic O-sources. Again, the same recommendation would be to add the stochiometric amount of HCL in the future.

Due to the age of the temperature reading from Baker et. al., 1998, it could be argued that in-cave temperatures are on average lower than 9.9 °C. Moreover, using a $\delta^{18}O_{H2O}$ from meteoric water rather than an in-cave sample or fluid inclusion will likely introduce some error (McDermott, 2004). However, considering the very large discrepancy in $\delta^{18}O_{PO4}$, these effects are only marginal in explaining the discrepancy.

Despite this, unlike Mercury Chamber, it is not known how much phosphate concentration exists in the calcite. It is possible that this facilitates the inclusion of secondary O is likely to be coming from alternative sources such as nitrate. This contrasts with Rukiesa Cave calcite which contains 130-375 ppb of PO_4-P (Baker et. al., 2007).

	Poole's Cavern	Chang & Blake 2015	Longinelli & Nuti 1973	Pucéat et al. (2010)
Estimated Temperature °C	5.90	-6.21	-8.57	-1.27
± 1 SD	0.61	4.90	1.72	1.72
°C difference from recorded (±1SD = ±0.1 °C)	-4.10	-16.21	-18.57	-11.27

Table 8.1: Predicted values of in-cave temperature for BFM-96-2, Brown's Folly Mine, UK for the last 100 years using equations 8.i to 8.iii from Longinelli & Nuti 1973, Pucéat et al., 2010, Chang & Blake 2015 (listed in discussion sections 8.1.1-8.1.3), and equation 8.vii. Current in-cave temperature is 9.9 ±0.1 °C (Baker et. al., 1998), assumed to not have changed much over the last 100 years. $\delta^{18}O_{H2O}$ used was -6.7‰ (GNIP database 1979 to 1996). $\delta^{18}O_{PO4}$ used was +21.2 ±0.4‰.

8.6.2 Mercury Chamber, Rukiesa Cave, Ethiopia

Our $\delta^{18}O_{PO4}$ measurements for calcite taken from MERC-1, Rukiesa Cave (Asrat et al., 2007, Asrat et al., 2008; Baker et al., 2007, Wynn et. al., 2021) gave a value of +21.2 ±0.2‰.

We know that current in cave temperatures are 18.93 ±0.61 °C (Baker et. al., 2007., Asrat et. al., 2008). $\delta^{18}O_{H2O}$ is currently -0.35‰ (Wynn P; Unpublished data). Assuming minimal change in temperature or $\delta^{18}O_{H2O}$ over the past 50-years we can calculate predictive temperatures from the literature and equation 8.vii from the Poole's cavern calibration (Table 8.2).

Results shows that equation 8.i from Longinelli & Nuti 1973 can predict in-cave temperature as 18.74 ±0.86 ◦C (Table 8.2), which is -0.2 °C away from expected values, well within tolerance of 18.93 ±0.61 °C. However, this is without applying the +2‰ alteration advocated by Pucéat et. al., 2010 to account for difference in sample preparation (bromination rather than the current silver-phosphate method).

Pucéat et al., 2010 (26.04 ±0.86 °C) and Chang & Blake 2015 (28.35 ±3.07 °C) over-predict temperature in this case by 7.11 and 9.42 °C respectively. As discussed, this could either mean that the model of Longinelli & Nuti, 1973 is a better analogue for temperature in Mercury Chamber or that $\delta^{18}O_{PO4}$ is slightly away from a true equilibrium with temperature. We calculate this as roughly -0.5‰. This could either be due to disequilibrium in the cave, as phosphate pools are not being fully overturned by microbes (Smith et. al., 2021), or mild prep fractionation as phosphate is being released from calcite, or analytical error.

Again, the Poole's Cavern equation 8.vii describing the relationship between PO_4-O and temperature vastly over-predicts temperature within Rukiesa cave. The likely reason for this is due to the high pH of Poole's Cavern waters exhibiting a positive fractionation on $\delta^{18}O_{PO4}$

compared to what would be expected in more neutral pH waters. For this reason, equation 8.vii may only be suitable for high-pH environments.

Despite these findings, the biggest question here is whether $\delta^{18}O_{PO4}$ in this case is being measured truly correct or coincidentally correct. Considering that the other calcite values processed in this study were ±0.2‰ away from the $\delta^{18}O_{PO4}$ for MERC-1. The only way to truly confirm this is to repeat the experiment once a methodology has been established, and tested, that ensures phosphate can be extracted from calcite without contamination or suffering from the effects of oxygen isotope exchange during acid hydrolysis of carbonate.

	Poole's Cavern	Chang & Blake, 2015	Longinelli & Nuti, 1973	Pucéat et al., 2010
Estimated Temperature °C	40.19	28.35	18.74	26.04
±1 SD	1.84	3.07	0.86	0.86
°C difference from recorded (±1SD = ±0.61 °C)	21.26	9.42	-0.20	7.11

Table 8.2: Predicted values of in-cave temperature for MERC-1, Rukiesa Cave for the last 50-years using equations 8.i to 8.iii from Longinelli & Nuti 1973, Pucéat et al., 2010, Chang & Blake 2015 (detailed in discussion sections 8.1.1-8.1.3), and equation 8.vii. Current in-cave temperature is 18.93 ±0.61 °C (Baker et. al., 2007., Asrat et. al., 2008), assumed to not have changed much over the last 100 years, and will be our aim. $\delta^{18}O_{H2O}$ used was -0.35‰ (Wynn P; Unpublished data). $\delta^{18}O_{PO4}$ used was 21.2 ±0.2‰.

8.7 $\delta^{18}O_{PO4}$ PALAEOTHERMOMETRY IN THE PLEISTOCENE AND THE ARCHEAN

In this final section we will discuss the efficacy of phosphate-oxygen-thermometry in a palaeoclimate context, testing the ability to extract independent temperature records.

The first dataset comes from some preliminary samples of drilled speleothem from Yarrangobilly Flowstone (Jersey Cave, South East Australia) that has grown periodically over the past 100,000 years (Figure 8.3). The second pushes the newly presented Poole's Cavern phosphate-oxygen-temperature relationship to temporal and environmental extremes, far outside its designed function, by trying to reconstruct ocean temperatures 3.2 to 3.5 billion years ago.

In all, these studies offer excellent promise for $\delta^{18}O_{PO4}$ palaeothermometry in cave environments, especially on the context of a multi-proxy climatic study where fluid inclusion data is available.

8.7.1 CAVE TEMPERATURE ESTIMATES FOR JERSEY CAVE, AUSTRALIA 99 TO 37 KA

Phosphate-Oxygen isotopes extracted from YB-F1 (Yarrangobilly Flowstone, Jersey Cave, South East Australia) under a NERC grant (Grant IP-1603-11115) are presented below and converted into in-cave temperature, using the temperature relationship detailed in discussion Section 8.5. This data set shows more variation in $\delta^{18}O_{PO4}$ than recorded in our calcite samples, ranging from +13 to +18‰ (Figure 8.3).

The Yarrangobilly speleothem grew between 99 to 37 ka, with a significant hiatus between 84.1 to 47.3 ka. Carbonate isotope, trace element and organic matter fluorescence records identify a drying episode between 99 ka towards the hiatus commencing at 84.1 Ka, followed by a wetter phase allowing recommencement of growth at 47.3 Ka. This climatic trend fits the record of interglacial and glacial conditions (Webb et. al., 2014).

However, due to the multiple confounding factors which drive carbonate isotope composition, deriving a pure temperature signal from the cave has thus far proved elusive.

Using fluid inclusion characterisation of $\delta^{18}O_{H2O}$, equation 8.vii can be used to try to derive palaeotemperature records from the Yarrangobilly flowstone record. Whilst fluid inclusion analysis has not been undertaken on the YB-F1 sample, data are available from a speleothem collected on Tasmania (Goede et. al., 1986). Whilst distant to Yarangobilly caves in NSW Australia, this is the nearest record that can enable at least a rough derivation of temperatures for the region and this period. However, given the distance between these sites, and the age of the analysis, any interpretation should be treated with caution without primary fluid inclusion data.

This Tasmanian $\delta^{18}O_{calcite}$ record is significant as it describes a rapid warming between 97 to 76 Ka (Goede et. al., 1986). The pollen records in Fletcher and Thomas, 2010 also suggest warming during this period.

Strangely, the fluid-inclusion $\delta^{18}O_{H2O}$ data between 99 and 84 Ka is not explicitly presented in Goede et. al., 1986. However, by taking dated $\delta^{18}O_{calcite}$ values and Equation 4 from Goede et. al., 1986 (δD_{fi} = 13.9 $\delta^{18}O_{calcite}$ + 1.6 (r = 0.85)), fluid-inclusion deuterium values (δD_{fi}) can be calculated (Table 8.3). Fluid-inclusion $\delta^{18}O_{H2O}$ can then be calculated from δD_{fi} by rearranging Equation 1 from Goede et. al., 1986 as $\delta^{18}O_{H2O}$ = (δD_{fi} - 6.9)/7 (Table 8.3).

Age (Ka)	$\delta^{18}O_{calcite}$ (PDB)‰	δD_{fi} (SMOW)‰	$\delta^{18}O_{H2O}$ (SMOW)‰
99	-5.00	-47.4	-7.76
87.8	-3.90	-32.1	-5.57
84.1	-4.10	-34.9	-5.97

Table 8.3: $\delta^{18}O_{H2O}$ values as calculated from $\delta^{18}O_{calcite}$, δD_{fi} and Equations 1 and 4 from Goede et. al., 1986.

With no other indication of palaeo-meteoric water between 47.3 to 37 Ka, the average contemporary drip-water $\delta^{18}O_{H2O}$ value from site HW3 in Yarrangobilly was used at -6.9 (±0.3)‰ (Tadros, et. al., 2016). Some preliminary data from Treble & Drysdale 2010 suggest that this value has not deviated much in the last 100-years. Other studies from Mairs Cave, in South Australia, show variation similar (-4.5 to -7.5‰ at 15-23 Ka (Treble et. al., 2017)). However as before, this should be treated with caution as modern $\delta^{18}O_{H2O}$ values are unlikely to apply to the last glacial maximum, and further highlight the need for primary fluid inclusion data.

$\delta^{18}O_{PO4}$ in this record ranged from 13.06 (SD ±0.71)‰ at 84.1 Ka to 17.7 (SD ±0.71)‰ at 47.3 Ka. Temperature records can then be calculated from the literature (Longinelli & Nuti, 1973., Chang & Blake, 2015) and this article. Current annual mean temperature inside the cave is 12 °C (Desmarchelier, 1999).

8.7.1.1 99.4 to 84.1 Ka

Results show an apparent increase in temperature between 99.4 and 84.1 Ka (Figure 8.4). This is consistent with Goede et. al., 1986 suggests that +4 °C warming did take place in Tasmania during this period between 100 to 76 Ka. Stacked temperature records from Fletcher et. al., 2010 agree with this, suggesting a +2 °C increase in temperature from Southern Ocean and Tasmanian reconstructions.

However, all our temperature models seem to exaggerate this temperature increase. Equation 8.iii of Chang & Blake, 2015 starts closest to contemporary temperatures, rising from 10 °C. However, an increase from 10 °C to 45 °C between 99 and 84.1 Ka, as well as the equation from Poole's cavern, is unrealistic for in-cave temperatures. At 84.1 Ka, Longinelli & Nuti, 1973 is more reasonable at 30 °C, but still exaggerated.

This discrepancy could be partly explained by variations in site-specific drip-water $\delta^{18}O_{H2O}$, which can only be accounted for by fluid-inclusion data taken directly from YB-F1. Another explanation could be due to a change in phosphate source. Phosphate concentrations did drop through this period by 200-ppb (Webb et. al., 2014), therefore a reduction in P from certain sources might be biasing the data higher. A multi-proxy analysis of YB-F1 might be able to prise-apart this discrepancy.

Overall, the disagreement in the new phosphate-oxygen equation (8.vii) away from realistic temperatures might mean that our model does not translate well to non-hyperalkaline caves.

8.7.1.2 47.3 to 37 Ka

As hydrological connections to the cave returned, speleothem growth resumed between 47.3 to 37 Ka. A large increase in P concentration (800 to 1400 ppb), and $\delta^{18}O_{calcite}$ becoming depleted in 18O are signs of enhanced rainfall during this period (Frisia et. al., 2012).

$\delta^{18}O_{PO4}$ describes temperatures 47.3 ka starting below or near current cave temps at 6 ±5 °C (Longinelli & Nuti, 1973) or 11 ±6 °C (Chang & Blake, 2015), that steadily increase over time. This temperature increase is consistent with the interglacial transition as described by Webb et. al., 2014. Again, values for Longinelli & Nuti, 1973 suggest the most realistic temperature values, increasing to 18 ±3 °C by the end of the period. The reconstruction using the Poole's cavern equation 8.vii is again suggesting exaggerated temperatures.

Between 38.4 and 37 Ka, $\delta^{18}O_{PO4}$ suggests a +11 to +15 °C increase in temperature. This is not supported by Fletcher et. al, 2010 which shows no significant increases in temperature until around 15 Ka, where temperatures rapidly increased towards today's values. An increase in mean annual air temperature is possible, just not to this magnitude. This observation could be due to the bias of isotopically lighter $\delta^{18}O_{H2O}$ as rainfall volumes increased. The findings from Web et. al., 2014 already suggest that this was occurring over the period from $\delta^{18}O_{calcite}$ values. In all, this signifies the importance and value of collecting fluid inclusion data to correct for meteoric water effects in phosphate-oxygen palaeothermometry.

8.7.1.3 Summary

In all, this is good evidence to suggest that $\delta^{18}O_{PO4}$ from speleothems can be used to predict in-cave palaeotemperature change. A better constraint on $\delta^{18}O_{H2O}$ values, through fluid-inclusion analysis, will likely yield more accurate results over palaeo-datasets.

Comparing each equation, Longinelli & Nuti, 1973 and Chang & Blake, 2015 produces values nearest to current and sensible cave temperatures. Our model likely over-estimates temperature in all cases, suggesting a potential poor application to non-hyperalkaline cave systems.

Despite this, the dynamics controlling phosphate-oxygen fractionation in Yarangobilly are not fully understood. For example, we are assuming $\delta^{18}O_{PO4}$ is always at equilibrium with temperature as driven by microbial turnover of P. The concentration of P may have also altered through time and, if in replete conditions, could affect the ability for microbes to overturn $\delta^{18}O_{PO4}$ to equilibrium with temperature. Moreover, comparative studies such as Smith et. al., 2021 have shown that sample equilibrium to temperature is not always the case in the literature.

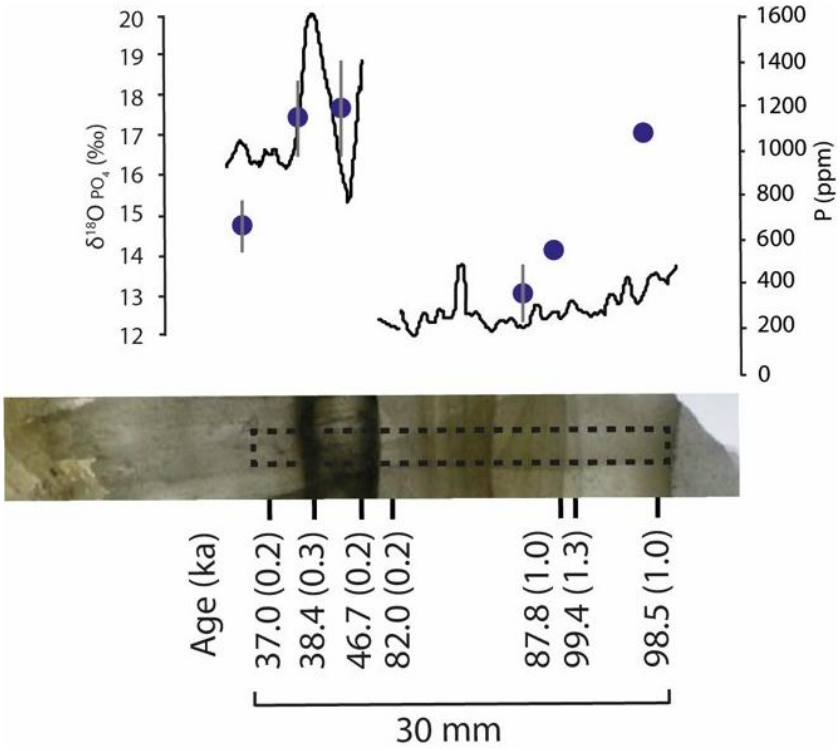

Figure 8.3: $\delta^{18}O_{PO4}$ data (unpublished) from calcite samples of YB-F1 (Yarangobilly caves, Australia) showing its variation through time (Wynn, unpublished 11/07/2019). P (ppm) data is provided from Webb. et. al., that shows its variation through time as controlled by water influx and is therefore an indicator of rainfall/aridity (Fairchild & Baker, 2010). This shows adequate P concentrations for processing to silver phosphate throughout. Figure from Wynn, 2019 (unpublished - BCRA Seminar).

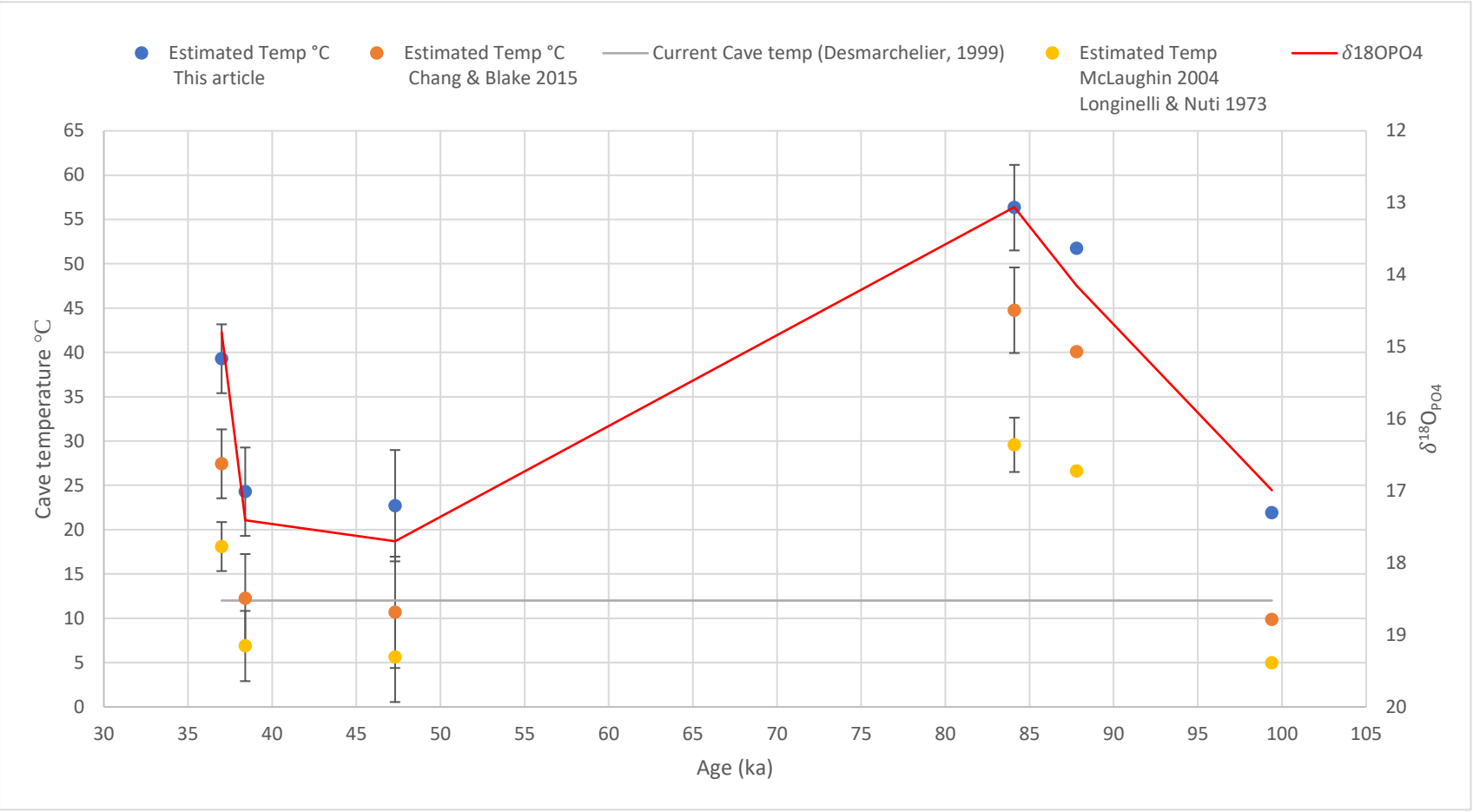

Figure 8.4: $\delta^{18}O_{PO4}$ temperature record for Yarangobilly Caves between 37 to 99 Ka. Taken from 6 U/Th date-matched drill samples that were processed to silver phosphate for isotopic analysis (Unpublished data, Wynn 2019). Equations 8.i to 8.iii from this article, Longinelli & Nuti 1973 and Chang & Blake 2015 were then used to calculate theoretical temperature. $\delta^{18}O_{H2O}$ values used in this calculation were taken from Tasmanian fluid-inclusions (Table 8.3) from Goede et. al., 1986 between 99 and 84 Ka. Contemporary drip-water values from HW3 (Tadros, et. al., 2016) were used as an estimate for 47.3 to 37 Ka. Current cave temperature, shown in grey, is 12 °C (Desmartchelier, 1999). Raw $\delta^{18}O_{PO4}$ trend is shown on the secondary axis in red. Error bars ±1 SD are given where possible, however the oldest two data points (87.8 Ka, 99.4 Ka) only yielded enough silver phosphate for 1 result.

8.7.2 OCEAN TEMPERATURES IN THE ARCHEAN

Oxygen and silicate isotope records from cherts suggest that ocean temperatures during the Archean, 3.2 to 3.5 Ga, were 55-80 °C (Karhu, J., 1986., Knauth, L., et. al., 2003., Robert F., et. al., 2006). This range is supported by phylogenetic records of 'resurrected proteins', which show that microorganisms in this period thrived in temperatures around 65 °C (Gaucher et. al., 2008). However conflicting results, such as using oxygen and hydrogen isotopes, suggests temperatures could be as low as 40 °C (Hren, et. al., 2009) or 0-50 °C (Krissansen-Totton, et. al., 2018). To date, there is still contention in the literature of exact temperature ranges from difference sources.

As such, Blake et. al., 2010 suggested the use of $\delta^{18}O_{PO4}$ as a novel thermometer for Archean Ocean temperatures. After extracting orthophosphate from iron-rich sedimentary rocks (Barberton Greenstone Belt, S. Africa), Blake et. al., 2010 was able to report $\delta^{18}O_{PO4}$ of 17.7-19.9‰ for 3.2-3.5 Ga (Chang & Blake, 2015). It is thought that iron oxides can scavenge PO_4 from the photic zones of oceans without alteration of the P-O bond and therefore further fractionation (Blake et. al., 2010). The iron-oxide then precipitates to the ocean floor, preserving the $\delta^{18}O_{PO4}$ signal. A preservation of this signal was justified, as Barberton rocks experienced only low-grade metamorphism and PO_4 is resistant to diagenesis (Chang & Blake, 2015).

This is an interesting observation, as Poole's Cavern has mention of iron-oxide based colloids in the literature (Hartland et. al., 2010). These exist in high concentrations and likely scavenge PO_4 in a similar way. Moreover, given the hyperalkaline nature of the waters, any microbes residing in the drip-waters are likely to be extremophiles. Actinobacteria, for example, show resistance to high temperatures as well as extremes of pH (Shivlata, et. al., 2015). Many

archaea and cyanobacteria are both alkaliphiles and hyperthermophiles (Rampelotto, 2013). For this reason, it is suggested that Poole's Cavern waters might be a surprisingly good analogue for the Archean ocean, as similar phenotypical characteristics might be present. As such, we can test equation 8.vii accordingly.

Blake et. al., (2010) used $\delta^{18}O_{PO4}$ and equation 8.i from Longinelli and Nuti, 1973 to calculate ocean temperatures as 26 to 35 °C. This was later amended by Chang & Blake 2015, using their new equation 8.iii, as 39 to 54 °C. $\delta^{18}O_{H2O}$ was assumed to be 0‰ as, apart from during glaciations, there is good evidence to suggest that meteoric ocean water has not altered much through geologic time (Blake et. al., 2010). As such, current $\delta^{18}O_{PO4}$ temperature estimates for the Archean are still below the range as suggested by chert records and outside the boundary of protein evolution.

Applying equation 8.vii from Poole's cavern to the $\delta^{18}O_{PO4}$ values from Blake et. al., 2010, and using a $\delta^{18}O_{H2O}$ of 0‰, we get a temperature range of 51 to 66 °C. This range is 12 °C higher than previous estimates by Chang & Blake, 2015, and fits closer to the current consensus of Archean ocean temperatures being between 55 and 80 °C from Si and O isotopes, as well as within range of resurrected protein models of early microorganisms at 65 °C.

One concern is that 51 to 66 °C might be in the range that might cause PPase enzymes to denature. This would inhibit the fractionation of orthophosphate by microbes, meaning that $\delta^{18}O_{PO4}$ is unlikely to be in equilibrium with temperature as inorganic fractionation processes do not readily occur (Chang & Blake, 2015., Smith et. al., 2021). For example, the optimum temperature for PPase in E. Coli is 45 °C, with full denaturisation at 60 °C (Cui, et. al., 2015).

However, many hyperthermophilic archaea, such as *Pyrococcus horikoshii*, host PPase that contain protein structures that make it thermally resistant to denaturisation at high

temperatures (Jeon et. al., 2005). PPase in these microbes overturn inorganic phosphate much more slowly but operate most effectively at 70 °C, with denaturisation taking place over 105 °C (Cui et. al., 2015). Moreover, 16S rRNA-based studies suggest that hyperthermophiles such as this are the most primitive known organisms, acting as the common ancestor in the phylogenetic tree of life (Stetter, 2006). They are likely contenders to be found 3.2 to 3.5 Ga.

To justify this, a careful study needs to be made to better understand the types of species that are thriving in Poole's Cavern waters, to see if there is any physiological connection to thermophiles or early microorganisms. This is important, as the specific metabolism mechanisms of P may affect $\delta^{18}O_{PO4}$. A glycerol dialkyl glycerol tetraethers (GDGTs) sweep of Poole's Cavern waters not only suggests a distinct microbial community compared to the soil system, but also shows evidence for high abundance of archaeal (41.5 %) and crenarchaeol (58.5 %) GDGTs (Blyth, et. al., 2014). GDGT membrane lipids, and particularly crenarchaeol GDGTs, are associated with hyperthermophiles by acting as a protective mechanism to extreme temperatures (Pitcher et. al., 2010). As such, crenarchaeol is mainly attributed to ammonium-oxidizing thaumarchaeota, that thrive in oligotrophic and hyperthermophilic conditions (Pester et. al., 2011). Species such as this might be expected in a culture analysis of Poole's Cavern waters and may have surprising ancestral roots to those found in the Archean.

It is therefore reasonable to suggest that our $\delta^{18}O_{PO4}$-temperature signal of 51 to 66 °C could have developed in Archean oceans 3.2 to 3.5 Ga, driven by the metabolism of early extremophiles. It however must be kept in mind that diagenesis of phosphate this old is possible, meaning that $\delta^{18}O_{PO4}$ may have altered through time or may not have been in equilibrium with temperature originally (Smith et. al., 2021).

9 - CONCLUSION

This research suggests the first evidence for potential Pyrophosphatase (PPase) activity in speleothem drip waters, signifying promise for $\delta^{18}O_{PO4}$ thermometry in caves. A statistically significant (R^2=0.69 p <0.01) relationship exists between $\delta^{18}O_{PO4}$ and temperature between 7 and 30 ^{o}C in Poole's Cavern drip-waters. This applies for the in-cave-system, and a closed-system with 100-ppb of additional orthophosphate, but shows non-equilibration when P concentrations surpass microbial needs. The gradient of change (-0.2‰/°C) is very similar to existing literature (e.g., Chang & Blake, 2015), however $\delta^{18}O_{PO4}$ values are consistently positively offset by the hyperalkaline pH of Poole's Cavern. This is a key first step in showcasing the potential for $\delta^{18}O_{PO4}$ as an in-cave chemical thermometer. However, the $\delta^{18}O_{PO4}$-temperature equation derived from Poole's Cavern is likely to only apply to hyperalkaline environments.

Secondly, this thesis evaluated $\delta^{18}O_{PO4}$ thermometry in contemporary speleothem material with mixed results. It has been shown that 'natural' $\delta^{18}O_{PO4}$ values in Poole's Cavern (that likely depict equilibration to in-cave temperature) can be successfully transferred between drip-water and speleothem material phases with minimal alteration. This suggests that $\delta^{18}O_{PO4}$ in speleothem material is representative of $\delta^{18}O_{PO4}$ in the drip-waters at the time of calcification which itself can 'log' cave temperature. This is complimented in a 100-yr-old speleothem from Ethiopia, which yields reasonable in-cave temperatures using existing $\delta^{18}O_{PO4}$-thermometry equations.

However, this does not apply to synthetic calcite or a speleothem from Brown's Folly Mine, likely due to acid hydrolysis and exchange of oxygen during calcite dissolution. In the future,

this can be solved by weighing the speleothem powder and stoichiometrically adding acid to minimise the duration of low pH conditions during dissolution.

Potential for $\delta^{18}O_{PO4}$ in palaeothermometry is also demonstrated. Data acquired in 2019 from an Australian speleothem seems to describe periods of temperature change that are temporally and regionally consistent for 99 to 37 ka. However, variation in $\delta^{18}O_{PO4}$ seems to describe exaggerated temperatures, possibly suggesting the need for better constraint of co-eval water values through fluid inclusion analysis to account for meteoric effects. Finally, following Chang & Blake, 2015, the phosphate-temperature equation generated from Poole's Cavern was applied to predict Archean ocean temperatures.

It seems that under the right conditions (with orthophosphate available to microbes but not in excess) $\delta^{18}O_{PO4}$-thermometry has real potential in speleothem palaeoclimatology. Considering that caves often represent average regional air temperature, and speleothems are invaluable as a temporally constrained climate archive, there is significance in furthering this technique for building an absolute temperature record.

For the future, it would be valuable to pursue building a fractionation equation with speleothem drip-waters at more typical pH (such as White Scar Cavern – pH 8) that will likely not be affected hyperalkalinity. There should be further investigation into issues during sample prep. Acid hydrolysis, for example, can be checked by dissolving calcite in an isotopically heavy medium. Opportunity should also be taken to establish a phosphate-temperature calibration within a cave system that hosts a speleothem record containing both fluid inclusions and phosphate. If the ensuing phosphate temperature record could be tested against a carbonate isotopologue time series, this would help to validate the technique against more conventional temperature proxies. This would provide the first absolutely dated

speleothem temperature record independent of competing environmental effects and kinetic fractionations.

10 – APPENDIX

10.1 $\delta^{18}O_{PO4}$ Isotope Data

$\delta^{18}O_{PO4}$ data for Poole's Cavern regression line at 100-ppb

Sample ID	Temp. °C	Temp. Range	PDOF ppb	Testing Date	Phosphate $\delta^{18}O$ (‰)	n=	SD (‰)	Notes
Keyworth Fridge 4	4	n/a	100	25/01/2021	16.98	3.00	0.51	Not included in trendline as noted equilibration not to work below 7 degrees
Poole's In Cave Temp 1	8.1	0.85	100	25/01/2021	22.60	2.00	2.30	Did not include in trendline: Very wide range. 1 result retracted due to +39% O
Poole's In Cave Temp 2	8.1	0.85	100	18/02/2021	22.03	2.00	3.27	Did not include in trendline: Very wide range. Average 16 % high O
Keyworth Incubator	16	n/a	100	25/01/2021	15.50	1.00	n/a	1 result.
Keyworth (lab temp)	21	n/a	100	25/01/2021	18.36	3.00	0.61	
Poole's 30 degree 25.1.21	30	n/a	100	25/01/2021	16.15	1.00	n/a	1 result. Result retracted due to high Oxygen % (+35.5 %)
LEC Cold Store 24hrs (4pt)	7.2	0.34	100	18/02/2021	20.11	3.00	0.31	
LEC Cold Store 6 days (4pt)	7.2	0.34	100	18/02/2021	20.61	2.00	0.06	1 result retracted due to low O % (-55 %)
Poole's 30C 100ppb 5 days	30	n/a	100	30/07/2021	16.2	3.00	0.8	
Poole's room 100ppb 5 days	22.6	0.89	100	30/07/2021	16.8	3.00	0.043	
Poole's 16C 100-ppb	16	n/a	100	30/07/2021	17.7	3.00	0.4	
Poole's lab Fridge 100ppb	4	n/a	100	30/07/2021	16.1	3.00	0.04	Not included in trendline as noted equilibration not to work below 7 degrees
8Lt Poole's Bulk Water 26/03/21	7.2	0.2	n/a	21/05/2021	20.2	3.0	0.5	
100-ppb DI water control	4 to 30	n/a	100	30/07/2021	18.2	3.0	0.4	DI Water check, not in trendline

Table 10.1: Raw data for the Phosphate-oxygen temperature relationship of Poole's Cavern waters spiked to 100-ppb. Data obtained from experiments undertaken at BGS Keyworth (25/01/21, 18/02/21), repeats at LEC (30/07/21) and two results from spiked waters left sealed in Poole's Cavern. Included is a result for 8Lt of un-spiked Poole's Cavern water, thought to represent in-cave temperature composition. Control data shows values for 100-ppb of potassium dihydrogen orthophosphate (PDOF) dissolved in boiled DI water and processed to silver phosphate (18.2 ±0.4‰).

Table 10.2: $\delta^{18}O_{PO4}$ data for Poole's Cavern waters dosed with 400-ppb PDOF

Sample ID	Date	Temperature °C	Phosphate $\delta^{18}O$ (‰)	Standard Deviation (‰)
Poole's 400ppb 4C	30/07/2021	4	15.8	0.2
6 2 day fridge	10/03/2021	7.0	16.0	0.1
72hr Pooles temp	05/03/2021	7	17.84	0.22
5 days Pooles temp	07/03/2021	7	15.15	0.38
5 24hr fridge	09/03/2021	7.1	15.9	0.1
7 72hr fridge	11/03/2021	7.2	16.4	0.2
Pooles in cave 0hr	02/03/2021	7.2	17.1	0.20
4hr Pooles temp	02/03/2021	7.2	15.77	0.48
8 11 days fridge	19/03/2021	7.3	16.6	0.4
1 0hr fridge	08/03/2021	7.4	16.0	0.3
2 4hr fridge	08/03/2021	7.4	16.5	0.3
3 8hr fridge	08/03/2021	7.4	17.1	0.4
4 12hr fridge	08/03/2021	7.4	17.4	0.1
F1	23/04/2021	7.9	17.3	0.10
F2	23/04/2021	7.9	17.6	0.20
F3	23/04/2021	7.9	17.2	0.10
F4	23/04/2021	7.9	17	0.30
Poole's FR 24H	04/06/2021	8	17.4	0.20
Poole's FR 72H	06/06/2021	8	16.7	0.30
0hr 16 degrees		16	17.2	0.2
24hr 16 degrees		16	16.6	0.2
48hr 16 degrees		16	16.9	0.0
7days 16 degrees		16	17.6	0.1
6 48hr Room	10/03/2021	20.2	17.1	0.2
5 24hr Room	09/03/2021	20.4	16.9	0.5
7 72hr Room	11/03/2021	20.5	17.2	0.3
8 11 days Room	19/03/2021	21.5	16.4	0.7
1 0hr Room	08/03/2021	22.3	17.7	0.2
2 4hr Room	08/03/2021	22.3	17.1	0.1
3 8hr Room	08/03/2021	22.3	16.9	0.1
4 12hr Room (23 Deg C)	08/03/2021	22.3	17.4	0.4
Room 2	19/04/2021	22.7	17.2	
Room 1	19/04/2021	22.7	18.5	0.30
Room 4	19/04/2021	22.7	17.3	0.30
Room 3	19/04/2021	22.7	16.3	0.50
Pooles 30C 72H	06/06/2021	31	16.3	0.20
Pooles 30C 24H	04/06/2021	32	17.3	0.20
0hr inc	08/03/2021	34	16.8	
4 72hr Incubator	11/03/2021	35	17.6	0.1
2 8hr incubator	08/03/2021	36	16.1	0.4
3 24hr incubator	09/03/2021	36	15.5	0.7
Inc 4	23/04/2021	38	17.7	0.40
Inc 3	23/04/2021	38	17.5	0.30
Inc 2	23/04/2021	38	17.6	0.40
Inc 1	23/04/2021	38	18	0.30

Table 10.3: $\delta^{18}O_{PO4}$ data for Poole's Cavern equilibration experiments with 400-ppb PDOF

Sample ID	Date	Temperature °C	Sample Location	Hours	Phosphate $\delta^{18}O$ (‰)	Standard Deviation (‰)	% O	Peak height (nA)	Comments
1 0hr fridge	08/03/2021	7.4	Cold Store	0	16.0	0.3	16.0	2.3	
2 4hr fridge	08/03/2021	7.4	Cold Store	4	16.5	0.3	16.1	2.3	
3 8hr fridge	08/03/2021	7.4	Cold Store	8	17.1	0.4	15.7	2.1	
4 12hr fridge	08/03/2021	7.4	Cold Store	12	17.4	0.1	16.1	2.3	
5 24hr fridge	09/03/2021	7.1	Cold Store	24	15.9	0.1	16.1	2.1	
6 2 day fridge	10/03/2021	7.0	Cold Store	48	16.0	0.1	16.1	2.4	
7 72hr fridge	11/03/2021	7.2	Cold Store	72	16.4	0.2	18.4	2.3	
8 11 days fridge	19/03/2021	7.3	Cold Store	264	16.6	0.4	16.9	2.5	
Pooles FR 24H	04/06/2021	8	Cold Store	24	17.4	0.20	15.50		
Pooles FR 72H	06/06/2021	8	Cold Store	72	16.7	0.30			
0hr 16 degrees		16	16 Deg	0	17.2	0.2	15.6	2.0	
24hr 16 degrees		16	16 Deg	24	16.6	0.2	15.2	3.7	
48hr 16 degrees		16	16 Deg	48	16.9	0.0	15.9	2.2	
7days 16 degrees		16	16 Deg	168	17.6	0.1	16.1	2.2	
1 0hr Room	08/03/2021	22.3	Room	0	17.7	0.2	15.9	2.0	
2 4hr Room	08/03/2021	22.3	Room	4	17.1	0.1	15.8	1.9	
3 8hr Room	08/03/2021	22.3	Room	8	16.9	0.1	15.7	2.1	
4 12hr Room (23 Deg C)	08/03/2021	22.3	Room	12	17.4	0.4	14.8	1.9	
5 24hr Room	09/03/2021	20.4	Room	24	16.9	0.5	15.7	2.0	
6 48hr Room	10/03/2021	20.2	Room	48	17.1	0.2	15.7	2.3	
7 72hr Room	11/03/2021	20.5	Room	72	17.2	0.3	15.4	2.2	
8 11 days Room	19/03/2021	21.5	Room	264	16.4	0.7	18.3	1.5	
0hr inc	08/03/2021	34	Incubator 36	0	16.8		14.70		
2 8hr incubator	08/03/2021	36	Incubator 36	8	16.1	0.4	16.9	2.5	
3 24hr incubator	09/03/2021	36	Incubator 36	24	15.5	0.7	16.9	2.2	
4 72hr Incubator	11/03/2021	35	Incubator 36	72	17.6	0.1	15.6	2.4	
Pooles 30C 24H	04/06/2021	32	30 degrees	24	17.3	0.20			within the range of samples above.
Pooles 30C 72H	06/06/2021	31	30 degrees	72	16.3	0.20			

Table 10.4: White Scar equilibration experiments at 100 and 400-ppb

Sample ID	Sample Location	Phosphate $\delta^{18}O$ (‰)	Standard Deviation (‰)	% O	Temperature °C	Date	PDOF ppb
WS FR 0H	White Scar	16.8	0.00		8	03/06/2021	400
WS FR 4H	White Scar	17.8	0.20		8	03/06/2021	400
WS FR 8H	White Scar	16.5	0.30		8	03/06/2021	400
WS FR 12H	White Scar	17	0.20		8	03/06/2021	400
WS FR 24H	White Scar	16.9	0.80	16.60	8	04/06/2021	400
WS FR 48H	White Scar	17.5	0.90	15.70	8	05/06/2021	400
WS FR1 72H	White Scar	17.4	0.20	16.10	8	06/06/2021	400
WS 7 FR 72H #2	White Scar	18.1	0.20		8	06/06/2021	400
WS ROOM 24H	White Scar	16.9	0.20		22	04/06/2021	400
WS ROOM 72H	White Scar	17.8	0.00	16.90	22	06/06/2021	400
WS 30C 24H	White Scar	17.1	0.20	16.60	31	04/06/2021	400
WS 30C 72H	White Scar	18.3	0.40		32	06/06/2021	400
White Scar 400ppb 4C	White Scar	16.6	0.3	15.9	4		400
White Scar 16 ºC 100-ppb	White Scar	18.7	0.2	15.4	16	30/07/2021	100
White Scar 100ppb 8 ºC	White Scar	17.8	0.3	15.4	8	30/07/2021	100

Table 10.5: 400-ppb PDOF in Boiled DI water

Sample ID	Date	Sample Type	Phosphate $\delta^{18}O$ (‰)	Standard Deviation (‰)	% O
DI 400ppb -3 boiled	30/07/2021	DI CHECK	17.8	0.5	15.9
DI 400ppb -4 boiled	30/07/2021	DI CHECK	18.5	0.2	15.7
DI 400ppb -2 boiled	30/07/2021	DI CHECK	18.4	0.3	15.6
Average			18.2 (n=3)	0.37 (range = 0.7)	

10.2 Colourimetry Equilibration data – P concentration change over time

10.2.1 SEAL Equilibration change with 100-ppb PDOF

Table 10.6: 100-ppb orthophosphate

Sample ID	Date	Hours	n=	Average mg/L	SD	Average ppb	SD ppb
Before	02/02/2021	-24	3	0.025	0.002	25.30	2.34
0hr	02/02/2021	0	3	0.067	0.004	66.60	3.98
8hr	02/02/2021	8	3	0.074	0.004	74.13	3.71
24hr	03/02/2021	24	3	0.072	0.001	71.93	1.46
72hr	05/02/2021	72	3	0.075	0.004	75.00	4.36
6 days	08/02/2021	144	3	0.079	0.005	79.33	4.73
10 days	12/02/2021	240	3	0.069	0.002	69.33	2.31
13 days	15/02/2021	312	3	0.074	0.002	74.33	1.53
14 days	16/02/2021	336	3	0.070	0.006	70.33	6.43
21 days	23/02/2021	504	3	0.068	0.004	68.00	3.61
29 days	03/03/2021	696	3	0.056	0.005	56.00	5.00

Table 10.7: 100-ppb orthophosphate 0.2 micron filtered

Sample ID	Date	Hours	n=	Average mg/L	SD	Average ppb	SD ppb
Before	02/02/2021	-24	3	0.016	0.001	15.93	0.81
0hr	02/02/2021	0	3	0.025	0.002	25.03	2.16
8hr	02/02/2021	8	3	0.023	0.005	23.20	4.82
24hr	03/02/2021	24	3	0.018	0.002	18.18	2.02
72hr	05/02/2021	72	3	0.023	0.003	22.67	3.06
6 days	08/02/2021	144	3	0.035	0.002	35.33	2.31
10 days	12/02/2021	240	3	0.020	0.005	20.33	4.62
13 days	15/02/2021	312	3	0.023	0.008	23.33	8.02
14 days	16/02/2021	336	3	0.020	0.002	20.33	1.53
21 days	23/02/2021	504	3	0.016	0.002	15.67	2.08
29 days	03/03/2021	696	3	0.019	0.005	19.00	4.58

Table 10.8: 100-ppb orthophosphate 0.45 micron filtered

Day	Date	Hours	n=	Average mg/L	SD	Average ppb	SD ppb
10 days	12/02/2021	240	3	0.029	0.002	29.33	2.08
13 days	15/02/2021	312	3	0.031	0.003	31.33	2.52
14 days	16/02/2021	336	3	0.032	0.005	31.67	4.93

Table 10.9: 100-ppb Total P

Hours	Date	n=	Average mg/L	SD	ppb	SD ppb
-24	02/02/2021	3	0.008	0.002	7.85	1.63
0	02/02/2021	3	0.059	0.002	58.70	2.42
8	02/02/2021	3	0.073	0.023	72.95	23.26
24	03/02/2021	3	0.054	0.003	54.15	3.18
72	05/02/2021	3	0.052	0.000	52.37	0.35
144	08/02/2021	3	0.048	0.014	47.85	14.45
240	12/02/2021	3	0.048	0.004	47.70	4.44
312	15/02/2021	3	0.048	0.008	48.30	8.28
336	16/02/2021	3	0.046	0.003	46.00	2.75

Table 10.10: 100-ppb DI water degradation test

Sample ID	Date	n=	Average mg/l	SD	ppb	SD
DI 3 DAYS - Total P	17/02/2021	3	0.10	0.01	98.77	6.37
DI Spike 100 ppb	16/02/2021	3	0.10	0.00	100.00	1.73
DI Spike 100 ppb 0.2 F	16/02/2021	3	0.09	0.00	88.33	0.58
DI Spike 100 ppb 0.45F	16/02/2021	3	0.10	0.00	100.67	2.52

10.2.2 SEAL Equilibration change with 400-ppb PDOF

Table 10.11: 400-ppb Orthophosphate (filtered and unfiltered)

Sample	n=	Average mg/L	SD	Hours
Pooles Blank Fridge	3	0.020	0.002	-24
Pooles Blank Fridge 0.2F	3	0.020	0.002	-24
Fridge Temp 0hr	3	0.399	0.007	0
Fridge Temp 0hr 0.2F	3	0.032	0.002	0
Room Temp 0hr	3	0.383	0.002	0
Room Temp 0hr 0.2F	3	0.030	0.004	0
Incubator 0hr	3	0.368	0.004	0
Incubator 0hr 0.2F	3	0.032	0.002	0
Fridge Temp 4hr	2	0.386	0.002	4
Fridge Temp 4hr 0.2F	3	0.029	0.003	4
Room Temp 4hr	3	0.371	0.002	4
Room Temp 4hr 0.2F	3	0.023	0.001	4
Fridge Temp 8hr	2	0.377	0.004	8
Fridge Temp 8hr 0.2F	3	0.012	0.001	8
Room Temp 8hr	3	0.367	0.008	8
Room Temp 8hr 0.2F	3	0.023	0.002	8
Incubator 8hr	3	0.332	0.008	8
Incubator 8hr 0.2F	3	0.025	0.001	8
Fridge Temp 12hr	3	0.39	0.008	12
Fridge Temp 12hr 0.2F	3	0.024	0.002	12
Room Temp 12hr	3	0.343	0.006	12
Room Temp 12hr 0.2F	3	0.021	0.002	12
Fridge Temp 24hr	3	0.363	0.009	24
Fridge Temp 24hr 0.2F	3	0.020	0.002	24
Room Temp 24hr	3	0.345	0.003	24
Room Temp 24hr 0.2F	3	0.022	0.001	24
Incubator 24hr	3	0.314	0.003	24
Incubator 24hr 0.2F	3	0.013	0.001	24
Fridge Temp 72hr	3	0.339	0.008	72
Fridge Temp 72hr 0.2F	3	0.023	0.001	72
Room Temp 72hr	3	0.302	0.006	72

Room Temp 72hr 0.2F	3	0.017	0.001	72
Incubator 72hr	3	0.232	0.002	72
Incubator 72hr 0.2F	3	0.018	0.002	72
Fridge Temp 7 days	2	0.355	0.016	168
Fridge Temp 7 days 0.2F	3	0.021	0.002	168
Room Temp 7 days	3	0.323	0.004	168
Room Temp 7 days 0.2F	3	0.015	0.001	168
Fridge Temp 11 days	3	0.346	0.003	264
Fridge Temp 11 days 0.2F	3	0.021	0.001	264
Room Temp 11 days	3	0.280	0.005	264
Room Temp 11 days 0.2F	3	0.014	0.001	264

Table 10.12: 400-ppb Total-P

Sample	n=	Average mg/L	SD	Hours
0hr Fridge 080321	3	0.40	0.00	0
4hr Fridge 080321	3	0.39	0.00	4
8hr Fridge 080321	3	0.40	0.00	8
12hr Fridge 080321 1	3	0.34	0.00	12
24hr Fridge 090321 1	3	0.34	0.00	24
72hr Fridge 110321 3	3	0.33	0.00	72
7 days Fridge 150321 1	3	0.35	0.00	168
11 days Fridge 190321 1	3	0.35	0.00	264
0hr Room 080321 1	3	0.35	0.00	0
4hr Room 080321 1	3	0.38	0.00	4
8hr Room 080321 1	3	0.36	0.00	8
12hr Room 080321 1	3	0.34	0.00	12
24hr Room 090321 1	3	0.34	0.00	24
72hr Room 110321 1	3	0.33	0.00	72
7 days Room 150321 1	3	0.32	0.00	168
11 days Room 190321 1	3	0.30	0.01	264
0hr Incubator 030321 1	3	0.36	0.00	0
8hr Incubator 080321 2	3	0.34	0.00	8
24hr Incubator 090321 1	3	0.30	0.00	24
72hr Incubator 110321 1	3	0.25	0.00	72

11 – REFERENCES

Alpert AE, Cohen AL, Oppo D, DeCarlo TM, Gove J, Young C., 2016. Comparison of equatorial Pacific sea surface temperature variability and trends with Sr/Ca records from multiple corals. Palaeoceanography 31:252–265

Bajnai, D., Guo, W., Spötl, C. *et al.* Dual clumped isotope thermometry resolves kinetic biases in carbonate formation temperatures. *Nat Commun* **11,** 4005 (2020). https://doi.org/10.1038/s41467-020-17501-0

Baker A., Genty D., Dreybodt W., Barnes W., Mockler N. and Grapes J. (1998) Testing theoretically predicted stalagmite growth rate with recently annually laminated samples: implications for past stalagmite deposition. Geochim. Cosmochim. Acta 62, 393–404. https://doi.org/10.1016/S0016-7037(97)00343-8

Baker A., Mockler N. and Barnes W. (1999) Fluorescence intensity variations of speleothem forming groundwaters: implications for palaeoclimate reconstruction. Water Resour. Res. 35, 407– 413.

Baker, A., Asrat, A., Fairchild, I.J., Leng, M.J., Wynn, P.M., Bryant, C., Genty, D. and Umer, M., 2007. Analysis of the climate signal contained within δ18O and growth rate parameters in two Ethiopian stalagmites. *Geochimica et Cosmochimica Acta*, *71*(12), pp.2975-2988.

Baker, A., Blyth, A.J., Jex, C.N., et al., 2019. Glycerol dialkyl glycerol tetraethers (GDGT) distributions from soil to cave: Refining the speleothem palaeothermometer. Organic Geochemistry, 136: 103890. doi:10.1016/j.orggeochem.2019.06.011.

Baker, A., Smart, P. L. & Lawrence Edwards, R., 1995. Palaeoclimate implications of mass spectrometric dating of a British flowstone. Geology 23, 10.1130/0091-7613(1995)023<0309:Piomsd>2.3.Co;2

Baldini, J.U., Bertram, R.A. and Ridley, H.E., 2018. Ground air: A first approximation of the Earth's second largest reservoir of carbon dioxide gas. Science of the Total Environment, 616, pp.1007-1013. https://doi.org/10.1016/j.scitotenv.2017.10.218

Baldini, J. U. L. 2010. Cave atmosphere controls on stalagmite growth rate and palaeoclimate records. Geological Society, London, Special Publications 336, 283–294, https://doi.org/10.1144/sp336.15

Baldini, J.U., 2001. Morphologic and dimensional linkage between recently deposited speleothems and drip water from Browns Folly Mine, Wiltshire, England. J. Cave Karst Stud, 63, pp.83-90.

Baldini, J.U., McDermott, F., Baker, A., Baldini, L.M., Mattey, D.P. and Railsback, L.B., 2005. Biomass effects on stalagmite growth and isotope ratios: A 20th century analogue from Wiltshire, England. Earth and Planetary Science Letters, 240(2), pp.486-494.

Baldini, J.U.L. 2002. Structure of the 8200-Year Cold Event Revealed by a Speleothem Trace Element Record. Science 296(5576), pp. 2203–2206. http://dx.doi.org/10.1126/science.1071776.

Barman, J., Samanta, A., Saha, B. and Datta, S., 2016. Mycorrhiza. Resonance, 21(12), pp.1093-1104.

Bar-Matthews, M., Ayalon, A., Matthews, A., Sass, E. and Halicz, L., 1996. Carbon and oxygen isotope study of the active water-carbonate system in a karstic Mediterranean cave: Implications for palaeoclimate research in semiarid regions. Geochimica et Cosmochimica Acta, 60(2), pp.337-347.

Bassil, N.M., Bryan, N. and Lloyd, J.R., 2015. Microbial degradation of isosaccharinic acid at high pH. The ISME journal, 9(2), pp.310-320.

Bassil, N.M., Small, J.S. and Lloyd, J.R., 2020. Enhanced microbial degradation of irradiated cellulose under hyperalkaline conditions. FEMS Microbiology Ecology.

Bernard, S., Daval, D., Ackerer, P. et al., 2017. Burial-induced oxygen-isotope re-equilibration of fossil foraminifera explains ocean palaeotemperature paradoxes. Nat Commun 8, 1134 (2017). https://doi.org/10.1038/s41467-017-01225-9

Bi, Q.-F., Zheng, B.-X., Lin, X.-Y., et al. (2018) The microbial cycling of phosphorus on long-term fertilized soil: Insights from phosphate oxygen isotope ratios. Chemical Geology, 483: 56–64.doi:10.1016/j.chemgeo.2018.02.013.

Blaauw, M., 2012. Out of tune: the dangers of aligning proxy archives. Quaternary Science Reviews Volume 36, 12 March 2012, Pages 38-49. https://doi.org/10.1016/j.quascirev.2010.11.012

Blake, R. E., Aleksandr V. Surkov, Lisa M. Stout, Hui Li, Sae Jung Chang, Deb P. Jaisi, Albert S. Colman, Yuhong Liang., 2016. DNA thermometry: A universal biothermometer in the 18O/16O ratio of PO4 in DNA. American Journal of Science Nov 2016, 316 (9) 813-838; DOI: 10.2475/09.2016.01

Blake, R.E., Alt, J.C. and Martini, A.M., 2001. Oxygen isotope ratios of PO4: an inorganic indicator of enzymatic activity and P metabolism and a new biomarker in the search for life. Proceedings of the National Academy of Sciences, 98(5), pp.2148-2153.

Blake, R.E., O'Neil, J.R. and Surkov, A.V., 2005. Biogeochemical cycling of phosphorus: insights from oxygen isotope effects of phosphoenzymes. American Journal of Science, 305(6-8), pp.596-620.

Blake, R.E., O'Neil, J.R., Garcia, G.A., 1997. Oxygen isotope systematics of biologically mediated reactions of phosphate: I. Microbial degradation of organophophorus compounds. Geochimica et Cosmochimica Acta 61, 4411–4422.

Blyth, A.J., Jex, C.N., Baker, A., Khan, S.J. and Schouten, S., 2014. Contrasting distributions of glycerol dialkyl glycerol tetraethers (GDGTs) in speleothems and associated soils. Organic geochemistry, 69, pp.1-10.

Bollyn, J., Faes, J., Fritzsche, A. and Smolders, E., 2017. Colloidal-bound polyphosphates and organic phosphates are bioavailable: a nutrient solution study. Journal of Agricultural and Food Chemistry, 65(32), pp.6762-6770.

Borsato, A., Frisia, S., Fairchild, I. J., Somogyi, A., and Susini, J.: Trace element distribution in annual stalagmite laminae mapped by micrometer-resolution X-ray fluorescence: implications for incorporation of environmentally significant species, Geochim. Cosmochim. Ac., 71, 1494–1512, 2007.

Bradley, C., Andy Baker, Catherine N. Jex, Melanie J. Leng., 2010. Hydrological uncertainties in the modelling of cave drip-water $\delta^{18}O$ and the implications for stalagmite palaeoclimate reconstructions, Quaternary Science Reviews, Volume 29, Issues 17–18, 2010, Pages 2201-2214, ISSN 0277-3791, https://doi.org/10.1016/j.quascirev.2010.05.017

Bradley, R., 2015. Palaeoclimatology: Reconstructing Climates of the Quaternary. Oxford: Elsevier. ISBN 978-0-12-386913-5.

Bradley, R.S., 2008. Holocene perspectives on future climate change. In: Battarbee, R.W., Binney, H.A. (Eds.), Natural Climate Variability and Global Warming: A Holocene Perspective. Wiley-Blackwell, Chichester, pp. 254–268.

Braganza, K., Gergis, J. L., Power, S. B., Risbey, J. S., and Fowler, A. M. (2009), A multiproxy index of the El Niño–Southern Oscillation, A.D. 1525–1982, J. Geophys. Res., 114, D05106, doi:10.1029/2008JD010896.

Bramwell, D, Dalton, K, Drinkwater, J, Hassall, J, Lorimer, K and Mackreth, K, 1983. Excavations at Poole's Cavern, Buxton: an interim report. Derbyshire Archaeological Journal, Vol.103, 47–74.

Bréant, C., Amaëlle Landais, Anaïs Orsi, Patricia Martinerie, Thomas Extier, Frédéric Prié, Barbara Stenni, Jean Jouzel, Valérie Masson-Delmotte, Markus Leuenberger, 2019. Unveiling the anatomy of Termination 3 using water and air isotopes in the Dome C ice core, East Antarctica, Quaternary Science Reviews, Volume 211, Pages 156-165, ISSN 0277-3791, https://doi.org/10.1016/j.quascirev.2019.03.025.

Brohan, P., J.J. Kennedy, I. Harris, S.F.B. Tett, P.D. Jones. 2006. "Uncertainty estimates in regional and global observed temperature changes: a new dataset from 1850". J. Geophys. Res. 111 (D12): D12106. doi:10.1029/2005JD006548.

Bryan SP, Marchitto TM., 2008. Mg/Ca–temperature proxy in benthic foraminifera: new calibrations from the Florida Straits and a hypothesis regarding Mg/Li. Palaeoceanography 23:PA2220

Buffle, J., Wilkinson, K.J., Stoll, S., Filella, M. and Zhang, J., 1998. A generalized description of aquatic colloidal interactions: the three-colloidal component approach. Environmental Science & Technology, 32(19), pp.2887-2899.

Burke, I.T., Mortimer, R.J., Palaniyandi, S., Whittleston, R.A., Lockwood, C.L., Ashley, D.J. and Stewart, D.I., 2012. Biogeochemical reduction processes in a hyper-alkaline leachate affected soil profile. Geomicrobiology Journal, 29(9), pp.769-779.

Chang, S. J., Ruth E. Blake, 2015. Precise calibration of equilibrium oxygen isotope fractionations between dissolved phosphate and water from 3 to 37°C, Geochimica et Cosmochimica Acta, Volume 150, 2015, Pages 314-329, ISSN 0016-7037, https://doi.org/10.1016/j.gca.2014.10.030

Chang, S.J., Blake, R.E. and Colman, A.S., 2021. Oxygen isotope exchange rates between phosphate and water catalyzed by inorganic pyrophosphatase: Implications for the biogeochemical cycle of phosphorus. Earth and Planetary Science Letters, 570: 117071. doi:10.1016/j.epsl.2021.117071.

Chang, S.J., Blake, R.E., Stout, L.M. and Kim, S.J., 2010. Oxygen isotope, micro-textural and molecular evidence for the role of microorganisms in formation of hydroxylapatite in limestone caves, South Korea. Chemical Geology, 276(3-4), pp.209-224. https://doi.org/10.1016/j.chemgeo.2010.06.007

Chapman, M. R., Shackleton, N. J., Zhao, M., and Eglinton, G., 1996. Faunal and alkenone reconstructions of subtropical North Atlantic surface hydrography and palaeotemperature over the last 28 kyr, Palaeoceanography, 11(3), 343– 357, doi:10.1029/96PA00041.

Charles, C.J., Rout, S.P., Garratt, E.J., Patel, K., Laws, A.P. and Humphreys, P.N., 2015. The enrichment of an alkaliphilic biofilm consortia capable of the anaerobic degradation of isosaccharinic acid from cellulosic materials incubated within an anthropogenic, hyperalkaline environment. FEMS microbiology ecology, 91(8).

Cheng, H., Edwards, R. L., Sinha, A., Spötl, C., Yi, L., Chen, S., Kelly, M., Kathayat, G., Wang, X., Li, X., Kong, X., Wang, Y., Ning, Y., & Zhang, H., 2016. The Asian monsoon over the past 640,000 years and ice age terminations. Nature, 534(7609), 640–646. https://doi.org/10.1038/nature18591

Cheng, H., Edwards, R.L., Shen, C.C., Polyak, V.J., Asmerom, Y., Woodhead, J., Hellstrom, J., Wang, Y., Kong, X., Spötl, C. and Wang, X., 2013. Improvements in ^{230}Th dating, ^{230}Th and ^{234}U half-life values, and U–Th isotopic measurements by multi-collector inductively coupled plasma mass spectrometry. Earth and Planetary Science Letters, 371, pp.82-91.

Clark, I D, Fontes, J C and Fritz, P, 1992. Stable isotope disequilibria in travertine from high pH waters: Laboratory investigations and field observations from Oman. Geochimica et Cosmochimica Acta, Vol.56, 2041–2050.

Cohn, M., 1953, A study of oxidative phosphorylation with ^{18}O-labeled inorganic phosphate: Journal of Biological Chemistry, v. 201, p. 735–750.

Colman, A.S., Blake, R.E., Karl, D.M., Fogel, M.L. and Turekian, K.K., 2005. Marine phosphate oxygen isotopes and organic matter remineralization in the oceans. Proceedings of the National Academy of Sciences, 102(37), pp.13023-13028.

Comas-Bru, L., Rehfeld, K., Roesch, C., Amirnezhad-Mozhdehi, S., Harrison, S.P., Atsawawaranunt, K., Ahmad, S.M., Brahim, Y.A., Baker, A., Bosomworth, M. and Breitenbach, S.F., 2020. SISALv2: a comprehensive speleothem isotope database with multiple age–depth models. Earth System Science Data, 12(4), pp.2579-2606.

Conte MH, Sicre M, Rühlemann C, Weber JC, Schulte S, Schulz-Bull D, Blanz T., 2006. Global temperature calibration of the alkenone unsaturation index ($U^{K'}_{37}$) in surface waters and comparison with surface sediments. Geochem Geophys Geosyst 7:Q02005

Cook, E. R., R. D. D'Arrigo, and M. E. Mann, 2002: A Well-Verified, Multiproxy Reconstruction of the Winter North Atlantic Oscillation Index since a.d. 1400. J. Climate, 15, 1754–1764, https://doi.org/10.1175/1520-0442(2002)015<1754:AWVMRO>2.0.CO;2.

Crowson, R. A., Showers, W. J., Wright, E. K., & Hoering, T. C., 1991. Preparation of Phosphate Samples for Oxygen Isotope Analysis. Analytical Chemistry, 63(20), 2397–2400. https://doi.org/10.1021/ac00020a038

Cuffey KM, Vimeux F., 2001. Covariation of carbon dioxide and temperature from the Vostok ice core after deuterium-excess correction. Nature 412:523–527

Cui, Y., Liu, F., Li, X., et al. (2015) Improvement in the Thermal Stability of Pyrophosphatase by Conjugation to Poly(N-isopropylacrylamide): Application to the Polymerase Chain Reaction. ACS Applied Materials & Interfaces, 7 (39): 21913–21918. doi:10.1021/acsami.5b06494

Dansgaard W, Johnsen SJ, Clausen HB, Dahl-Jensen D, Gundestrup NS, Hammer CU, Hvidberg CS, Steffensen JP, Sveinbjoornsdottie AE, Jouzel J, Bond G., 1993. Evidence for general instability of past climate from a 250-kyr ice-core record. Nature 364:218–220

Dansgaard, W. and Johnsen, S. J., 1969. “A Flow Model and a Time Scale for the Ice Core from Camp Century, Greenland,” Journal of Glaciology. Cambridge University Press, 8(53), pp. 215–223. doi: 10.3189/S0022143000031208.

Darling, W.G., BATH, A.H., GIBSON, J.J. and ROZANSKI, K., 2006. Isotopes in water. In Isotopes in palaeoenvironmental research (pp. 1-66). Springer, Dordrecht. https://doi.org/10.1007/1-4020-2504-1_01

Davies, C. L., Surridge, B. W. J., & Gooddy, D. C., 2014. Phosphate oxygen isotopes within aquatic ecosystems: Global data synthesis and future research priorities. Science of the Total Environment, 496, 563–575. https://doi.org/10.1016/j.scitotenv.2014.07.057

Davison, W., Zhang, H., 1994. In-situ speciation measurements of trace components in natural waters using thin-film gels. Nature 367 (6463), 546–548. https://doi:10.1038/367546a0

de Boer, e. j., R. Tjallingii, M.I. Vélez, K.F. Rijsdijk, A. Vlug, G.-J. Reichart, A.L. Prendergast, P.G.B. de Louw, F.B.V. Florens, C. Baider, H. Hooghiemstra Climate variability in the SW Indian Ocean from an 8000-yr long multi-proxy record in the Mauritian lowlands shows a middle to late Holocene shift from negative IOD-state to ENSO-state Quat. Sci. Rev., 86 (2014), pp. 175-189, 10.1016/j.quascirev.2013.12.026

Deakin, P, et al., 1968. Poole’s Cavern Survey. [Eldon Pothole Club.]

DeCarlo TM, Gaetani GA, Cohen AL, Foster GL, Alpert AE, Stewart JA., 2016. Coral Sr-U thermometry. Palaeoceanography 31:626–638

Dekens PS, Lea DW, Pak DK, Spero HJ., 2002. Core top calibration of Mg/Ca in tropical foraminifera: refining palaeotemperature estimation. Geochem Geophys Geosyst 3:1–29

Dennis, P.F., Rowe, P.J. and Atkinson, T.C., 2001. The recovery and isotopic measurement of water from fluid inclusions in speleothems. Geochimica et Cosmochimica Acta, 65(6), pp.871-884.

Desmarchelier JM. 1999. High-resolution palaeoenvironmental information from southeast Australian speleothems. PhD Thesis, University of Tasmania.

D'Hondt, S. and Arthur, M.A., 1996. Late Cretaceous oceans and the cool tropic paradox. Science, 271(5257), pp.1838-1841.

Dorale, J.A. and Liu, Z., 2009. Limitations of Hendy test criteria in judging the palaeoclimatic suitability of speleothems and the need for replication. Journal of cave and karst studies, 71(1), pp.73-80.

Dorale, J.A., Edwards, R.L., Ito, E., and Gonzalez, L.A., 1998, Climate and vegetation history of the mid-continent from 75 to 25 ka: A speleothem record from Crevice Cave, Missouri, USA: Science, v. 282, p. 1871–1874

Drysdale, R., Couchoud, I., Zanchetta, G. et al. Magnesium in subaqueous speleothems as a potential palaeotemperature proxy. Nat Commun 11, 5027 (2020). https://doi.org/10.1038/s41467-020-18083-7

Dwyer Gary S and Chandler Mark A., 2009. Mid-Pliocene sea level and continental ice volume based on coupled benthic Mg/Ca palaeotemperatures and oxygen isotopes Phil. Trans. R. Soc. A.367157–168 http://doi.org/10.1098/rsta.2008.0222

Elderfield H, Ferretti P, Greaves M, Crowhurst S, McCave IN, Hodell D, Piotrowski AM., 2012. Evolution of ocean temperature and ice volume through the Mid-Pleistocene climate transition. Science 337:704–709

Engel, J., Woodhead, J., Hellstrom, J., Maas, R., Drysdale, R. and Ford, D., 2019. Corrections for initial isotopic disequilibrium in the speleothem U-Pb dating method. Quaternary Geochronology, 54, p.101009.

Esper, J., Cook, E.R., Schweingruber, F.H. 8576228100;7202259586;7004223231; Low-frequency signals in long tree-ring chronologies for reconstructing past temperature variability (2002) Science, 295 (5563), pp. 2250-2253. DOI: 10.1126/science.1066208

Fairchild, I.J. and Hartland, A., 2010. Trace element variations in stalagmites: controls by climate and by karst system processes. EMU Notes in Mineralogy, 10(7), pp.259-287.

Fairchild, I.J. et al., 2006. Modification and preservation of environmental signals in speleothems. Earth-Science Reviews 75(1–4), pp. 105–153. http://dx.doi.org/10.1016/j.earscirev.2005.08.003

Fairchild, I.J., Baker, A., Borsato, A., Frisia, S., Hinton, R.W., McDERMOTT, F.R.,Tooth, A.F., 2001. Annual to sub-annual resolution of multiple trace-element trends in speleothems. Journal of the Geological Society, 158(5), pp.831-841.

Fairchild, I.J., Borsato, A., Tooth, A.F., Frisia, S., Hawkesworth, C.J., Huang, Y., McDermott, F. & Spiro, B., 2000. Controls on trace element (Sr-Mg) compositions of carbonate cave waters: implications for speleothem climatic records. Chemical Geology 166, 255-269.

Fairchild, IJ, & Baker, A 2012. Speleothem Science: From Process to Past Environments, John Wiley & Sons, Incorporated, Hoboken. Available from: ProQuest Ebook Central. [19 October 2020]. https://onlinelibrary.wiley.com/doi/book/10.1002/9781444361094

Fitriatin, B.N., Yuniarti, A., Turmuktini, T. and Ruswandi, F.K., 2014. The effect of phosphate solubilizing microbe producing growth regulators on soil phosphate, growth and yield of maize and fertilizer efficiency on Ultisol. Eurasian Journal of Soil Science, 3(2), p.101.

Fletcher, M.-S. and Thomas, I., 2010. A quantitative Late Quaternary temperature reconstruction from western Tasmania, Australia. Quaternary Science Reviews, 29 (17–18): 2351–2361. doi:10.1016/j.quascirev.2010.06.012.
Ford, D. and Williams, P.D., 2013. Karst hydrogeology and geomorphology. John Wiley & Sons.

Ford, T and Gunn, J, 1992. Caves and Karst of the Peak District. [Buxton: British Cave Research Association.] 32pp.
Frappier, A., D. Sahagian, L.A. González, S.J. Carpenter El Niño events Recorded by Stalagmite Carbon Isotopes Science, 298, 2002, p. 565, 10.1126/science.1076446

Frisia, S. and Borsato, A., 2010. Karst, in: Carbonates in Continental Settings, edited by: Alonso-Zarza, A. M. and Tanner, L. H., Developments in Sedimentology, Elsevier, Amsterdam, 269–318, 2010.

Frisia, S., A. Borsato, J. Susini, 2008. Synchrotron radiation applications to past volcanism archived in speleothems: an overview. J. Volcanol. Geotherm. Res. 2008, 177, 96. doi:10.1016/J.JVOLGEORES.2007.11.010

Frisia, S., Borsato, A., Drysdale, R. N., Paul, B., Greig, A., and Cotte, M., 2012. A re-evaluation of the palaeoclimatic significance of phosphorus variability in speleothems revealed by high-resolution synchrotron micro XRF mapping, Clim. Past, 8, 2039–2051, https://doi.org/10.5194/cp-8-2039-2012

Gagan, M.K., Ayliffe, L.K., Hopley, D., Cali, J.A., Mortimer, G.E., Chappell, J., McCulloch, M.T. and Head, M.J., 1998. Temperature and surface-ocean water balance of the mid-Holocene tropical western Pacific. Science, 279(5353), pp.1014-1018.

Gascoyne, M., 1992. Palaeoclimate determination from cave calcite deposits. Quaternary Science Reviews 11, 609–632.

Gascoyne, M., Ford, D.C. and Schwarcz, H.P., 1983. Rates of cave and landform development in the Yorkshire Dales from speleothem age data. Earth Surface Processes and Landforms, 8(6), pp.557-568.

Gat, J.R., Mook, W.G. and Meijer, H.A., 2001. Environmental isotopes in the hydrological cycle. Principles and Applications UNESCO/IAEA Series, 2, pp.63-7.

Genty, D., Baker, A., Massault, M., Proctor, C., Gilmour, M., Pons-Branchu, E. and Hamelin, B., 2001. Dead carbon in stalagmites: carbonate bedrock palaeodissolution vs. ageing of soil organic matter. Implications for ^{13}C variations in speleothems. Geochimica et Cosmochimica Acta, 65(20), pp.3443-3457.

George, S., Jan Esper, 2019. Concord and discord among Northern Hemisphere palaeotemperature reconstructions from tree rings, Quaternary Science Reviews, Volume 203, 2019, Pages 278-281, ISSN 0277-3791, https://doi.org/10.1016/j.quascirev.2018.11.013.

George, T.S., Giles, C.D., Menezes-Blackburn, D., Condron, L.M., Gama-Rodrigues, A.C., Jaisi, D., Lang, F., Neal, A.L., Stutter, M.I., Almeida, D.S. and Bol, R., 2018. Organic phosphorus in the terrestrial environment: a perspective on the state of the art and future priorities. Plant and Soil, 427(1-2), pp.191-208. 10.1007/s11104-017-3391-x.

Geyh, M.A. and Franke, H.W., 1970. Zur Wachstumsgeschwindigkeit von Stalagmiten (On the growth rates of stalagmites). Atompraxis, 16(1), pp.46-48.

Ghosh, P., J. Adkins, H. Affek, B. Balta, W. Guo, E.A. Schauble, D. Schrag, J.M. Eiler., 2006. ^{13}C–^{18}O bonds in carbonate minerals: A new kind of palaeothermometer Geochim. Cosmochim. Acta, 70 (2006), pp. 1439-1456 https://doi.org/10.1016/j.gca.2005.11.014

Glennie, E, 1953. Hydrological tests at Poole's Cavern, Buxton, Derbyshire. Newsletter of the Cave Research Group of Great Britain, Nos 45/46, 5–10.

Goede, A., Green, D.C. and Harmon, R.S., 1986. Late Pleistocene palaeotemperature record from a Tasmanian speleothem. Australian Journal of Earth Sciences, 33(3), pp.333-342.

Goldhammer, T., Max, T., Brunner, B., Einsiedl, F., & Zabel, M., 2011. Marine sediment pore-water profiles of phosphate $\delta^{18}O$ using a refined micro-extraction. Limnology and Oceanography Methods, 9, 110–120.

Griffiths, M.L., Drysdale, R.N., Vonhof, H.B., Gagan, M.K., Zhao, J.X., Ayliffe, L.K., Hantoro, W.S., Hellstrom, J.C., Cartwright, I., Frisia, S. and Suwargadi, B.W., 2010. Younger Dryas–Holocene temperature and rainfall history of southern Indonesia from δ18O in speleothem calcite and fluid inclusions. Earth and Planetary Science Letters, 295(1-2), pp.30-36.

Grimes, S. T., David.P. Mattey, Margaret E. Collinson, Jerry J. Hooker, 2004. Using mammal tooth phosphate with freshwater carbonate and phosphate palaeoproxies to obtain mean palaeotemperatures, Quaternary Science Reviews, Volume 23, Issues 7–8, 2004, Pages 967-976, ISSN 0277-3791, https://doi.org/10.1016/j.quascirev.2003.06.023

Grootes, P.M., Stuiver, M., Thompson, L.G. and Mosley-Thompson, E., 1989. Oxygen isotope changes in tropical ice, Quelccaya, Peru. Journal of Geophysical Research: Atmospheres, 94(D1), pp.1187-1194.

Hartland, A, Fairchild, I J, Lead, J R, Dominguez-Villar, D, Baker, A, Gunn, J, Baalousha, M and Ju-Nam, Y, 2010. The dripwaters and speleothems of Poole's Cavern: a review of recent and ongoing research, Cave and Karst Science, Vol.36, 37–46.

Hartland, A, Fairchild, I J, Müller, W and Dominguez-Villar, D, 2014. Preservation of NOM-metal complexes in a modern hyperalkaline stalagmite: Implications for speleothem trace element geochemistry. Geochimica et Cosmochimica Acta, Vol.128, 29–43

Hartland, A, Fairchild, I, Lead, J and Baker, A, 2010. Fluorescent properties of organic carbon in cave dripwaters. Science of the Total Environment, Vol.408, 5940–5950.

Heathwaite, A. L., 1997. Sources and pathways of phosphorus loss from agriculture. H. Tunney, O.T. Careton, P.C. Brookes, A.E. Johnstone (Eds.), Phosphorus Loss From Soil to Water, CAB International, Wallingford, UK pp. 205-223

Helfenstein, J., Pistocchi, C., Oberson, A., Tamburini, F., Goll, D. S., and Frossard, E., 2020. Estimates of mean residence times of phosphorus in commonly considered inorganic soil phosphorus pools, Biogeosciences, 17, 441–454, https://doi.org/10.5194/bg-17-441-2020

Hellstrom, J., 2006. U-Th dating of speleothems with high initial 230Th using stratigraphical constraint. Quaternary Geochronology. 1. 289-295. 10.1016/j.quageo.2007.01.004.

Hellstrom, J., McCulloch, M. & Stone, J., 1998. A Detailed 31,000-Year Record of Climate and Vegetation Change, from the Isotope Geochemistry of Two New Zealand Speleothems. Quaternary Research 50, 167–178, https://doi.org/10.1006/qres.1998.1991

Hellstrom, J., Sniderman, K., Drysdale, R. et al., 2020. Speleothem growth intervals reflect New Zealand montane vegetation response to temperature change over the last glacial cycle. Sci Rep 10, 2492 (2020). https://doi.org/10.1038/s41598-020-58317-8

Hellstrom, J.C. and McCulloch, M.T., 2000. Multi-proxy constraints on the climatic significance of trace element records from a New Zealand speleothem. Earth and Planetary Science Letters, 179(2), pp.287-297.

Henkes., G. A., Benjamin H. Passey, Ethan L. Grossman, Brock J. Shenton, Thomas E. Yancey, Alberto Pérez-Huerta, Temperature evolution and the oxygen isotope composition of Phanerozoic oceans from carbonate clumped isotope thermometry, Earth and Planetary Science Letters, Volume 490, 2018, Pages 40-50, ISSN 0012-821X, https://doi.org/10.1016/j.epsl.2018.02.001.

Herbert T. D., 2014. 8.15: alkenone palaeotemperature determinations. In: Holland HD, Turekian KK (eds) Treatise on geochemistry, 2nd edn. Elsevier, Oxford, pp 399–433

Hernández, A., Celia Martin-Puertas, Paola Moffa-Sánchez, Eduardo Moreno-Chamarro, Pablo Ortega, Simon Blockley, Kim M. Cobb, Laia Comas-Bru, Santiago Giralt, Hugues Goosse, Jürg Luterbacher, Belen Martrat, Raimund Muscheler, Andrew Parnell, Sergi Pla-Rabes, Jesper Sjolte, Adam A. Scaife, Didier Swingedouw, Erika

Wise, Guobao Xu, 2020. Modes of climate variability: Synthesis and review of proxy-based reconstructions through the Holocene, Earth-Science Reviews, Volume 209, 2020, 103286, ISSN 0012-8252, https://doi.org/10.1016/j.earscirev.2020.103286.

Herron, M. M. and Langway, C. C., 1980. "Firn Densification: An Empirical Model," Journal of Glaciology. Cambridge University Press, 25(93), pp. 373–385. doi: 10.3189/S0022143000015239.

Hertzberg J.E., Schmidt M.W., 2017. Palaeotemperatures. In: White W. (eds) Encyclopaedia of Geochemistry. Encyclopedia of Earth Sciences Series. Springer, Cham. https://doi.org/10.1007/978-3-319-39193-9_131-1

Hertzberg JE, Schmidt MW, Bianchi TS, Smith RW, Shields MR, Marcantonio F., 2016. Comparison of eastern tropical Pacific TEX_{86} and *Globigerinoides ruber* Mg/Ca derived sea surface temperatures: insights from the Holocene and Last Glacial Maximum. Earth Planet Sci Lett 434:320–332

Hessl, A., K.J. Allen, T. Vance, N.J. Abram, K.M. Saunders Reconstructions of the southern annular mode (SAM) during the last millennium Prog. Phys. Geogr. Earth Environ., 41 (2017), pp. 834-849, 10.1177/0309133317743165

Hill, C. & Forti, P. (1997) Cave Minerals of the World. 2nd edition. National Speleological Society, Huntsville, Alabama.

Hilton, R.J., Andros, N.D. and Watt, R.K., 2012. The ferroxidase center is essential for ferritin iron loading in the presence of phosphate and minimizes side reactions that form Fe (III)-phosphate colloids. BioMetals, 25(2), pp.259-273.

Hoffmann, D.L., Prytulak, J., Richards, D.A., Elliott, T., Coath, C.D., Smart, P.L. and Scholz, D., 2007. Procedures for accurate U and Th isotope measurements by high precision MC-ICPMS. International Journal of Mass Spectrometry, 264(2-3), pp.97-109.

Hren, M. T., Tice, M. M. & Chamberlain, C. P., 2009. Oxygen and hydrogen isotope evidence for a temperate climate 3.42 billion years ago. Nature 462, 205–208.

Hua, Q., McDonald, J., Redwood, D., Drysdale, R., Lee, S., Fallon, S. and Hellstrom, J., 2012. Robust chronological reconstruction for young speleothems using radiocarbon. Quaternary Geochronology, 14, pp.67-80.

Huang, Y., Fairchild, I.J., Borsato, A., Frisia, S., Cassidy, N.J., McDermott, F. and Hawkesworth, C.J., 2001. Seasonal variations in Sr, Mg and P in modern speleothems (Grotta di Ernesto, Italy). Chemical Geology, 175(3-4), pp.429-448. https://doi.org/10.1016/S0009-2541(00)00337-5

Ishikawa, M. and Ichikuni, M.: Coprecipitation of phosphate with calcite, Chem. J., 15, 283–288, 1981.

Jaglan, S., Anil K. Gupta, Hai Cheng, Steven C. Clemens, Som Dutt, S. Balaji, 2020. Indian summer monsoon variability during the last millennium as recorded in stalagmite from Baratang Mahadev cave, Andaman Islands, Palaeogeography, Palaeoclimatology, Palaeoecology, Volume 557, 2020, 109908, ISSN 0031-0182, https://doi.org/10.1016/j.palaeo.2020.109908

Jaisi, D.P. and Blake, R.E., 2010. Tracing sources and cycling of phosphorus in Peru Margin sediments using oxygen isotopes in authigenic and detrital phosphates. Geochimica et Cosmochimica Acta, 74(11), pp.3199-3212.

Jeon, S.-J. and Ishikawa, K. (2005) Characterization of the Family I inorganic pyrophosphatase fromPyrococcus horikoshiiOT3. Archaea, 1 (6): 385–389. doi:10.1155/2005/591628.

Jones, T. J., Daniel J. Lunt, Daniela N. Schmidt, Andy Ridgwell, Appy Sluijs, Paul J. Valdes, Mark Maslin., 2013. Climate model and proxy data constraints on ocean warming across the Palaeocene–Eocene Thermal Maximum, Earth-Science Reviews, Volume 125, 2013, Pages 123-145, ISSN 0012-8252, https://doi.org/10.1016/j.earscirev.2013.07.004.

Kaczka R. J., Barbara Spyt, Karolina Janecka, Ilka Beil, Ulf Büntgen, Tobias Scharnweber, Daniel Nievergelt, Martin Wilmking, 2018. Different maximum latewood density and blue intensity measurements techniques reveal similar results, Dendrochronologia, Volume 49, 2018, Pages 94-101, ISSN 1125-7865, https://doi.org/10.1016/j.dendro.2018.03.005.

Kapsner, W., Alley, R., Shuman, C. et al. Dominant influence of atmospheric circulation on snow accumulation in Greenland over the past 18,000 years. Nature 373, 52–54 (1995). https://doi.org/10.1038/373052a0

Karhu, J. & Epstein, S. The implication of the oxygen isotope records in coexisting cherts and phosphates. Geochim. Cosmochim. Acta 50, 1745–1756 (1986).

Karl, D. M., & Tien, G., 1992. MAGIC: A sensitive and precise method for measuring dissolved phosphorus in aquatic environments. Limnology and Oceanography, 37(1), 105–116. https://doi.org/10.4319/lo.1992.37.1.0105

Kendall, A.C. and Broughton, P.L., 1978. Origin of fabrics in speleothems composed of columnar calcite crystals. Journal of Sedimentary Research, 48(2), pp.519-538.

Knauth, L. P. & Lowe, D. R. High Archean climatic temperature inferred from oxygen isotope geochemistry of cherts in the 3.5 Ga Swaziland Supergroup, South Africa. Geol. Soc. Am. Bull. 115, 566–580 (2003).

Koch, P.L., Zachos, J.C. and Dettman, D.L., 1995. Stable isotope stratigraphy and palaeoclimatology of the Palaeogene Bighorn Basin (Wyoming, USA). Palaeogeography, Palaeoclimatology, Palaeoecology, 115(1-4), pp.61-89.

Koltai, G., Cheng, H. and Spötl, C., 2018. Palaeoclimate significance of speleothems in crystalline rocks: a test case from the Late Glacial and early Holocene (Vinschgau, northern Italy). Climate of the Past, 14(3), p.369.https://doi.org/10.5194/cp-14-369-2018

Krissansen-Totton, J. et al. 2018. Constraining the climate and ocean pH of the early Earth with a geological carbon cycle model. Proceedings of the National Academy of Sciences 115(16), pp. 4105–4110. Available at: http://dx.doi.org/10.1073/pnas.1721296115

Krom, M. D., Herut, B., and Mantoura, R. F. C., 2004, Nutrient budget for the Eastern Mediterranean: Implications for phosphorus limitation: Limnology and Oceanography, v. 49, 1582–1592.

Kucera M., 2007. Planktonic foraminifera as tracers of past oceanic environments, Chapter 6. In: Hillaire-Marcel C, de Vernal A (eds) Developments in marine geology. Elsevier, Oxford, pp 213–262

Landais A, Caillon N, Grachev A, Barnola JM, Chapellaz J, Jouzel J, Masson-Delmotte V, Leuenberger M., 2004. Quantification of rapid temperature change during DO event 12 and phasing with methane inferred from air isotopic measurements. Earth Planet Sci Lett 225:221–232

Landais, A., Yang, J.-W., Pasquier, N., Grisart, A., Brandon, M., Extier, T., Prié, F., Minster, B., Piel, C., Sauze, J., Milcu, A., Stenni, B., and Blunier, T., 2020. Triple isotopic composition of oxygen in water and dioxygen during deglaciations recorded in the EPICA Dome C ice core to link climate, biosphere productivity and water cycle, EGU General Assembly 2020, Online, 4–8 May 2020, EGU2020-5961, https://doi.org/10.5194/egusphere-egu2020-5961

Lavergne, A., Daux, V., Villalba, R., Pierre, M., Stievenard, M., Vimeux, F., et al. (2016). Are the oxygen isotopic composition of Fitzroya cupressoides and Nothofagus pumilio cellulose promising proxies for climate reconstructions in northern Patagonia? J. Geophys. Res. 121, 767–776. doi: 10.1002/2015JG003260

Lawrence, K. T., Pearson, A., Castañeda, I. S., Ladlow, C., Peterson, L. C., & Lawrence, C. E., 2020. Comparison of late Neogene Uk'37 and TEX86 palaeotemperature records from the eastern equatorial Pacific at orbital resolution. Palaeoceanography and Palaeoclimatology, 35, e2020PA003858. https://doi.org/10.1029/2020PA003858

Lechleitner, F. A., Thorsten Dittmar, James U.L. Baldini, Keith M. Prufer, Timothy I. Eglinton, 2017. Molecular signatures of dissolved organic matter in a tropical karst system, Organic Geochemistry, Volume 113, 2017, Pages 141-149, ISSN 0146-6380, https://doi.org/10.1016/j.orggeochem.2017.07.015.

Lee, DH., Choi, SL., Rha, E. et al. 2015. A novel psychrophilic alkaline phosphatase from the metagenome of tidal flat sediments. BMC Biotechnol 15, 1 (2015). https://doi.org/10.1186/s12896-015-0115-2

Leutert, T.J., Philip F. Sexton, Aradhna Tripati, Alison Piasecki, Sze Ling Ho, A. Nele Meckler, 2019. Sensitivity of clumped isotope temperatures in fossil benthic and planktic foraminifera to diagenetic alteration, Geochimica et Cosmochimica Acta, Volume 257, 2019, Pages 354-372, ISSN 0016-7037, https://doi.org/10.1016/j.gca.2019.05.005.

Li, H., Sinha, A., André, A.A., Spötl, C., Vonhof, H.B., Meunier, A., Kathayat, G., Duan, P., Voarintsoa, N.R.G., Ning, Y. and Biswas, J., 2020. A multimillennial climatic context for the megafaunal extinctions in Madagascar and Mascarene Islands. Science advances, 6(42), p.eabb2459.

Liang Y, Blake RE., 2006. Oxygen isotope signature of P-i regeneration from organic compounds by phosphomonoesterases and photooxidation. Geochim Cosmochim Acta 2006; 70:3957.

Liang, Y., Blake, R. E., 2009. Compound- and enzyme-specific phos-phodiester hydrolysis mechanisms revealed by $d^{18}O$ of dissolved inorganic phosphate: Implications for marine P cycling. Geochim. Cosmochim. Ac. 73, 3782–3794.

Liu, G., Li, X., Chiang, H.W., Cheng, H., Yuan, S., Chawchai, S., He, S., Lu, Y., Aung, L.T., Maung, P.M. and Tun, W.N., 2020. On the glacial-interglacial variability of the Asian monsoon in speleothem δ18O records. Science advances, 6(7), p.eaay8189. https://doi.org/10.1016/j.jenvman.2020.111618

Longinelli, A. and Nuti, S., 1973a. Revised phosphate-water isotopic temperature scale. Earth and Planetary Science Letters, 19(3), pp.373-376.

Longinelli, A. and Nuti, S., 1973b. Oxygen isotope measurements of phosphate from fish teeth and bones. Earth and Planetary Science Letters, 20(3), pp.337-340.

Luz, B. and Kolodny, Y., 1985. Oxygen isotope variations in phosphate of biogenic apatites, IV. Mammal teeth and bones. Earth and planetary science letters, 75(1), pp.29-36.

Macleod, G, Fallick, A E and Hall, A J, 1991. The mechanism of carbonate growth on concrete structures, as elucidated by carbon and oxygen isotope analyses. Chemical Geology, Vol.86, 335–343.

Maloney, P., 1992, The molecular and cell biology of anion transport by bacteria: BioEssays, v. 14, p. 757–762.

Marchitto TM, Curry WB, Lynch-Stieglitz J, Bryan SP, Cobb KM, Lund DC., 2014. Improved oxygen isotope temperature calibrations for cosmopolitan benthic foraminifera. Geochim Cosmochim Acta 130:1–11

Mason, H. E., Frisia, S., Tang, Y., Reeder, R. J., and Phillips, B., 2007. Phosphorus speciation in calcite speleothems determined from solid-state NMR spectroscopy, Earth Planet. Sci. Lett., 254, 313– 322, 2007.

Masson-Delmotte V, Dreyfus G, Braconnot P, Johnsen S, Jouzel J, Kageyama M, Landais A, Loutre M-F, Nouet J, Parrenin F, Raynaud D, Stenni B, Tuenter E., 2006. Past temperature reconstructions from deep ice cores: relevance for future climate change. Clim Past 2:145–165

Matthews, A., Ayalon, A. and Bar-Matthews, M., 2000. D/H ratios of fluid inclusions of Soreq cave (Israel) speleothems as a guide to the Eastern Mediterranean Meteoric Line relationships in the last 120 ky. Chemical Geology, 166(3-4), pp.183-191.

McConnaughey, T. 13C and 18O isotopic disequilibrium in biological carbonates: II. In vitro simulation of kinetic isotope effects. Geochim. Cosmochim. Acta53, 163–171 (1989).

McCulloch, M.T., Gagan, M.K., Mortimer, G.E., Chivas, A.R. and Isdale, P.J., 1994. A high-resolution Sr/Ca and δ18O coral record from the Great Barrier Reef, Australia, and the 1982–1983 El Niño. Geochimica et Cosmochimica Acta, 58(12), pp.2747-2754.

McDermott et.al., 2004. Palaeo-climate reconstruction from stable isotope variations in speleothems: a review. Quaternary Science Reviews Volume 23, Issues 7–8, April 2004, Pages 901-918. https://doi.org/10.1016/j.quascirev.2003.06.021

McDermott F., Schwarcz H., Rowe P.J., 2006. ISOTOPES IN SPELEOTHEMS. In: Leng M.J. (eds) Isotopes in Palaeoenvironmental Research. Developments in Palaeoenvironmental Research, vol 10. Springer, Dordrecht. https://doi.org/10.1007/1-4020-2504-1_05

McDermott, F., Mattey, D.P. and Hawkesworth, C., 2001. 2001: Centennial-scale Holocene climate variability revealed by a high-resolution speleothem? ^{18}O record from SW Ireland. Science 294, 1329-31.

McDermott, F., T.C. Atkinson, I.J. Fairchild, L.M. Baldini, D.P. Mattey, 2011. A first evaluation of the spatial gradients in $\delta^{18}O$ recorded by European Holocene speleothems, Global and Planetary Change, Volume 79, Issues 3–4, 2011, Pages 275-287, https://doi.org/10.1016/j.gloplacha.2011.01.005

McGarry, S., Miryam Bar-Matthews, Alan Matthews, Anton Vaks, Bettina Schilman, Avner Ayalon, 2004. Constraints on hydrological and palaeotemperature variations in the Eastern Mediterranean region in the last 140ka given by the δD values of speleothem fluid inclusions, Quaternary Science Reviews, Volume 23, Issues 7–8, 2004, Pages 919-934, ISSN 0277-3791, https://doi.org/10.1016/j.quascirev.2003.06.020

McLaughlin, K., Cade-Menun, B.J. and Paytan, A., 2006. The oxygen isotopic composition of phosphate in Elkhorn Slough, California: A tracer for phosphate sources. Estuarine, Coastal and Shelf Science, 70(3), pp.499-506.

McTainsh GH. 1989. Quaternary aeolian dust processes and sedi-ments in the Australian region. Quaternary Science Reviews8: 235–253

Nagra, G., Treble, P.C., Andersen, M.S., Fairchild, I.J., Coleborn, K. and Baker, A., 2016. A post-wildfire response in cave dripwater chemistry. Hydrol. Earth Syst. Sci, 20, pp.2745-2758.

Nanson GC, Price DM, Short SA. 1992. Wetting and drying of Australia over the past 300 ka. Geology 20: 791–794.

Newton, K, Fairchild, I and Gunn, J, 2015. Rates of calcite precipitation from hyperalkaline waters, Poole's Cavern, Derbyshire, UK. Cave and Karst Science, Vol.42, 116–124.

Nisbeth, C. S., Tamburini, F., Kidmose, J., Jessen, S., and O'Connell, D. W., 2019. Analysis of oxygen isotopes of inorganic phosphate (δ18Op) in freshwater: A detailed method description, Hydrol. Earth Syst. Sci. Discuss. [preprint], https://doi.org/10.5194/hess-2019-469, 2019

Page KJ, Kemp J, Nanson GC. 2009. Late Quaternary evolution of Riverine Plain palaeochannels, south-eastern Australia. Australian Journal of Earth Sciences 56: S19–S33.

Pearson, P. N., 2012. Oxygen Isotopes in Foraminifera: Overview And Historical Review. In Reconstructing Earth's Deep-Time Climate—The State of the Art in 2012. https://doi.org/10.1017/S1089332600002539

Pester, M., Schleper, C. and Wagner, M. (2011) The Thaumarchaeota: an emerging view of their phylogeny and ecophysiology. Current Opinion in Microbiology, 14 (3): 300–306. doi:10.1016/j.mib.2011.04.007.

Petersen, S. V., Defliese, W. F., Saenger, C., Daëron, M., Huntington, K. W., John, C. M., et al (2019). Effects of improved 17O correction on interlaboratory agreement in clumped isotope calibrations, estimates of mineral-specific offsets, and temperature dependence of acid digestion fractionation. Geochemistry, Geophysics, Geosystems, 20, 3495– 3519. https://doi.org/10.1029/2018GC008127

Pistocchi, C., Federica Tamburini, Gerard Gruau, André Ferhi, Dominique Trevisan, Jean-Marcel Dorioz, 2017. Tracing the sources and cycling of phosphorus in river sediments using oxygen isotopes: Methodological adaptations and first results from a case study in France, Water Research, Volume 111, 2017, Pages 346-356, https://doi.org/10.1016/j.watres.2016.12.038

Pitcher, A., Rychlik, N., Hopmans, E. et al. 2010. Crenarchaeol dominates the membrane lipids of Candidatus Nitrososphaera gargensis, a thermophilic Group I.1b Archaeon. ISME J 4, 542–552. https://doi.org/10.1038/ismej.2009.138

Pitty, A, 1966. An approach to the study of karst water illustrated by results from Poole's Cavern, Buxton. University of Hull, Occasional Papers in Geography, Vol.5, 210–230.
Porcelli, D. and Swarzenski, P.W., 2003. The behavior of U-and Th-series nuclides in groundwater. Reviews in Mineralogy and Geochemistry, 52(1), pp.317-361.

Prahl FG, Wakeham SG., 1987. Calibration of unsaturation patterns in long-chain ketone compositions for palaeotemperature assessment. Nature 330:367–369

Quinn, T.M. and Sampson, D.E., 2002. A multiproxy approach to reconstructing sea surface conditions using coral skeleton geochemistry. Palaeoceanography, 17(4), pp.14-1.

Rampelotto, P.H. Extremophiles and Extreme Environments. Life 2013, 3, 482-485. https://doi.org/10.3390/life3030482

Ravelo AC, Hillaire-Marcel C., 2007. The use of oxygen and carbon isotopes of foraminifera in palaeoceanography, Chapter 18. In: Hillaire-Marcel C, de Vernal A (eds) Developments in marine geology. Elsevier, Oxford, pp 735–764

Redfield AC., 1958. The biological control of chemical factors in the environment. Am Sci 46:230A–2221

Richards, D.A., Dorale J. A., 2003. Uranium-series Chronology and Environmental Applications of Speleothems. Reviews in Mineralogy and Geochemistry 52(1), pp. 407–460. http://dx.doi.org/10.2113/0520407

Robert, F. & Chaussidon, M. A palaeotemperature curve for the Precambrian oceans based on silicon isotopes in cherts. Nature 443, 969–972 (2006).

Rossi, C., Lozano, R. P., Isanta, N., and Hellstrom, J., 2010. Manganese stromatolites in caves: El Soplao (Cantabria, Spain), Geology, 38, 1119–1122, 2010.

ROWBERRY, M., FRONTERA, C., BAROŇ, I., KUČERA, J., KŘIVÁNEK, L. and MARTÍ, X., 2020. A novel positioning system for three-dimensional fracture displacement monitoring in the British Cave Science Centre, Poole's Cavern, Buxton, Derbyshire. Cave and Karst Science, 47(3), pp.146-152.

Rozanski, K., Araguás-Araguás, L. and Gonfiantini, R. (1993). Isotopic Patterns in Modern Global Precipitation. In Climate Change in Continental Isotopic Records (eds P.K. Swart, K.C. Lohmann, J. Mckenzie and S. Savin). https://doi.org/10.1029/GM078p0001

Samperiz, A., Laura F. Robinson, Joseph A. Stewart, Ivo Strawson, Melanie J. Leng, Brad E. Rosenheim, Emily R. Ciscato, Katharine R. Hendry, Nadiezhda Santodomingo, 2020. Stylasterid corals: A new palaeotemperature archive, Earth and Planetary Science Letters, Volume 545, 2020, 116407,ISSN 0012-821X, https://doi.org/10.1016/j.epsl.2020.116407

Schindler, D.W., 1974. Eutrophication and recovery in experimental lakes: implications for lake management. Science, 184(4139), pp.897-899.

Schmidt MW, Chang P, Hertzberg JE, Them TR, Ji L, Otto-Bliesner BL., 2012. Impact of abrupt deglacial climate change on tropical Atlantic subsurface temperatures. Proc Natl Acad Sci 109:14348–14352

Schmidt MW, Lynch-Stieglitz J., 2011. Florida Straits deglacial temperature and salinity change: implications for tropical hydrologic cycle variability during the Younger Dryas. Palaeoceanography 26:PA4205

Schmidt, G.A., LeGrande, A.N. and Hoffmann, G., 2007. Water isotope expressions of intrinsic and forced variability in a coupled ocean-atmosphere model. Journal of Geophysical Research: Atmospheres, 112(D10).

Scholz, D. and Hoffmann, D., 2008. 230Th/U-dating of fossil corals and speleothems. Quaternary Science Journal, 57(1-2), pp.52-76.

Scholz, D., Hoffmann, D.L., Hellstrom, J. and Ramsey, C.B., 2012. A comparison of different methods for speleothem age modelling. Quaternary Geochronology, 14, pp.94-104.

Schott, W., 1935. Die Foraminiferen in dem äquatorialen Tein des Atlatischen Ozeans Dt. Atlant. Exped. Meteor 1925–1927, 3 (3B) (1935), pp. 43-134

Schouten S, Hopmans EC, Schefuß E, Sinninghe Damsté JS., 2002. Distributional variations in marine crenarchaeotal membrane lipids: a new tool for reconstructing ancient sea water temperatures? Earth Planet Sci Lett 204:265–274

Schwarcz, H.P., 1986. Geochronology and isotopic geochemistry of speleothems. In: Fritz, P., Fontes, J.Ch. (Eds.), Handbook of Environmental Isotope Geochemistry. Elsevier, Amsterdam, pp. 271–303.

Severinghaus, J., Sowers, T., Brook, E. et al. Timing of abrupt climate change at the end of the Younger Dryas interval from thermally fractionated gases in polar ice. Nature 391, 141–146 (1998). https://doi.org/10.1038/34346

Sharpley, A.N. and Rekolainen, S., 1997. Phosphorus in Agriculture and Its Environmental Implications. In: Tunney, H., Carton, O.T., Brookes, P.C. and Johnston, A.E., Eds., Phosphorus Loss from Soil to Water. Proceedings of a Workshop, Wexford, 29-31 September 1995, 1-53.

Shen, C. C., Lin, K., Duan, W., Jiang, X., Partin, J. W., Edwards, R. L., Cheng, H., & Tan, M., 2013. Testing the annual nature of speleothem banding. Scientific reports, 3, 2633. https://doi.org/10.1038/srep02633

Shen, C., Chung-Che Wu, Hai Cheng, R. Lawrence Edwards, Yu-Te Hsieh, Sylvain Gallet, Ching-Chih Chang, Ting-Yong Li, Doan Dinh Lam, Akihiro Kano, Masako Hori, Christoph Spötl, 2012. High-precision and high-resolution carbonate ^{230}Th dating by MC-ICP-MS with SEM protocols, Geochimica et Cosmochimica Acta, Volume 99, 2012, Pages 71-86, ISSN 0016-7037, https://doi.org/10.1016/j.gca.2012.09.018

Shen, Chuan-Chou & Edwards, R & Cheng, Hai & Dorale, Jeffrey & Thomas, Rebecca & Moran, S & Weinstein, Sarah & Edmonds, Henrietta., 2002. Uranium and thorium isotopic and concentration measurements by magnetic sector inductively coupled plasma mass spectrometry. Chemical Geology. 185. 165-178. 10.1016/S0009-2541(01)00404-1.

Shen, J, Smith, AC, Claire, MW, Zerkle, AL. Unraveling biogeochemical phosphorus dynamics in hyperarid Mars-analogue soils using stable oxygen isotopes in phosphate. Geobiology. 2020; 18: 760– 779. https://doi.org/10.1111/gbi.12408

Shivlata, L. and Satyanarayana, T. (2015) Thermophilic and alkaliphilic Actinobacteria: biology and potential applications. Frontiers in Microbiology, 6. doi:10.3389/fmicb.2015.01014.

Sinclair, D. J., 2011. Two mathematical models of Mg and Sr partitioning into solution during incongruent calcite dissolution: Implications for dripwater and speleothem studies, Chemical Geology, Volume 283, Issues 3–4, 2011, Pages 119-133, ISSN 0009-2541, https://doi.org/10.1016/j.chemgeo.2010.05.022

Smith, A., Wynn, P., Barker, P. et al. North Atlantic forcing of moisture delivery to Europe throughout the Holocene. Sci Rep 6, 24745 (2016). https://doi.org/10.1038/srep24745

Smith, A.C., Pfahler, V., Tamburini, F., Blackwell, M.S. and Granger, S.J., 2021. A review of phosphate oxygen isotope values in global bedrocks: characterising a critical endmember to the soil phosphorus system. Journal of Plant Nutrition and Soil Science, 184(1), pp.25-34. https://doi.org/10.1002/jpln.202000513

Smith, A.C., Pfahler, V., Tamburini, F., et al. (2021) A review of phosphate oxygen isotope values in global bedrocks: Characterising a critical endmember to the soil phosphorus system. Journal of Plant Nutrition and Soil Science, 184 (1): 25–34. doi:10.1002/jpln.202000513

Smith, C.L., Fairchild, I.J., Spötl, C., Frisia, S., Borsato, A., Moreton, S.G. and Wynn, P.M., 2009. Chronology building using objective identification of annual signals in trace element profiles of stalagmites. Quaternary Geochronology, 4(1), pp.11-21.

Smith, S.L., Rizoulis, A., West, J.M. and Lloyd, J.R., 2016. The microbial ecology of a hyper-alkaline spring, and impacts of an alkali-tolerant community during sandstone batch and column experiments representative of a geological disposal facility for intermediate-level radioactive waste. Geomicrobiology Journal, 33(6), pp.455-467.

Smith, TM., Reynolds RW, Peterson TC, Lawrimore J., 2008. Improvements to NOAA's historical merged land-ocean surface temperature analysis. J Climate 21:2283–2296

Smithson, P, 1991. Interrelationships between cave and outside air temperatures. Theoretical and Applied Climatology, Vol.44, 65–73.

Smithson, P, 1993. Vertical temperature structure in a cave environment. Geoarchaeology, Vol.8, 229–240.

Spadin, F. and Marti, D. and Hidalgo-Staub, R. and Rička, J. and Fleitmann, D. and Frenz, M. 2015. Technical Note: How accurate can stalagmite formation temperatures be determined using vapour bubble radius measurements in fluid inclusions? Clim. Past, 11, 905–913, 2015 www.clim-past.net/11/905/2015/ doi:10.5194/cp-11-905-2015

Spötl, C., Mangini, A., Frank, N., Eichst . adter, R., Burns, S., 2002. Start of the last interglacial period at 135 ka: evidence from a high Alpine speleothem. Geology 30 (9), 815–818.

Stetter, K.O. (2006) Hyperthermophiles in the history of life. Philosophical Transactions of the Royal Society B: Biological Sciences, 361 (1474): 1837–1843. doi:10.1098/rstb.2006.1907.

Stüeken, E.E., Tino, C., Arp, G., et al. (2020) Nitrogen isotope ratios trace high-pH conditions in a terrestrial Mars analog site. Science Advances, 6 (9): eaay3440. doi:10.1126/sciadv.aay3440.

Svendsen, l., S. Hetzinger, N. Keenlyside, Y. Gao Marine-based multiproxy reconstruction of Atlantic multidecadal variability Geophys. Res. Lett., 41 (2014), pp. 1295-1300, 10.1002/2013GL059076

Svensson, A., Andersen, K. K., Bigler, M., Clausen, H. B., Dahl-Jensen, D., Davies, S. M., Johnsen, S. J., Muscheler, R., Parrenin, F., Rasmussen, S. O., Röthlisberger, R., Seierstad, I., Steffensen, J. P., and Vinther, B. M., 2008. A

60,000-year Greenland stratigraphic ice core chronology, Clim. Past, 4, 47–57, https://doi.org/10.5194/cp-4-47-2008

Tadros, C.V., Treble, P.C., Baker, A., et al. (2016) ENSO–cave drip-water hydrochemical relationship: a 7-year dataset from south-eastern Australia. Hydrology and Earth System Sciences, 20 (11): 4625–4640. doi:10.5194/hess-20-4625-2016.

Tamburini, F., after Karl D.M, Tien G., 1992. MAGIC: A sensitive and precise method for measuring dissolved phosphorus in aquatic environments. Limnol. Oceanogr. 37, 105–116.

Tamburini, F., Bernasconi, S. M., Angert, A., Weiner, T., & Frossard, E., 2010. A method for the analysis of the $\delta^{18}O$ of inorganic phosphate extracted from soils with HCl. European Journal of Soil Science, 61(6), 1025–1032. https://doi.org/10.1111/j.1365-2389.2010.01290.x

Tamburini, F., Pfahler, V., Bünemann, E.K., Guelland, K., Bernasconi, S.M. and Frossard, E., 2012. Oxygen isotopes unravel the role of microorganisms in phosphate cycling in soils. Environmental science & technology, 46(11), pp.5956-5962. https://doi.org/10.1021/es300311h

Treble PC, Chappell J, Gagan MK, et al. 2005. In situ measurementof seasonal d18O variations and analysis of isotopic trends in amodern speleothem from southwest Australia. Earth and PlanetaryScience Letters 233: 17–32

Treble, P., Drysdale, R., 2010. Speleothem palaeo-rainfall archives in southwest and southeast Australia. Ansto presentation. Past Global Changes. https://pastglobalchanges.org/sites/default/files/download/docs/meeting-products/presentations/2010-aus2k-1st-wkshp/11-Aus2K_treble.pdf [Accessed September 2021]

Treble, P.C., Baker, A., Ayliffe, L.K., et al., 2017. Hydroclimate of the Last Glacial Maximum and deglaciation in southern Australia's arid margin interpreted from speleothem records (23–15 ka). Climate of the Past, 13 (6): 667–687. doi:10.5194/cp-13-667-2017.

Tripati A, Eagle R, Thiagarajan N, Gagnon A, Bauch H, Halloran P, Eiler J., 2010. ^{13}C-^{18}O isotope signatures and 'clumped isotope' thermometry in foraminifera and coccoliths. Geochim Cosmochim Acta 74:5697–5717

Van Breukelen, M.R., Vonhof, H.B., Hellstrom, J.C., Wester, W.C.G. and Kroon, D., 2008. Fossil dripwater in stalagmites reveals Holocene temperature and rainfall variation in Amazonia. Earth and Planetary Science Letters, 275(1-2), pp.54-60. https://doi.org/10.1016/j.epsl.2008.07.060

Vettoretti G, Peltier WR. The impact of insolation, greenhouse gas forcing and ocean circulation changes on glacial inception. The Holocene. 2011;21(5):803-817. doi:10.1177/0959683610394885

WEBB, M., DREDGE, J., BARKER, P.A., MÜLLER, W., JEX, C., DESMARCHELIER, J., HELLSTROM, J. and WYNN, P.M. (2014), Quaternary climatic instability in south-east Australia from a multi-proxy speleothem record. J. Quaternary Sci., 29: 589-596. https://doi.org/10.1002/jqs.2734

Wefer G, Berger WH, Bijma J, Fischer G., 1999. Clues to ocean history: a brief overview of proxies. In: Fischer G, Wefer G (eds) Use of proxies in palaeoceanography: examples from the South Atlantic. Springer, Berlin, pp 1–68

White, J., 2019. TinyTag temperature data collected at White Scar between October 2016 and August 2019.

Wilson, R., Kevin Anchukaitis, Keith R. Briffa, Ulf Büntgen, Edward Cook, Rosanne D'Arrigo, Nicole Davi, Jan Esper, Dave Frank, Björn Gunnarson, Gabi Hegerl, Samuli Helama, Stefan Klesse, Paul J. Krusic, Hans W. Linderholm, Vladimir Myglan, Timothy J. Osborn, Miloš Rydval, Lea Schneider, Andrew Schurer, Greg Wiles, Peng Zhang, Eduardo Zorita, 2016. Last millennium northern hemisphere summer temperatures from tree rings: Part I: The long term context, Quaternary Science Reviews, Volume 134, 2016, Pages 1-18, ISSN 0277-3791, https://doi.org/10.1016/j.quascirev.2015.12.005

Wolf, A., Roberts, W.H.G., Ersek, V. et al. Rainwater isotopes in central Vietnam controlled by two oceanic moisture sources and rainout effects. Sci Rep 10, 16482 (2020). https://doi.org/10.1038/s41598-020-73508-z

Woodhead, J., John Hellstrom, Robyn Pickering, Russell Drysdale, Bence Paul, Petra Bajo, 2012. U and Pb variability in older speleothems and strategies for their chronology, Quaternary Geochronology, Volume 14, 2012, Pages 105-113, https://doi.org/10.1016/j.quageo.2012.02.028

Wuchter C, Shouten S, Coolen MJL, Sinninghe Damsté JS., 2004. Temperature-dependent variation in the distribution of tetraether membrane lipids of marine Crenarchaeota: implications for TEX86 palaeothermometry. Palaeoceanography 19:PA4028

Wynn P. M., Fairchild Ian J., Spötl Christoph, Hartland Adam, Mattey Dave, Fayard Barbara, Cotte Marine, 2014. Synchrotron X-ray distinction of seasonal hydrological and temperature patterns in speleothem carbonate. Environmental Chemistry 11, 28-36.

Wynn, P. M., Ian J. Fairchild, Andrea Borsato, Christoph Spötl, Adam Hartland, Andy Baker, Silvia Frisia, James U.L., Baldini., 2018. Sulphate partitioning into calcite: Experimental verification of pH control and application to seasonality in speleothems, Geochimica et Cosmochimica Acta, Volume 226, 2018, Pages 69-83, ISSN 0016-7037, https://doi.org/10.1016/j.gca.2018.01.020

Wynn, P.M., Ambler, S., Grefe, I., Soto, D.X., Surridge, B.W.J., Gabitov, R.I., Barker, P.A., Anwar, J., Quin, A., Pereira, M.G. and Grant, H.K., 2021. Contemporary systematics of vadose zone nitrate capture by speleothem carbonate. Chemical Geology, 571, p.120172.

Wynn, P.M., Fairchild, I.J., Baker, A., Baldini, J.U. and McDermott, F., 2008. Isotopic archives of sulphate in speleothems. *Geochimica et Cosmochimica Acta*, *72*(10), pp.2465-2477.

Wynn, P.M., Fairchild, I.J., Frisia, S., Spötl, C., Baker, A. and Borsato, A., 2010. High-resolution sulphur isotope analysis of speleothem carbonate by secondary ionisation mass spectrometry. Chemical Geology, 271(3-4), pp.101-107.

Young, M.B., McLaughlin, K., Kendall, C., Stringfellow, W., Rollog, M., Elsbury, K., Donald, E.,Paytan,A.,2009.Characterizing the oxygen isotopic composition of phosphate sources to aquatic ecosystems. Environmental Science and Technology 43, 5190–5196.

Žák, K., Onac, B.P. and Perşoiu, A., 2008. Cryogenic carbonates in cave environments: A review. Quaternary International, 187(1), pp.84-96. https://doi.org/10.1016/j.quaint.2007.02.022

Zhang Zi-Yin, Gong Dao-Yi, He Xue-Zhao, Lei Yang-Na & Feng Sheng-Hui (2010) Statistical Reconstruction of the Antarctic Oscillation Index Based on Multiple Proxies, Atmospheric and Oceanic Science Letters, 3:5, 283-287, DOI: 10.1080/16742834.2010.11446883

Zhao, J., Xia, Q., Collerson, K., 2001. Timing and duration of the last interglacial inferred from high resolution U-series chronology of stalagmite growth in Southern Hemisphere. Earth and Planetary Science Letters 184, 635–644.

Zhou, Y.L., Yang, Y., Chen, M., Zhao, Z.W. and Jiang, H.L., 2014. To improve the performance of sediment microbial fuel cell through amending colloidal iron oxyhydroxide into freshwater sediments. Bioresource technology, 159, pp.232-239.

Zohar, I., Shaviv, A., Klass, T., Roberts, K., & Paytan, A., 2010. Method for the analysis of oxygen isotopic composition of soil phosphate fractions. Environmental Science and Technology, 44(19), 7583–7588. https://doi.org/10.1021/es100707f